



THE UNIVERSITY *of* EDINBURGH

Edinburgh Research Explorer

## The 4D evolution of the Teutonic Bore Camp VHMS deposits, Yilgarn Craton, Western Australia

**Citation for published version:**

Barrote, VR, Mcnaughton, NJ, Tessalina, SG, Evans, NJ, Talavera, C, Zi, J & Mcdonald, BJ 2020, 'The 4D evolution of the Teutonic Bore Camp VHMS deposits, Yilgarn Craton, Western Australia', *Ore Geology Reviews*, vol. 120, pp. 103448. <https://doi.org/10.1016/j.oregeorev.2020.103448>

**Digital Object Identifier (DOI):**

[10.1016/j.oregeorev.2020.103448](https://doi.org/10.1016/j.oregeorev.2020.103448)

**Link:**

[Link to publication record in Edinburgh Research Explorer](#)

**Document Version:**

Peer reviewed version

**Published In:**

Ore Geology Reviews

**General rights**

Copyright for the publications made accessible via the Edinburgh Research Explorer is retained by the author(s) and / or other copyright owners and it is a condition of accessing these publications that users recognise and abide by the legal requirements associated with these rights.

**Take down policy**

The University of Edinburgh has made every reasonable effort to ensure that Edinburgh Research Explorer content complies with UK legislation. If you believe that the public display of this file breaches copyright please contact [openaccess@ed.ac.uk](mailto:openaccess@ed.ac.uk) providing details, and we will remove access to the work immediately and investigate your claim.



## Manuscript Details

<b>Manuscript number</b>	OR GEO_2019_778_R1
<b>Title</b>	The 4D evolution of the Teutonic Bore Camp VHMS deposits, Yilgarn Craton, Western Australia
<b>Article type</b>	Research paper

### Abstract

The Teutonic Bore Camp, comprised of the Teutonic Bore, Jaguar and Bentley deposits, is one of the most significant volcanic-hosted massive sulphide (VHMS) camps in Western Australia. Despite being extensively studied, only recently there have been advances in the understanding of the mechanism that drove the formation of mineralisation. It has been recognized by recent studies that the volcanic-hosted deposits from the Teutonic Bore Camp represent replacement-type VHMS systems, with significant input of fluids and metals from a magmatic source. This paper tests the existing hypothesis that the nearby Penzance granite acted as the metals source and/or thermal engine driving the development of these ore deposits. New age constraints on the formation of the host volcanic sequence at the Bentley deposit and the crystallization of the Penzance granite allows for the construction of a 4D evolutionary model for the ore system. A new U-Pb SHRIMP monazite age of  $2681.9 \pm 4.5$  Ma indicates that the Penzance granite post-dates the host stratigraphy at Bentley (ca. 2693 Ma) and is probably coeval with mineralisation. All zircons (Penzance, Bentley units I and III) have very similar  $\epsilon_{\text{Hf}}(i)$ , with most values between -1 and +6, slightly higher than the  $\epsilon_{\text{Hf}}(i)$  of zircons from other granites and volcanics within the Kurnalpi Terrain, and indicative of juvenile sources. The mean Th/U ratios are  $\sim 0.7$  and  $\sim 0.6$  for the Penzance and Bentley zircons, respectively. All zircons have similar Ce/Nd(CN) ratios. The chemical similarities between the zircons from the granite and the volcanic rocks at Bentley support a shared magmatic source between the Penzance and the Teutonic Bore Camp sequence. The Penzance granite is the likely source of heat, and potentially metals, which drove the VHMS mineralisation at the Teutonic Bore Camp.

<b>Keywords</b>	Penzance; Teutonic Bore; Volcanic-hosted massive sulphide; Archean; Geochronology; 4D modelling
<b>Corresponding Author</b>	Vitor Rodrigues Barrote
<b>Corresponding Author's Institution</b>	Curtin University
<b>Order of Authors</b>	Vitor Rodrigues Barrote, Neal McNaughton, Svetlana Tesselina, Noreen Evans, Cristina Talavera, Jian-Wei Zi, Bradley McDonald
<b>Suggested reviewers</b>	Susan Belford, John Percival, Haoyang Zhou, Christopher Yeats

## Submission Files Included in this PDF

### File Name [File Type]

Cover letter.docx [Cover Letter]

Reply to reviewers.docx [Response to Reviewers]

MS with changes marked.docx [Revised Manuscript with Changes Marked]

Highlights.docx [Highlights]

GraphicAbstract.tif [Graphical Abstract]

MS with no changes marked.docx [Manuscript File]

Figure Captions.docx [Figure]

Fig1.jpg [Figure]

Fig2.jpg [Figure]

Fig3.jpg [Figure]

Fig4.jpg [Figure]

Fig5.jpg [Figure]

Fig6.jpg [Figure]

Fig7.jpg [Figure]

Fig8.jpg [Figure]

Fig9.jpg [Figure]

Fig10.jpg [Figure]

Fig11.jpg [Figure]

declaration-of-conflict of-interests.docx [Conflict of Interest]

Sup1\_Methods.docx [e-Component]

## Submission Files Not Included in this PDF

### File Name [File Type]

Table 1.xlsx [Table]

Sup2\_SHRIMP\_Zircon.xlsx [e-Component]

Sup3\_Hf\_Zircon.xlsx [e-Component]

Sup4\_TE\_Zircon.xlsx [e-Component]

To view all the submission files, including those not included in the PDF, click on the manuscript title on your EVISE Homepage, then click 'Download zip file'.

## Research Data Related to this Submission

### Data set

<https://data.mendeley.com/datasets/jpwjnwcnv2/draft?a=97413372-af5a-4ce3-96d8-180bf090118b>

Data for: The magmatic 4D evolution of the Teutonic Bore Camp VHMS deposits, Yilgarn Craton, Western Australia

Electronic Supplementary Material for "The 4D evolution of the Teutonic Bore Camp VHMS deposits, Yilgarn Craton, Western Australia" The Teutonic Bore Camp, comprised of the Teutonic Bore, Jaguar and Bentley deposits, is one of the most significant volcanic-hosted massive sulphide (VHMS) camps in Western Australia. Despite being extensively studied, only recently there have been advances in the understanding of the mechanism that drove the formation of mineralisation. It has been recognized by recent studies that the volcanic-hosted deposits from the Teutonic Bore Camp represent replacement-type VHMS systems, with significant input of fluids and metals from a magmatic source. This paper tests the existing hypothesis that the nearby Penzance granite acted as the metals source and/or thermal engine driving the development of these ore deposits. New age constraints on the formation of the host volcanic sequence at the Bentley deposit and the crystallization of the Penzance granite allows for the construction of a 4D evolutionary model for the ore system. A new U-Pb SHRIMP monazite age of  $2681.9 \pm 4.5$  Ma indicates that the Penzance granite post-dates the host stratigraphy at Bentley (ca. 2693 Ma) and is probably coeval with mineralisation. All zircons (Penzance, Bentley units I and III) have very similar  $\epsilon_{\text{Hf}}(i)$ , with most values between -1 and +6, slightly higher than the  $\epsilon_{\text{Hf}}(i)$  of zircons from other granites and volcanics within the Kurnalpi Terrain, and indicative of juvenile sources. The mean Th/U ratios are  $\sim 0.7$  and  $\sim 0.6$  for the Penzance and Bentley zircons, respectively. All zircons have similar Ce/Nd(CN) ratios. The chemical similarities between the zircons from the granite and the volcanic rocks at Bentley support a shared magmatic source between the Penzance and the Teutonic Bore Camp sequence. The Penzance granite is the likely source of heat, and potentially metals, which drove the VHMS mineralisation at the Teutonic Bore Camp.

1 Vitor Barrote  
2 School of Earth and Planetary Sciences  
3 Curtin University  
4 Kent St, Bentley WA 6102  
5 Phone: +6145 1929556  
6 Email: vitorbarrote@hotmail.com  
7

8 28.01.2020  
9

10 Dear Editor,  
11

12 I am pleased to re-submit the manuscript "The magmatic 4D evolution of the Teutonic Bore Camp VHMS deposits,  
13 Yilgarn Craton, Western Australia", on behalf of myself, Vitor Barrote and my co-authors.  
14

15 We have greatly appreciated the helpful and constructive revisions to this important work and continue to appreciate  
16 your consideration. We have addressed the concerns raised by the reviewers and editors and believe that the  
17 manuscript should be now suitable for publication.  
18

19 We attach a rebuttal letter that indicates how we have addressed the comments as well as a version of the manuscript  
20 with tracked changes.  
21

22  
23  
24 Sincerely,  
25

26  
27  
28  
29  
30  
31  
32  
33  
34  
35  
36  
37  
38  
39  
40  
41  
42  
43  
44  
45  
46  
47  
48  
49  
50  
51  
52  
53  
54  
55  
56  
57  
58  
59



Vitor Barrote

1  
2  
3  
4 Authors' response to reviewers' comments

5 Manuscript title: –The 4D evolution of the Teutonic Bore Camp VHMS deposits, Yilgarn  
6 Craton, Western Australia  
7

8 Authors: Vitor Barrote, Neal McNaughton, Svetlana Tessalina, Noreen Evans, Cristina  
9 Talavera, Jian-Wei Zi, Bradley McDonald  
10  
11

12  
13 Manuscript number: ORGEO\_2019\_778

14 Date: 28<sup>th</sup> January 2020  
15  
16  
17  
18

19 Dear editor,  
20

21  
22 The authors would like to thank you for your positive reviews, advice, and critiques in how to  
23 further correct and improve this manuscript. We have addressed comments below; editor and  
24 reviewer's comments are indicated in red font, whereas our response is indicated in black font,  
25 for easy reading. In addition to the main comments presented below we have also accepted and  
26 appropriately modified the manuscript based on all the comments made by reviewer 1 in the  
27 tracked version of the revised manuscript. Our response to these comments can be seen in the  
28 tracked version that we have re-submitted.  
29  
30  
31  
32

### 33 **Comments from the editors and reviewers:**

#### 34 **-Editor**

35  
36  
37 *In addition to the reviewers comment, I think that you should try to frame your study within a*  
38 *broader context. As it stands your paper is very much a local study which should be better*  
39 *integrated within the broader context of VHMS in Precambrian time. Also you should limit the*  
40 *use of acronyms to the minimum.*  
41  
42

43 We have attempted to better clarify the broader impact of our observations to VHMS systems  
44 in the Precambrian, as suggested. We have re-phrased the last paragraph of the introduction to  
45 present to the reader our intention to reflect upon this broader subject aided by the upcoming  
46 study presented. We have also re-shaped our final paragraph of section 5.5 where we expose  
47 how the observations presented in this study could potentially impact the exploration of  
48 Precambrian VHMS.  
49

50  
51 Apart from well established acronyms such as VHMS, HFSE and MSWD we have altered the  
52 text and limited our use of acronyms (e.g. Teutonic Bore and Eastern Goldfields Superterrane).  
53

#### 54 **-Reviewer 1**

55  
56  
57  
58  
59

60  
61  
62 This work reports original geochronological data on the volcanic stratigraphy of the Teutonic  
63 Bore Camp, it adds important constraints on the evolution of the associated VHMS deposits,  
64 and is therefore worthy of publication on Ore Geology Review.  
65  
66

67 I have attached a track change version of the manuscript with some recommendations, but, in  
68 particular, I'd like to emphasise some aspects that should be considered by the authors with  
69 care.  
70

71  
72  
73 **1- The first section of the geological background (paragraph 1.1) needs to be revised to improve**  
74 **its clarity. This is a pivotal part of the manuscript that should be crystal clear to the readers,**  
75 **otherwise the following parts will miss of a solid base of understanding.**  
76

77 We have addressed the Geological Background section and based on the additional comments  
78 from this reviewer we have modified it to improve its clarity. We believe that this modified  
79 version will be much easier for the readers to understand.  
80

81  
82 **2- All the tables, apart from table 3, should be moved to the ESMs in a spreadsheet form, in**  
83 **order to be more accessible and to avoid large text gaps within the final manuscript.**  
84

85 We intend to do this, if agreed upon by the Editors and we submit the revised version of the  
86 manuscript with tables 1, 2, 4 and 5 as supplementary material. Also as suggested by the  
87 reviewer within the text we have re-shaped the Methods section and added much of the  
88 information to the ESM.  
89

90  
91 **3- There is bold claim in the discussion that needs to be further discussed or modified. I am**  
92 **referring to the end of paragraph 4.4 where it is suggested that "the Penzance granite is a strong**  
93 **candidate to have acted as the probable magmatic source of sulphur to the mineralisation, and**  
94 **consequently, metals." Whereas the suggestion that the Penzance granite could have acted as a**  
95 **sulfur source is coherent with the isotopic data discussed in Chen et al. (2015), the assumption**  
96 **that metals were sourced from the granite magma is unsupported.**  
97  
98

99 We have modified this part of the text as not to extrapolate on the proposed discussions and  
100 present to the reader unsupported arguments. We have limited ourselves to affirm that Chen et  
101 al. (2015) presents evidence for sulphur supply from magmatic sources only. The supply of  
102 metals remains a possibility, although there is no evidence at this point that this is the case.  
103

#### 104 **-Reviewer 2**

105  
106  
107 The manuscript provides geochronological constraints on the granite and host sequences for  
108 the Teutonic Bore (TB) camp. The authors suggest the involvement of granite in the VHMS  
109 mineralization. The topic of the study is suitable for Ore Geology Reviews. However, two  
110 important points require attention in preparing your revision so that the resulting manuscript  
111 can be evaluated for publication.  
112  
113  
114  
115  
116  
117  
118

119  
120  
121  
122  
123  
124  
125  
126  
1. I am confused with the term “magmatic 4D evolution”. I read the manuscript several times and haven’t found it out. In my view, magmatic evolution should involve the geochemical evolution and dynamical processes, rather than solely providing age data. I think the authors should clarify what the 4D evolution really means.

127  
128  
129  
130  
131  
132  
133  
134  
135  
136  
We have refrained from using the term “magmatic 4D evolution” and instead consistently use “4D evolution”, including modification of the title. The concept of 4D evolution or 4D evolutionary model in this article refers to the addition of time constrains to previously known processes involving magmatism and volcanism, which include geochemical evolution, development of the stratigraphical sequence and development of mineralisation as a consequence of these processes. We have added our definition of the concept to the introduction in order to clarify to the reader the meaning of 4D evolutionary model in this context.

137  
138  
139  
140  
141  
142  
143  
2. The authors also declare that they constructed a 4D evolutionary model for the ore system (lines 24-26 and section 5.4). I definitely do not see this point in the text. Actually, in this manuscript, the authors just conduct geochronological study on the host rock and a granite in the deposits. They even do not obtain the direct ages for mineralization. How do this reveal the 4D evolution of ore systems?

144  
145  
146  
147  
148  
149  
150  
151  
152  
As addressed in the first comment, the 4D evolutionary model refers to the constrain of processes in time, which was achieved by combining extensive new original geochronological observations with previous studies that focused on geochemistry, stratigraphy and other techniques. We have added our definition of the concept to the introduction in order to clarify to the reader the meaning of 4D evolutionary model in this context. We have also added an explanation of the concept in section 5.4 in order not to confuse the reader and to clarify the outcome of the study.

153  
154  
155  
156  
Additionally, do not overstate the temporal association between granite intrusion and mineralization.

157  
158  
159  
160  
161  
162  
163  
We understand the reviewers concern and share his view. We have replaced likely coeval to possibly coeval. We have evidence that the mineralisation is younger than the host rocks that are dated in this study based on stratigraphic observation presented in Belford et al. (2015). However the lack of a reliable age for the Teutonic Bore mineralisation prevents us from demonstrating the association between granite and ore formation.

164  
165  
166  
167  
**Some minor comments are:**

168  
169  
170  
Q1 Lines 483-484: Why do similar Th/U ratios of zircon suggest a magma consanguinity? Any reference?

171  
172  
173  
174  
175  
176  
177  
According to Kirkland et al. (2015), parental magma composition is one of four factors that may contribute to variations in the Th/U of a zircon crystal.



178  
179  
180 We have added that information to the main text and included the reference in our  
181 Bibliography.  
182

183 Q2 Lines 499-506: The authors argue the possible involvement of granite in VHMS  
184 mineralization. What do you mean for “interaction” (line 499)? I do not see the speciality of  
185 granitoid veins within the volcanics as well as volcanic xenoliths within the granite. In my  
186 view, it just indicates that granite postdate the volcanics.  
187  
188

189 We have re-phrased this passage to clarify the ideas presented. The argument presented here  
190 absolutely indicates only that the granite postdates the volcanics. The reason why we  
191 demonstrate that these rocks interact is to refute the idea that granite and volcanics are part of  
192 separate systems that were tectonically placed in contact.  
193  
194

195 Q3 Conclusion section: “The age of the TB camp mineralisation is likely coeval to the intrusion  
196 of the Penzance granite at ca. 2682 Ma.” How do you draw the synchronicity for the  
197 mineralization and granite intrusion? Do not overstate their association before you can offer a  
198 reliable age for the TB mineralization.  
199  
200

201 We understand the reviewers concern and share his view. We have replaced likely coeval to  
202 possibly coeval. We have evidence that the mineralisation is younger than the host rocks that  
203 are dated in this study based on stratigraphic observation presented in Belford et al. (2015).  
204 However the lack of a reliable age for the Teutonic Bore mineralisation prevents us from  
205 demonstrating the association between granite and ore formation.  
206  
207  
208  
209  
210  
211  
212  
213  
214  
215  
216  
217  
218  
219  
220  
221  
222  
223  
224  
225  
226  
227  
228  
229  
230  
231  
232  
233  
234  
235  
236

1  
2  
3  
4  
5  
6  
7  
8  
9  
10 1 The ~~magmatic~~ 4D evolution of the Teutonic Bore Camp VHMS  
11 2 deposits, Yilgarn Craton, Western Australia  
12 3

13 4 Vitor R. Barrote<sup>1,2,3</sup>, Neal J. McNaughton<sup>1</sup>, Svetlana G. Tessalina<sup>1</sup>, Noreen J. Evans<sup>1,2</sup>,  
14 5 Cristina Talavera<sup>1,4,5</sup>, Jian-Wei Zi<sup>1,5,6</sup>, Bradley J. McDonald<sup>1,2</sup>  
15 6  
16 7

17 8 1- John de Laeter Centre and The Institute for Geoscience Research (TIGeR), Curtin  
18 9 University, Kent St, Bentley, WA 6102, Australia

20 10 2- School of Earth and Planetary Sciences, Curtin University, Kent St, Bentley, WA 6102,  
21 11 Australia

22 12 2-3- [School of Earth, Atmosphere and Environment, Monash University, Clayton,](#)  
23 13 [Victoria 3800, Australia](#)

24 14 3-4- School of Geosciences, University of Edinburgh, The King's Building, James  
25 15 Hutton Road, EH9 3FE, Edinburgh, UK

26 16 4-5- State Key Lab of Geological Processes and Mineral Resources, China  
27 17 University of Geosciences

28 18 Declarations of interest: none

29 19  
30 20  
31 21  
32 22  
33 23  
34 24  
35 25  
36 26  
37 27  
38 28  
39 29  
40 30  
41 31  
42 32  
43 33  
44 34  
45 35  
46 36  
47 37  
48 38  
49 39  
50 40  
51 41  
52 42  
53 43  
54 44  
55 45  
56 46  
57 47  
58 48  
59 49

17 **ABSTRACT**

18 The Teutonic Bore (TB) eCamp, comprised of the Teutonic Bore, Jaguar and Bentley  
19 deposits, is one of the most significant volcanic-hosted massive sulphide (VHMS) camps in  
20 Western Australia. Despite being extensively studied ~~in the past~~, only recently there have been  
21 advances in the understanding of the mechanism that drove the formation of mineralisation. It  
22 has been recognized by recent studies that the volcanic-hosted deposits from the ~~TB~~Teutonic  
23 Bore Camp represent replacement-type VHMS systems, with significant input of fluids and  
24 metals from a magmatic source. This paper tests the existing hypothesis that the nearby

**Commented [1]:** Be consistent with the capital letter. Personally I do not have any preference, but keep it uniform throughout the text.

**Commented [2R2]:** We made sure to keep it consistently capital throughout the text.

25 Penzance granite acted as the metals source and/or thermal engine driving the development of  
26 these ore deposits.

27 New age constraints on the formation of the host volcanic sequence at the Bentley deposit  
28 and the crystallization of the Penzance granite allows for the construction of a 4D evolutionary  
29 model for the ore system. A new U-Pb SHRIMP monazite age of  $2681.9 \pm 4.5$  Ma indicates  
30 that the Penzance granite post-dates the host stratigraphy at Bentley (ca. 2693 Ma) and is  
31 probably coeval with mineralisation. All zircons (Penzance, Bentley units I and III) have very  
32 similar  $\delta\text{Hf}_{(i)}$ , with most values between -1 and +6, slightly higher than the  $\delta\text{Hf}_{(i)}$  of zircons  
33 from other granites and volcanics within the Kurnalpi Terrain, and indicative of juvenile  
34 sources. The mean Th/U ratios are  $\sim 0.7$  and  $\sim 0.6$  for the Penzance and Bentley zircons,  
35 respectively. All zircons have similar Ce/Nd<sub>(CN)</sub> ratios. The chemical similarities between the  
36 zircons from the granite and the volcanic rocks at Bentley support a shared magmatic source  
37 between the Penzance and the [Teutonic Bore](#) Camp sequence. The Penzance granite is the  
38 likely source of heat, and potentially metals, which drove the VHMS mineralisation at the  
39 [Teutonic Bore](#) Camp.

40 Keywords: Penzance; Teutonic Bore; Volcanic-hosted massive sulphide; Archean;  
41 Geochronology; 4D modelling

## 42 1 INTRODUCTION

43 Using an extensive database of compiled whole-rock geochemistry and U-Pb  
44 geochronology, Hollis et al (2015) proposed a link between VHMS mineralisation and the  
45 emplacement of HFSE-enriched syn-volcanic intrusions, throughout the Archean Yilgarn  
46 Craton, including the Eastern Goldfield Superterrane ([EGS](#)). Despite the apparent geographical  
47 and broadly coeval association between VHMS ores and HFSE-enriched intrusions, [the](#)  
48 [identification of a genetic link link requires would benefit from](#) further [geochronological and](#)  
49 [isotopic evidencedemonstration by detailed geochronology and isotopic geochemistry.](#)

119  
120  
121  
122  
123  
124  
125  
126  
127  
128  
129  
130  
131  
132  
133  
134  
135  
136  
137  
138  
139  
140  
141  
142  
143  
144  
145  
146  
147  
148  
149  
150  
151  
152  
153  
154  
155  
156  
157  
158  
159  
160  
161  
162  
163  
164  
165  
166  
167  
168  
169  
170  
171  
172  
173  
174  
175  
176  
177

50 The number of significant VHMS occurrences in the Yilgarn Craton is small compared to  
51 other Archean terrains with ~~similar characteristics~~ such as the Superior Province of Canada  
52 ([Hollis et al., 2015](#)). Previous studies suggested that this ~~is~~ could be due to under-exploration  
53 and the use of techniques inappropriate for mineral prospecting in the Yilgarn Craton (Butt et  
54 al., 2017; Ellis, 2004; Hollis et al., 2017, 2015; McConachy et al., 2004). Unlike classic VHMS  
55 systems, replacement-type VHMS systems, such as those in the ~~EGSE~~ Eastern Goldfield  
56 ~~Superterrane~~, do not precipitate onto the seafloor ~~and~~ ~~but rather replace slightly older host~~  
57 ~~stratigraphy~~. ~~As a consequence~~, although some stratigraphic control can be observed within  
58 replacement-type mineralisation, it is not an inevitable feature (Doyle and Allen, 2003).

59 Historically, ~~the search~~ exploration for VHMS occurrences within the Teutonic Bore ~~(TB)~~  
60 area was focused on key stratigraphic horizons. However, the known deposits formed at  
61 different stratigraphic positions and show significant differences in the geometry of  
62 mineralisation, compared to ~~TB~~ Teutonic Bore (Chen et al., 2015; Parker et al., 2017). This led  
63 to a significant time gap between the discoveries of the ~~TB~~ Teutonic Bore deposit in 1976, and  
64 the Jaguar and Bentley deposits ~~(in 2004 and 2008, respectively)~~ (Ellis, 2004; ~~Independence~~  
65 ~~Group NL (IGO), 2015~~; Parker et al., 2017).

66 To better understand ~~this inconsistent lack of stratigraphic control on the~~ position of  
67 orebodies ~~within the stratigraphy~~ at the ~~TB~~ Teutonic Bore eCamp, and a possible link between  
68 high-field-strength-elements (HFSE)-enriched granite emplacement and ore precipitation, this  
69 work re-examines and expands the database of geochronology and isotopic/geochemical  
70 fingerprints for the igneous rock units. This includes re-assessment of the geochronological  
71 data from the nearby HFSE-enriched granite, the Penzance granite (Champion and Cassidy,  
72 2002; Geoscience Australia ~~(GA)~~ 2019), and the volcanic sequence from the ~~TB~~ Teutonic  
73 Bore eCamp (Nelson, 1995), with additional U-Pb ~~Sensitive High-Resolution Ion Microprobe~~  
74 ~~(SHRIMP)~~ dating of zircon and ~~monazites~~.

**Commented [3]:** Such as... please mention an example.

**Commented [4R4]:** We have provided an example.

**Commented [5]:** I recommend to rephrase this sentence. The main clause depends on the subordinate, it should be the opposite. It might be difficult to understand to those readers which are not familiar with the topic.

**Commented [6R6]:** We have merged the information from the subordinate to the main clause.

**Commented [7]:** Brackets are not necessary

**Commented [8R8]:** Change accepted

**Commented [9]:** I recommend to minimise the use of unpublished references when it is not indispensable, as they are a not transparent means by nature.

**Commented [10R10]:** Reference removed

**Commented [11]:** I recommend to clarify to the reader the nature of the inconsistency. It is mentioned above that the VHMS being of a replacive nature are expected to form in the same stratigraphic position, but it is not clear enough, I believe this is an important point that should be emphasised more.

**Commented [12R12]:** We have modified the sentence to clarify the inconsistency (i.e. lack of stratigraphic control).

**Commented [13]:** This acronym is never utilised I the text, so it can be deleted.

**Commented [14R14]:** Ok

**Commented [15]:** The acronym needs to be resolved once at the beginning, but being a known technique it can be omitted in the abstract.

**Commented [16R16]:** Ok

**Commented [17]:** Mineral names are uncountable.

**Commented [18R18]:** We have modified the text to adhere to this rule.

178  
179  
180  
181  
182  
183  
184  
185  
186  
187 75 These geochronological studies are complemented by zircon Hf-isotopiee and trace  
188 76 element analyseis-on-zireons- efrom the Bentley volcanic sequence and Penzance granite, and  
189 77 compilation of detailed stratigraphy, whole-rock geochemistry and sulphur isotope data from  
190 78 previous studies (Belford et al., 2015; Chen et al., 2015; Das, 2018; Isaac, 2015; Sedgmen et  
191 79 al., 2007). [The present work combines the improved geochronological constrains presented](#)  
192 80 [here to the current 3D understanding of the geological processes at place, to develop a 4D](#)  
193 81 [evolutionary model of the deposits at the Teutonic Bore Camp.](#)

198 82 Reliable and precise ages for magmatism and ore-hosting volcanism, combined with  
199 83 traditional and isotopic geochemistry, allows testing of the hypothesis of a genetic relationship  
200 84 between the HFSE-rich Penzance granite and the [FBTeutonic Bore](#) Camp deposits. The results  
201 85 [could](#) have implications for future exploration for [Precambrian](#) VHMS deposits, not only in the  
202 86 well-established [FBTeutonic Bore eCamp](#), but also in *greenfields* throughout the [EGSEastern](#)  
203 87 [Goldfield Superterrane](#) and [potentially, other terranes elsewhere](#) in the Yilgarn Craton.

## 208 88 **12 GEOLOGICAL BACKGROUND**

### 209 89 **12.1 Geology of the Teutonic Bore Camp**

210 90 The Teutonic Bore, Jaguar and Bentley VHMS deposits, along with several other smaller  
211 91 occurrences, form the [FBTeutonic Bore](#) Camp (Independence Group NL (~~x~~ IGO),  
212 92 2015). The [FBTeutonic Bore](#) Camp is [located near the town of Leonora](#), within the Kurnalpi  
213 93 Terrane of the [EGSEastern Goldfield Superterrane](#), Yilgarn Craton (Figure 1). The deposits  
214 94 ~~from~~ the [FBTeutonic Bore eCamp](#) are hosted by the [FBTeutonic Bore](#) volcanic complex,  
215 95 which comprises pillow basalt, overlain and interlayered with volcanoclastic units, coherent  
216 96 rhyolite, andesite and thin sedimentary units (Belford et al., 2015; Parker et al., 2017 and  
217 97 references therein). [The prefix “meta” is assumed but omitted when addressing the Archean](#)

**Commented [19]:** Elsewhere in the Yilgarn or specifically in certain terranes? Please specify.

**Commented [20R20]:** The other Terranes within the Yilgarn are understudied, so studies similar to this if conducted in such regions could impact the understanding and consequently exploration strategies for these locations. Due to the unavailability of such constrains we refrain from specifying which Terranes.

“More data is required in the South West, Burtville and Yamarna terranes, and a number of greenstone belts of the Youanmi Terrane (e.g. Twin Peaks, Tallering) in order to clearly delineate regions of prospectivity and establish temporal, geochemical and stratigraphic associations to mineralization. Localized studies are required in order to establish volcanological settings for a number of deposits and their controlling factors.” Hollis et al 2015

**Commented [21]:** If you want to provide a geographical reference, the location of town of Leonara should be included in the geological map.

**Commented [22R22]:** We have included the town of Leonora in the geological map and have described the symbology in the caption.

237  
238  
239  
240  
241  
242  
243  
244  
245  
246  
247  
248  
249  
250  
251  
252  
253  
254  
255  
256  
257  
258  
259  
260  
261  
262  
263  
264  
265  
266  
267  
268  
269  
270  
271  
272  
273  
274  
275  
276  
277  
278  
279  
280  
281  
282  
283  
284  
285  
286  
287  
288  
289  
290  
291  
292  
293  
294  
295

98 ~~stratigraphic sequence of the Yilgarn Craton, because all rocks are metamorphosed to some~~  
99 ~~extent (Czarnota et al., 2010).~~

100 The volcanic stratigraphy and the distribution of the three deposits, as well as other known  
101 uneconomic ore bodies, have a NW-SE trend (Figure 1). ~~This trend coincides with the general~~  
102 ~~alignment of regional structures, such as the fault that bounds the TB~~Teutonic Bore volcanic  
103 ~~complex to the west (Hallberg and Thompson, 1985; Parker et al., 2017).~~The TB volcanic  
104 ~~sequence is bounded by a syenogranite to the east. Although the nature of the contact with the~~  
105 ~~volcanics is unclear, its attitude follows the general trend of stratigraphy and orebody~~  
106 ~~distribution. Additionally, this trend coincides with the general alignment of regional~~  
107 ~~structures, such as the fault that bounds the TB volcanic complex to the west (Hallberg and~~  
108 ~~Thompson, 1985; Parker et al., 2017).~~

109 The stratigraphy at the TBTeutonic Bore eCamp comprises a predominantly laterally  
110 continuous lithofacies association between the three deposits (Figure 2A). ~~Disruption of the~~  
111 ~~stratigraphic sequence by later dolerite intrusions causes inconsistencies in the stratigraphic~~  
112 ~~continuity between deposits (Belford et al., 2015; Das, 2018), although individual deposits can~~  
113 ~~occur in locally restricted facies (Das, 2018). The prefix “meta” is assumed but omitted when~~  
114 ~~addressing the Archean stratigraphic sequence of the Yilgarn Craton, because all rocks are~~  
115 ~~metamorphosed to some extent (Czarnota et al., 2010).~~

116 ~~Disruption of the stratigraphic sequence by later dolerite intrusions causes inconsistencies~~  
117 ~~in the stratigraphic continuity between deposits (Belford et al., 2015; Das, 2018).~~  
118 Nonetheless,Therefore, the volcanic sequence that hosts the mineralisation can be broadly  
119 subdivided ~~in six units as follow from bottom to top (Figure 2B; Belford et al., 2015; Parker et~~  
120 ~~al., 2017), as depicted in Figure 2B, and comprises six units, from bottom to top:~~

I. Footwall Rhyolite: ~~from~~ 200 m to over 1 km thick. Mainly coherent, either massive  
or flow-banded, with minor breccia (Parker et al., 2017), ~~and with calc-alkaline to~~

**Commented [23]:** I recommend to anticipate this at L91 when you first mention the rocks within the TB complex. Here this sentence creates a logic gap between the sentence that precedes and the one that follows.

**Commented [24R24]:** We repositioned the passage.

**Commented [25]:** This sentence continues the regional analysis started in L92-93. I recommend to avoid logic gaps and to keep this sentence close and connected with the one in L92-93.

**Commented [26R26]:** We have re-shaped the paragraph to satisfy that.

**Commented [27]:** This sentence is unclear. Please rephrase trying to be more specific and avoiding the use of generic terminology such as “the attitude of the contact”.

**Commented [28R28]:** We have erased this sentence and focused on describing the interaction between granite and volcanics further down. It was repetitive as well.

**Commented [29]:** This sentence continues the regional analysis started in L92-93. I recommend to avoid logic gaps and to keep this sentence close and connected with the one in L92-93.

**Commented [30R30]:** We have re-shaped the paragraph to satisfy that.

**Commented [31]:** This sentence is redundant, I recommend to simplify it.

**Commented [32R32]:** We removed this information from this section, we agree with the reviewer that it was unclear. Furthermore it was not necessary to the understanding of the stratigraphy.

**Commented [33]:** This part of the sentence is unclear. Please rephrase in a way in which the spatial relationships can be clearer, in particular in respect to the VHMS deposits.

**Commented [34R34]:** We removed this information from this section, we agree with the reviewer that it was unclear. Furthermore it was not necessary to the understanding of the stratigraphy and relationship between deposits.

**Commented [35]:** I recommend to anticipate this at L91 when you first mention the rocks within the TB complex. Here this sentence creates a logic gap between the sentence that precedes and the one that follows.

**Commented [36R36]:** We have moved this part to the first paragraph of this section.

**Commented [37]:** This sentence is redundant, I recommend to simplify it.

**Commented [38R38]:** We removed this information from this section, we agree with the reviewer that it was unclear. Furthermore it was not necessary to the understanding of the stratigraphy and relationship between deposits.

**Commented [39]:** Citation should always be located at the end of the sentence before punctuation.

**Commented [40R40]:** Ok

**Commented [41]:** Of the six units listed, for only the first is reported the thickness. I recommend to be consistent

**Commented [42R42]:** We have added the requested information to the text.

296  
297  
298  
299  
300  
301  
302  
303  
304  
305  
306  
307  
308  
309  
310  
311  
312  
313  
314  
315  
316  
317  
318  
319  
320  
321  
322  
323  
324  
325  
326  
327  
328  
329  
330  
331  
332  
333  
334  
335  
336  
337  
338  
339  
340  
341  
342  
343  
344  
345  
346  
347  
348  
349  
350  
351  
352  
353  
354

- 123 ~~transitional~~. The magmatic affinity ~~is calc-alkaline to transitional~~ (Belford et al.,  
124 2015). This package is footwall to all three deposits.
- 125 II. Sedimentary rocks partly derived from the rhyolite, locally coarse but grading to  
126 arenite, siltstone and shale. This is the host unit to [the Bentley deposit](#). [The thickness](#)  
127 [range from 0 to 70 m according to Parker et al. \(2017\)](#)
- 128 III. Transitional to tholeiitic basalt/ transitional andesite [with thickness between 30 and](#)  
129 [170 m, with:](#) ~~display~~ massive or pillowed habit, commonly intercalated with shale  
130 rich sediments (Parker et al., 2017). This package is host to the ~~FB~~[Teutonic Bore](#)  
131 deposit and upper lens at Bentley (e.g.: Flying Spur, Brooklands, Comet:  
132 Independence Group NL (IGO), 2015) and overlays the lower orebody at the  
133 Bentley deposit (Arnage: Independence Group NL (IGO), 2015). Belford et al.  
134 (2015) names this unit Footwall Andesite (FA) and Footwall Basalt (FB), relative  
135 to their position to the mineralised zone at Jaguar.
- 136 IV. Upper sedimentary horizon (mineralised package from Belford et al., 2015):  
137 ~~consistings of a~~ ~~C~~ complex assemblage of intercalated dacite (called MPD by  
138 Belford et al., 2015), conglomerate, pumice-rich breccia, laminated sediment,  
139 laminated chert and massive sulphide (Belford et al., 2015). Unit IV marks a  
140 geochemical break in magmatic affinity, from tholeiitic/transitional of the  
141 underlying basalts/andesites to calc-alkaline in the overlying lavas. [The thickness](#)  
142 [is typically within 20 to 40 m \(Parker et al., 2017\)](#).
- 143 V. Upper basalt and andesite of calc-alkaline affinity: ~~consistings of~~ massive and  
144 pillowed basalt and andesite lavas with minor volcanic breccias, ~~and:~~ ~~I~~ intercalated  
145 with mostly carbonaceous shales (Belford et al., 2015). [The total thickness of this](#)  
146 [unit ranges between about 200 to 700 m \(Parker et al., 2017\)](#).

355  
356  
357  
358  
359  
360  
361  
362  
363  
364  
365  
366  
367  
368  
369  
370  
371  
372  
373  
374  
375  
376  
377  
378  
379  
380  
381  
382  
383  
384  
385  
386  
387  
388  
389  
390  
391  
392  
393  
394  
395  
396  
397  
398  
399  
400  
401  
402  
403  
404  
405  
406  
407  
408  
409  
410  
411  
412  
413

147 VI. Hangingwall rhyolite: uppermost stratigraphic unit, described by Belford et al.  
148 (2015) from a single drillhole. The thickness of this unit is estimated to be between  
149 100 to 500m according to Parker et al. (2017).

150 ~~VI.~~  
151 The Teutonic Bore volcanic sequence is bounded to the east ~~The area east of TB is occupied~~  
152 by a large composite batholith (Figure 1) named the Kent Complex by Champion and Cassidy  
153 (2002) and part of the Penzance Supersuite (Hollis et al., 2015). The Penzance Supersuite  
154 consists of HFSE-enriched granites with biotite and/or amphibole in quartz and feldspar rich  
155 rocks. These granites are characterised by variably elevated total Fe, MgO, Y, LREE, Zr,  
156 coupled with low to moderate Al<sub>2</sub>O<sub>3</sub>, K<sub>2</sub>O, Rb, Sr and moderate Na<sub>2</sub>O (Champion and Cassidy,  
157 2002).

158 The relationship between the Penzance granite and the volcanic sequence in the  
159 ~~TB~~Teutonic Bore Camp area remains unclear. Earlier studies (e.g.: Hallberg and Thompson,  
160 1985) suggest an irregular contact between the granite and the volcanic rocks, with  
161 anastomosing veins of granitoid extending into adjacent extrusive rocks and a number of  
162 xenoliths of volcanic rocks within the intrusive granite. The Penzance granite is one of several  
163 HFSE-enriched intrusions in the Yilgarn Craton that occurs in close proximity to VHMS  
164 deposits or occurrences hosted by equally HFSE-enriched volcanics (Hollis et al., 2015).

165 The Jaguar deposit was classified as a replacement-type VHMS deposit by Belford (2010).  
166 This classification relied on evidence including replacement front texture, absence of chimney  
167 structures, and rapid emplacement of the host volcanic sequence, according to the criteria  
168 proposed by Doyle and Allen (2003). Later studies (Chen et al., 2015; Das, 2018; Parker et al.,  
169 2017) have identified similar textures in Bentley and other smaller occurrences and,  
170 consequently, the replacement-type VHMS model is accepted within the ~~TB~~Teutonic Bore  
171 Camp.



414  
415  
416  
417  
418  
419  
420  
421  
422  
423  
424  
425  
426  
427  
428  
429  
430  
431  
432  
433  
434  
435  
436  
437  
438  
439  
440  
441  
442  
443  
444  
445  
446  
447  
448  
449  
450  
451  
452  
453  
454  
455  
456  
457  
458  
459  
460  
461  
462  
463  
464  
465  
466  
467  
468  
469  
470  
471  
472

Despite the predominance of sub-seafloor replacement processes, Belford (2010) observed features that indicate possible above seafloor activity. The development of thin beds of translucent chert with colloform intergrowths of chert and sulphide is interpreted as products of a waning hydrothermal system that had vented fluid to the sediment–water interface and deposited precipitates onto the seafloor (Belford et al., 2015). Massive sulphides conformably overlain by, and gradational upwards into, ~~these~~ narrow beds of laminated chert intercalated with finely-bedded sulphide-rich mudstone, support the idea of a progressive disruption of the mineral activity and indicate that some sulphide precipitation might have taken place very near or at seafloor (Belford et al., 2015).

The occurrence of massive sulphide clasts in the surrounding breccias and conglomerates, which were the result of rapid erosion and mass flow, indicates that the sulphide body was formed contemporaneously with the deposition of the upper sedimentary horizon (IV) (Belford et al., 2015). Similar features have not been observed in either the Bentley or the [Teutonic Bore](#) deposits.

#### 1.22.2 Geochronology of the [Teutonic Bore](#) sequence and the Penzance granite

The SHRIMP zircon age of  $2692 \pm 4$  Ma (Nelson, 1995) is the only published age for the volcanic sequence at the [Teutonic Bore](#) eCamp and comes from a porphyritic dacite with unclear stratigraphic position (Belford et al., 2015). ~~Detailed geochronology was attempted by~~ Additionally, Das (2018), ~~reported an ID-TIMS U-Pb age of  $2692 \pm 1.5$  Ma for a sample of coherent Footwall Rhyolite (unit IV) from Jaguar. These analysis remain unpublished and no data table or sample characterization is provided by Das (2018). in felsic rocks well constrained within the stratigraphic sequence, however only one ID-TIMS U-Pb zircon age was reported. The age of  $2692 \pm 1.5$  Ma for a sample of coherent Footwall Rhyolite (unit IV) from Jaguar remains unpublished.~~

**Commented [43]:** Here you are referring to the content of a Master's thesis not accessible to the readers. Please provide more details as its content is very relevant to this study. Also, I recommend to reword the sentences as it appears that Das has "attempted" (try??) to acquire detailed geochronology, but has managed to obtain a single analysis. Is this true? How is such information relevant to this study?

**Commented [44R44]:** We have reworded the sentence as suggested.

I wish I could provide more details. The only reference in the thesis to this data is "The rarity of dateable minerals in the mafic succession is a major difficulty in the process of lithostratigraphic correlation. Therefore, the best way to obtain the age of a mafic succession is by dating the crosscutting felsic rocks that have dateable minerals in abundance. Until now, the age of the Teutonic Bore Volcanic Complex was constrained from a porphyritic dacite from north of Teutonic Bore deposit at SHRIMP zircon age of  $2962 \pm 4$  Ma (Nelson, 1995). The footwall rhyolite samples for dating were selected from the drill core at Teutonic Bore, Jaguar and Bentley after removing the weathered surface and inclusions. A sample of the coherent footwall rhyolite from Jaguar (Sample # 13JUDD002) was dated using the ID-TIMS U-Pb analysis of Zircon and gave the age of  $2692.6 \pm 1.5$  Ma."

473  
474  
475  
476  
477  
478  
479  
480  
481  
482  
483  
484  
485  
486  
487  
488  
489  
490  
491  
492  
493  
494  
495  
496  
497  
498  
499  
500  
501  
502  
503  
504  
505  
506  
507  
508  
509  
510  
511  
512  
513  
514  
515  
516  
517  
518  
519  
520  
521  
522  
523  
524  
525  
526  
527  
528  
529  
530  
531

196 The reported ages for the Penzance granite are  $2679 \pm 8\text{Ma}$  (Champion and Cassidy, 2002)  
197 and  $2686 \pm 9\text{Ma}$  (Geoscience Australia (GA), 2019, sample ID 96969076). The two ages are  
198 derived from the same analyses and calculated from the same a single dataset from for sample  
199 ID 96969076. No explanation is provided by either references as to the reason behind the  
200 difference in age calculation from a single set of analysis.

**Commented [45]:** It is unclear whether these two ages are derived from the same analyses, or from distinct analyses from zircon extracted from the same sample. Please explain better. Also, include the sample ID in the citation as it has not been contextualised in the text.

**Commented [46R46]:** We have modified the text to clarify that the two ages were calculated from the same single dataset. How these two authors have obtained different ages is not clear and there is no detailed information available. That is one of the reasons why we have decided to attempt dating this rock from newly collected samples from the same location. We accepted the insertion of the sample number to the citation.

**Commented [47]:** Information regarding the sample is redundant as drillcore names and depths are repeated. The coordinate of the samples is available only for sample 96969076. I recommend to simplify this part by summarising the sample info in a table, it would be clearer and shorter.

**Commented [48R48]:** The description of the sampling procedure for the Penzance is necessary to understanding the significance of the new age determination and how it compared to the previous data available. We have moved the rest of the methods to the ESM

**Commented [49]:** The methods can be summarised within the manuscript and the full version moved into the ESM.

**Commented [50R50]:** We moved the methods to the ESM

**Commented [51]:** This is implied in the citation, it is not necessary to restate it.

**Commented [52R52]:** Ok

## 23 SAMPLES AND METHODS

### 2.13.1 Penzance samples

203 Samples from the Penzance granite were collected from three different positions within  
204 the same quarry (Lat. -28.264050, Long. 121.077888, Penzance Quarry in Figure 1). They were  
205 collected from the same quarry as sample ID 96969076 from the Geochron Delivery database  
206 of Geoscience Australia (2019), according to those records. Each one of the three samples was  
207 processed separately and treated as different samples, the analyses were combined only in the  
208 data processing phase of each technique.

### 2.23.2 Bentley samples

210 Two samples were collected from different positions within the footwall rhyolite (unit I) in  
211 the Bentley deposit. Sample 15BUDD78 – 111.60 m was collected from drillhole 15BUDD78  
212 at 111.60 meters depth, from a distal position to the ore. Sample 15BUDD137 – 398.60 m was  
213 collected from a younger higher stratigraphic position within the sequence, a stringer zone to  
214 the lower massive sulphide lens (Arnage), from a different drillhole (15BUDD137).

**Commented [53]:** It is not clear what this is about. If it is the specific name of the lens provide the reader with a scheme that represents the locations of the different lenses. As it is, this name does not provide the reader with any useful information. Please contextualise

215 Two samples (15BUDD120 - 228.42 and 15BUDD120 - 226.04) of the transitional andesite  
216 (unit III), were collected from a single drillhole (15BUDD120), within two meters of each  
217 other. The transitional andesite at the sampled point is hangingwall to the lower lens (Arnage),  
218 but it is in the stringer zone for the upper lens, marked by the occurrence of disseminated  
219 sulphides.

**Commented [54R54]:** We have removed that reference as it is not fundamental to the understanding of the ideas.

### 3.3 Analytical techniques

Zircon and Monazites were analysed on the SHRIMP II at the John de Laeter Centre, Curtin University (JdLC). Additionally, Zircon Lu–Hf isotopes and rare earth element (REE) abundances were measured over two analytical sessions using laser ablation split stream inductively coupled plasma mass spectrometry (LA-SS-ICPMS). The analyses were conducted in zircons from the same samples that were analysed by SHRIMP, but not necessarily on the same grain or over the same spot as the SHRIMP analysis. Detailed description of the conditions and procedures are provided in Supplementary Material 1.

### **2.3—SHRIMP U–Pb dating of Zircon and Monazites**

#### *2.3.1—Mount preparation*

~~Zircon and monazite grains were separated from crushed rock samples using a Frantz magnetic separator and heavy liquids (methylene iodide). Grains were handpicked, mounted in epoxy resin discs and polished to expose their interiors. The zircon crystals were characterized by cathodoluminescence (CL) imaging, and monazite crystals by back-scattered electron (BSE) microscopy using the Mira3, at the Microscopy and Microanalysis Facility, John de Laeter Centre, Curtin University. The epoxy mounts were carbon coated for SEM imaging and Au coated before each SHRIMP analytical session.~~

~~Polished thin sections prepared from samples of transitional andesite (unit III) were examined to identify suitable zircon grains for SHRIMP geochronology using the Tescan Integrated Mineral Analyzer (TIMA-GM) and back-scattered electron (BSE) microscopy using the Mira3, at the Microscopy and Microanalysis Facility, John de Laeter Centre, Curtin University. Portions of the thin sections containing grains large enough (>15 µm) for ion microprobe analysis were drilled out, in ~3 mm plugs, and cast in 25 mm epoxy mounts. The reference materials were in a separate mount that was cleaned and Au coated with the sample mounts before each SHRIMP analytical session.~~

### 2.3.2 Zircon

Selected areas of the imaged zircon were analysed on the SHRIMP II at the John de Laeter Centre, Curtin University (JdLC). The analytical procedures for the Curtin consortium SHRIMP II have been described by de Laeter and Kennedy (1998) and Kennedy and de Laeter (1994) and are similar to those described by Compston et al. (1984) and Williams (1998). For the larger zircons in grain mounts, a 20–25  $\mu\text{m}$  elliptical spot was used, with a mass-filtered  $\text{O}_2^-$  primary beam of  $\sim 2.8\text{--}3.0$  nA, whereas a 10–12  $\mu\text{m}$  spot of  $\sim 0.5$  nA was used on the smaller zircons in polished thin sections. Data for each spot was collected in sets of six scans on the zircons through the mass range of  $^{196}\text{Zr}2\text{O}^+$ ,  $^{204}\text{Pb}^+$ , Background,  $^{206}\text{Pb}^+$ ,  $^{207}\text{Pb}^+$ ,  $^{208}\text{Pb}^+$ ,  $^{238}\text{U}^+$ ,  $^{248}\text{ThO}^+$  and  $^{254}\text{UO}^+$ . The  $^{206}\text{Pb}/^{238}\text{U}$  age standard and U-content standard used was M257 (561.3 Ma and 840 ppm U; Nasdala et al., 2008) while OGC zircon was utilized as the  $^{207}\text{Pb}/^{206}\text{Pb}$  standard, to monitor instrument induced mass fractionation (3465.4  $\pm$  0.6 Ma; Stern et al., 2009). The  $^{207}\text{Pb}/^{206}\text{Pb}$  dates obtained on OGC zircons during the SHRIMP sessions matched the  $^{207}\text{Pb}/^{206}\text{Pb}$  standard age within uncertainty and no fractionation correction was warranted. The common Pb correction was based on the measured  $^{204}\text{Pb}$  content (Compston et al., 1984). The correction formula for Pb/U fractionation is  $^{206}\text{Pb}^+ / ^{238}\text{U}^+ = a ( ^{254}\text{UO}^+ / ^{238}\text{U}^+ )^b$  (Claoué-Long et al., 1995) using the parameter values of Black et al. (2003). The constant “a” is determined empirically from analyses of the standard during each analytical session. The programs SQUID II and Isoplot (Ludwig, 2011, 2009) were used for data processing.

### 2.3.3 Monazite

The U–Th–Pb analyses were performed using the high spatial resolution capability of the SHRIMP II at the JdLC. Monazite was analysed in two analytical sessions. Grains were analysed using a 30  $\mu\text{m}$  Köhler aperture,  $\sim 0.3$  nA primary ion beam ( $\text{O}_2^-$ ) and a  $\sim 10$   $\mu\text{m}$  analysis spot. Energy filtering was not applied, and the post-collector retardation lens was activated to reduce stray ion arrivals. The mass resolution ( $M/\Delta M$  at 1% peak height) was

650  
651  
652  
653  
654  
655  
656  
657  
658  
659  
660  
661  
662  
663  
664  
665  
666  
667  
668  
669  
670  
671  
672  
673  
674  
675  
676  
677  
678  
679  
680  
681  
682  
683  
684  
685  
686  
687  
688  
689  
690  
691  
692  
693  
694  
695  
696  
697  
698  
699  
700  
701  
702  
703  
704  
705  
706  
707  
708

>5000. French ( $^{206}\text{Pb}/^{238}\text{U}$  age 514 Ma) was used as the primary Pb/U reference material, and Z2908 and Z2234 were the secondary reference materials used to monitor matrix effects (Fletcher et al., 2010). Z2908 ( $^{207}\text{Pb}/^{206}\text{Pb}$  age 1796 Ma) was also analysed to monitor and correct for instrumental mass fractionation of  $^{207}\text{Pb}$  from  $^{206}\text{Pb}$ . SQUID II software (Ludwig, 2009) was used for initial data reduction including  $^{204}\text{Pb}$  correction. Matrix effects in  $^{206}\text{Pb}/^{238}\text{U}$  were corrected following established protocols detailed by Fletcher et al. (2010). 9 analyses of Z2908 yielded a mean  $^{207}\text{Pb}/^{206}\text{Pb}$  age of  $1796.7 \pm 5.4$  Ma (MSWD = 1.7). An insignificant fractionation correction (0.02%) was applied to sample data, with no augmentation of sample precision required based on the reproducibility of  $^{207}\text{Pb}/^{206}\text{Pb}$  in the reference materials.  $^{207}\text{Pb}/^{206}\text{Pb}$  dates from individual analyses are presented with  $1\sigma$  internal precision, whereas weighted mean  $^{207}\text{Pb}/^{206}\text{Pb}$  dates are reported at 95% confidence limits.

#### 2.4 LA-SS-ICPMS of Zircon — Trace elements and Hf isotopes

Zircon Lu–Hf isotopes and rare earth element (REE) abundances were measured over two analytical sessions using laser ablation split stream inductively coupled plasma mass spectrometry (LA-SS-ICPMS). The analyses were conducted in zircons from the same samples that were analysed by SHRIMP, but not necessarily on the same grain or over the same spot as the SHRIMP analysis. Isotopic and elemental data were collected simultaneously using a Resonetics S-155-LR 193 nm excimer laser coupled to a Nu Plasma II multicollector and Agilent 7700s quadrupole mass spectrometer in the GeoHistory Facility, JdLC at Curtin University.

Samples 15BUDD120 — 228.42 and 15BUDD120 — 226.04 m, from the Transitional andesite (unit III) were analysed with a laser spot diameter of 24  $\mu\text{m}$ , with 2.7 J/cm<sup>2</sup> on-sample laser energy, repetition rate of 10 Hz, ablation time of 25 seconds and ~30 seconds of background capture before and after each analysis. Two cleaning pulse preceded analysis. The spot size and ablation time in this case were limited by the smaller size of the zircons.

Commented [55]: This acronym should be open up once the first time it is mentioned.

Commented [56R56]: Ok

295 The remaining samples were analysed with a laser spot diameter of 50  $\mu\text{m}$ , with 2.7 J/cm<sup>2</sup>  
296 on-sample laser energy, repetition rate of 10 Hz, ablation time of 40 seconds and ~45 seconds  
297 of total baseline acquisition.

298 Zircon standard P1 (Li et al., 2010; chips of Penglai zircon characterised in-house for trace  
299 element composition) was used as the primary standard to calculate element concentrations  
300 using <sup>91</sup>Zr as the internal reference isotope and assuming 43.14% Zr in zircon, and to correct  
301 for instrument drift.

302 Lu-Hf isotopic data were measured simultaneously for <sup>172</sup>Yb, <sup>173</sup>Yb, <sup>175</sup>Lu, <sup>176</sup>Hf+Yb+Lu,  
303 <sup>177</sup>Hf, <sup>178</sup>Hf, <sup>179</sup>Hf and <sup>180</sup>Hf on the Faraday array. Time resolved data was baseline subtracted  
304 and reduced using Iolite3.5 (DRS after Woodhead et al., 2004), where <sup>176</sup>Yb and <sup>176</sup>Lu were  
305 removed from the 176 mass signal using  $^{176}\text{Yb}/^{173}\text{Yb} = 0.7962$  (Chu et al., 2002) and  
306  $^{176}\text{Lu}/^{175}\text{Lu} = 0.02655$  (Chu et al., 2002) with an exponential law mass bias correction assuming  
307  $^{172}\text{Yb}/^{173}\text{Yb} = 1.35274$  (Chu et al., 2002). The interference corrected <sup>176</sup>Hf/<sup>177</sup>Hf was  
308 normalized to  $^{179}\text{Hf}/^{177}\text{Hf} = 0.7325$  (Patchett and Tatsumoto, 1980) for mass bias correction.  
309 Zircons from the Mud Tank carbonatite locality were analysed together with the samples in  
310 each session to determine corrected, standard referenced <sup>176</sup>Hf/<sup>177</sup>Hf (Table 1). Zircon  
311 standards with a range of REE contents (FC1-91500, Plešovice and GJ-1; references and data  
312 in Table 1) were run to verify the method. All analysed standards fell within 2 $\sigma$  error of reported  
313 <sup>176</sup>Hf/<sup>177</sup>Hf values, although uncertainties on the 24 micron beam run were, understandably,  
314 significantly higher. In addition, the corrected <sup>178</sup>Hf/<sup>177</sup>Hf and <sup>180</sup>Hf/<sup>177</sup>Hf ratios (for the 50  
315 micron beam run) were calculated to monitor the accuracy of the mass bias correction and  
316 yielded an average value of  $1.467193 \pm 12$  and  $1.886808 \pm 11$  (n=184), which is within the  
317 range of values reported by Thirlwall and Anezkievich (2004). Calculation of  $\epsilon_{\text{Hf}}$  values  
318 employed the decay constant of Scherer et al. (2001) and the Chondritic Uniform Reservoir  
319 (CHUR) values of Blichert-Toft and Albarède (1997).

Table 1: Summary of the Hf isotope measurements of standard materials used interspersed with analyses of unknown zircons. Mean values were calculated using the built-in statistics from the Iolite software (Paton et al., 2011)

Standard Material	50 $\mu\text{m}$	24 $\mu\text{m}$	Reference Value
	Corrected $^{176}\text{Hf}/^{177}\text{Hf}$	Corrected $^{176}\text{Hf}/^{177}\text{Hf}$	
Mud Tank	0.282505 $\pm$ 14 (MSWD = 0.70, n = 14)	0.282507 $\pm$ 64 (MSWD = 2.9, n = 6)	0.282505 $\pm$ 44 (Woodhead and Hergt, 2005)
FC1	0.282182 $\pm$ 9 (MSWD = 0.31, n = 9)	0.282229 $\pm$ 150 (MSWD = 3.9, n = 6)	0.282172 $\pm$ 42 (Woodhead and Hergt, 2005)
91500	0.282306 $\pm$ 11 (MSWD = 0.71, n = 14)	0.282235 $\pm$ 130 (MSWD = 2.4, n = 6)	0.282306 $\pm$ 40 (Woodhead et al., 2004)
Plešovice	0.282477 $\pm$ 8 (MSWD = 0.3, n = 10)	0.282470 $\pm$ 51 (MSWD = 0.49, n = 6)	0.282482 $\pm$ 13 (Sláma et al., 2008)
GJ1	0.282016 $\pm$ 12 (MSWD = 0.69, n = 14)	0.281201 $\pm$ 110 (MSWD = 1.1, n = 6)	0.282000 $\pm$ 5 (Morel et al., 2008)

## 34 RESULTS

### 3.14.1 U-Pb SHRIMP Zircon dating

#### 3.1.14.1.1 Footwall rhyolite (unit I) – Bentley Footwall

Fourteen analyses on 14 zircons from sample 15BUDD78 – 111.60 m were performed (Table 2 Supplementary Material 2). Using only analyses within 3% of concordant yields a mean  $^{207}\text{Pb}/^{206}\text{Pb}$  age of  $2696.5 \pm 4.2$  Ma (95% c.l., n=12; mean square weighted deviation, MSWD=1.04, Figure 3). The average and range of Th/U ratio from the most concordant SHRIMP analyses for this sample are 0.60 and 0.45-0.72, respectively.

A second sample from unit I was dated. Twenty-seven analyses from 27 zircons from sample 15BUDD137 – 398.60 m were collected (Table 2 Supplementary Material 2). The mean  $^{207}\text{Pb}/^{206}\text{Pb}$  age obtained for analyses within 4% of concordant and with <0.3% common Pb was  $2691.7 \pm 2.5$  Ma (95% c.l.; n=25; MSWD=0.95, Figure 3). The average and range of Th/U ratio from the most concordant SHRIMP analyses are 0.63 and 0.41-0.84, respectively.

The CL images of zircons from the two unit I, footwall rhyolite samples show grains with continuous oscillatory zoning and no discernible core and/or rims, as shown in Figure 4, and have with sizes that range from about 50 to 100  $\mu\text{m}$  (Figure 4). Their morphologies, Th/U and ages are indistinguishable, and combining the most concordant data, the resulting age of

Commented [57]: I recommend to move Table 2 into the ESMs in a spreadsheet format, so that the data can be more easily accessible. We should save colleagues from wasting their time doing copy/pasting from tables within pdf.

Commented [58R58]: Ok

Commented [59]: This sentences should be better linked or combined.

Commented [60R60]: Ok

827  
828  
829 337 2692.9 ± 2.1 Ma (95% cl; n=37; MSWD=1.05) is our best estimate of the age of the footwall  
830  
831 338 rhyolite at Bentley.

833  
834 339 3.1.24.1.2 *Transitional andesite (unit III) – Bentley Hangingwall*

835  
836 340 The samples from the transitional andesite were treated as two separate samples for the  
837  
838 341 geochronology portion of this study. However, these samples were taken 2 meters apart, from  
839  
840 342 the same drillcore (15BUDD120), and were within the same stratigraphic facies. The CL  
841  
842 343 images show zircons with continuous oscillatory zoning, and ~~are ranging from~~ 15 to 30 µm in  
843  
844 344 diameter (Figure 5).

845  
846 345 Sample 15BUDD120 – 226.04 m yielded 24 dates from 20 zircons. Considering only the  
847  
848 346 13 results with <5% discordance ([Table 2Supplementary Material 2](#)), the MSWD is 2.7 and  
849  
850 347 indicates an age spread not consistent with a single age population. Omitting the three youngest  
851  
852 348 ages as statistical outliers probably influenced by diffusional Pb-loss, ~~yields a mean age for~~ the  
853  
854 349 remaining population ~~yields a mean age~~ of 2693.2 ± 5.8 Ma (95% cl; n= 10; MSWD=0.88,  
855  
856 350 Figure 3). The average and range of Th/U from the SHRIMP analyses of the more concordant  
857  
858 351 zircons from this sample is 0.90 and 0.39-1.55, respectively.

859  
860 352 Sample 15BUDD120 – 228.42 has 18 dates from 16 grains. The ages <5% discordant and  
861  
862 353 <0.1% common Pb yield a mean <sup>207</sup>Pb/<sup>206</sup>Pb age of 2693.6 ± 6.0 Ma (95% cl, n=9;  
863  
864 354 MSWD=0.24, Figure 3; [Table 2Supplementary Material 2](#)). The average and range of Th/U of  
865  
866 355 the more concordant zircons is 0.95 and 0.73-1.31, respectively.

867  
868 356 The ages obtained for the two adjacent samples from the same stratigraphical facies agree  
869  
870 357 within error. Hence, the data can be combined to obtain a mean <sup>207</sup>Pb/<sup>206</sup>Pb age for the  
871  
872 358 Transitional Andesite (unit III) of 2693.4 ± 4.1 Ma (95% c.l., n=19; MSWD=0.55). The average  
873  
874 359 Th/U from the zircons used in this mean age calculation was 0.92.

875  
876  
877  
878  
879 360



886  
887  
888  
889  
890  
891  
892  
893  
894  
895  
896  
897  
898  
899  
900  
901  
902  
903  
904  
905  
906  
907  
908  
909  
910  
911  
912  
913  
914  
915  
916  
917  
918  
919  
920  
921  
922  
923  
924  
925  
926

361

Table 13: SHRIMP isotopic data for monazite from the Penzance granite (mounts N18-06, 16)

Penzance granite (mount N18-06, 16)																
Mount grain-spot	ppm U	ppm Th	$\frac{^{232}\text{Th}}{^{238}\text{U}}$	4f206 (%)	4f208 (%)	$\frac{^{207}\text{Pb}^*}{^{206}\text{Pb}^*}$	$\pm 1\sigma$ err	$\frac{^{206}\text{Pb}^*}{^{238}\text{U}}$	$\pm 1\sigma$ err	$\frac{^{207}\text{Pb}^*}{^{235}\text{U}}$	$\pm 1\sigma$ err	$\frac{^{208}\text{Pb}^*}{^{232}\text{Th}}$	$\pm 1\sigma$ err	$\frac{^{207}\text{Pb}/^{206}\text{Pb}}{\text{Age (Ma)}}$	$1\sigma$ err	% Disc.
$\leq 5\%$ discordance and $< 0.5\%$ 4f206																
N18-06B.B-5	207	12986	63.00	-0.02	0.00	0.1865	0.0022	0.5074	0.0114	13.044	0.3320	0.137	0.0026	2711	19	+2
N18-16C.8-3	629	12531	20.00	-0.01	-0.01	0.1863	0.0010	0.5232	0.0101	13.435	0.2720	0.148	0.0032	2709	9	0
N18-16A.1-6	508	15332	30.00	-0.06	-0.02	0.1862	0.0014	0.5092	0.0069	13.075	0.2050	0.142	0.0030	2709	12	+2
N18-06B.G-2	215	14282	66.00	0.02	0.00	0.1855	0.0022	0.5170	0.0097	13.224	0.2950	0.141	0.0026	2703	19	+1
N18-06B.A-6	789	32172	41.00	0.00	0.00	0.1853	0.0015	0.5092	0.0090	13.010	0.2560	0.140	0.0029	2701	13	+2
N18-16A.1-1	448	11587	26.00	0.00	0.00	0.1852	0.0026	0.5288	0.0091	13.499	0.3020	0.152	0.0032	2700	23	-1
N18-06B.B-7	310	11884	38.00	-0.04	-0.01	0.1851	0.0018	0.5140	0.0088	13.119	0.2620	0.138	0.0028	2699	16	+1
N18-06B.G-5	345	16469	48.00	-0.06	-0.01	0.1847	0.0019	0.4933	0.0085	12.563	0.2540	0.136	0.0024	2696	17	+4
N18-06B.A-5	573	19934	35.00	0.43	0.11	0.1844	0.0017	0.5213	0.0094	13.257	0.2710	0.144	0.0028	2693	15	0
N18-06B.K-2	1134	74444	66.00	0.34	0.04	0.1842	0.0016	0.4894	0.0085	12.430	0.2430	0.136	0.0027	2691	14	+5
N18-16B.6-2	926	62647	68.00	0.05	0.01	0.1842	0.0010	0.4854	0.0078	12.327	0.2130	0.142	0.0030	2691	9	+5
N18-16D.15-1	602	14098	23.00	0.02	0.01	0.1841	0.0009	0.5092	0.0083	12.929	0.2250	0.147	0.0030	2690	8	+1
N18-16C.8-5	664	14242	21.00	-0.05	-0.02	0.1841	0.0012	0.5198	0.0080	13.193	0.2240	0.141	0.0030	2690	11	0
N18-16C.8-6	466	11320	24.00	0.01	0.00	0.1840	0.0013	0.4927	0.0118	12.502	0.3140	0.144	0.0029	2689	12	+4

927  
928  
929  
930  
931  
932  
933  
934  
935  
936  
937  
938  
939  
940  
941  
942  
943  
944  
945  
946  
947  
948  
949  
950  
951  
952  
953  
954  
955  
956  
957  
958  
959  
960  
961  
962  
963  
964  
965  
966  
967

<u>N18-16D.16-1</u>	<u>1039</u>	<u>19243</u>	<u>19.00</u>	<u>0.03</u>	<u>0.01</u>	<u>0.1839</u>	<u>0.0007</u>	<u>0.5021</u>	<u>0.0120</u>	<u>12.729</u>	<u>0.3110</u>	<u>0.147</u>	<u>0.0033</u>	<u>2688</u>	<u>6</u>	<u>+2</u>
<u>N18-16G.18-1</u>	<u>1002</u>	<u>69393</u>	<u>69.00</u>	<u>0.32</u>	<u>0.04</u>	<u>0.1838</u>	<u>0.0009</u>	<u>0.4905</u>	<u>0.0102</u>	<u>12.430</u>	<u>0.2690</u>	<u>0.149</u>	<u>0.0035</u>	<u>2687</u>	<u>8</u>	<u>+4</u>
<u>N18-06B.A-7</u>	<u>1097</u>	<u>38290</u>	<u>35.00</u>	<u>0.01</u>	<u>0.00</u>	<u>0.1835</u>	<u>0.0014</u>	<u>0.5314</u>	<u>0.0097</u>	<u>13.442</u>	<u>0.2700</u>	<u>0.146</u>	<u>0.0029</u>	<u>2685</u>	<u>13</u>	<u>-2</u>
<u>N18-06B.G-7</u>	<u>216</u>	<u>12340</u>	<u>57.00</u>	<u>0.07</u>	<u>0.01</u>	<u>0.1832</u>	<u>0.0020</u>	<u>0.5244</u>	<u>0.0095</u>	<u>13.249</u>	<u>0.2840</u>	<u>0.143</u>	<u>0.0028</u>	<u>2682</u>	<u>18</u>	<u>-1</u>
<u>N18-16D.14-1</u>	<u>129</u>	<u>6945</u>	<u>54.00</u>	<u>-0.03</u>	<u>-0.01</u>	<u>0.1832</u>	<u>0.0019</u>	<u>0.5022</u>	<u>0.0137</u>	<u>12.685</u>	<u>0.3700</u>	<u>0.152</u>	<u>0.0032</u>	<u>2682</u>	<u>17</u>	<u>+2</u>
<u>N18-16A.1-4</u>	<u>279</u>	<u>15220</u>	<u>54.00</u>	<u>-0.01</u>	<u>0.00</u>	<u>0.1831</u>	<u>0.0016</u>	<u>0.5303</u>	<u>0.0114</u>	<u>13.390</u>	<u>0.3120</u>	<u>0.152</u>	<u>0.0032</u>	<u>2681</u>	<u>14</u>	<u>-2</u>
<u>N18-06B.B-6</u>	<u>308</u>	<u>10496</u>	<u>34.00</u>	<u>0.03</u>	<u>0.01</u>	<u>0.1830</u>	<u>0.0018</u>	<u>0.4883</u>	<u>0.0107</u>	<u>12.323</u>	<u>0.2980</u>	<u>0.137</u>	<u>0.0028</u>	<u>2681</u>	<u>16</u>	<u>+4</u>
<u>N18-06B.G-4</u>	<u>178</u>	<u>11404</u>	<u>64.00</u>	<u>0.04</u>	<u>0.01</u>	<u>0.1828</u>	<u>0.0023</u>	<u>0.4965</u>	<u>0.0095</u>	<u>12.515</u>	<u>0.2870</u>	<u>0.139</u>	<u>0.0026</u>	<u>2679</u>	<u>20</u>	<u>+3</u>
<u>N18-06B.K-3</u>	<u>895</u>	<u>38759</u>	<u>43.00</u>	<u>0.02</u>	<u>0.00</u>	<u>0.1827</u>	<u>0.0015</u>	<u>0.4817</u>	<u>0.0083</u>	<u>12.135</u>	<u>0.2340</u>	<u>0.136</u>	<u>0.0026</u>	<u>2678</u>	<u>13</u>	<u>+5</u>
<u>N18-16A.1-3</u>	<u>515</u>	<u>14308</u>	<u>28.00</u>	<u>-0.01</u>	<u>0.00</u>	<u>0.1827</u>	<u>0.0010</u>	<u>0.5205</u>	<u>0.0105</u>	<u>13.111</u>	<u>0.2760</u>	<u>0.147</u>	<u>0.0032</u>	<u>2677</u>	<u>9</u>	<u>-1</u>
<u>N18-16C.8-1</u>	<u>638</u>	<u>13479</u>	<u>21.00</u>	<u>0.00</u>	<u>0.00</u>	<u>0.1824</u>	<u>0.0014</u>	<u>0.5182</u>	<u>0.0072</u>	<u>13.035</u>	<u>0.2110</u>	<u>0.147</u>	<u>0.0032</u>	<u>2675</u>	<u>13</u>	<u>-1</u>
<u>N18-06B.A-1</u>	<u>863</u>	<u>31292</u>	<u>36.00</u>	<u>-0.02</u>	<u>0.00</u>	<u>0.1824</u>	<u>0.0015</u>	<u>0.5070</u>	<u>0.0088</u>	<u>12.750</u>	<u>0.2490</u>	<u>0.149</u>	<u>0.0030</u>	<u>2675</u>	<u>14</u>	<u>+1</u>
<u>N18-06B.B-3</u>	<u>296</u>	<u>11665</u>	<u>39.00</u>	<u>-0.09</u>	<u>-0.02</u>	<u>0.1823</u>	<u>0.0020</u>	<u>0.5334</u>	<u>0.0095</u>	<u>13.405</u>	<u>0.2850</u>	<u>0.144</u>	<u>0.0029</u>	<u>2674</u>	<u>18</u>	<u>-3</u>
<u>N18-06B.B-1</u>	<u>188</u>	<u>10313</u>	<u>55.00</u>	<u>0.05</u>	<u>0.01</u>	<u>0.1821</u>	<u>0.0023</u>	<u>0.5124</u>	<u>0.0099</u>	<u>12.868</u>	<u>0.2980</u>	<u>0.144</u>	<u>0.0026</u>	<u>2672</u>	<u>21</u>	<u>0</u>
<u>N18-06B.G-3</u>	<u>475</u>	<u>24369</u>	<u>51.00</u>	<u>-0.03</u>	<u>-0.01</u>	<u>0.1821</u>	<u>0.0017</u>	<u>0.4923</u>	<u>0.0083</u>	<u>12.363</u>	<u>0.2420</u>	<u>0.136</u>	<u>0.0026</u>	<u>2672</u>	<u>15</u>	<u>+3</u>
<u>N18-16A.6-1</u>	<u>1052</u>	<u>69743</u>	<u>66.00</u>	<u>-0.01</u>	<u>0.00</u>	<u>0.1821</u>	<u>0.0007</u>	<u>0.5010</u>	<u>0.0077</u>	<u>12.581</u>	<u>0.2020</u>	<u>0.150</u>	<u>0.0033</u>	<u>2672</u>	<u>6</u>	<u>+2</u>
<u>N18-16C.8-2</u>	<u>605</u>	<u>11778</u>	<u>19.00</u>	<u>0.00</u>	<u>0.00</u>	<u>0.1821</u>	<u>0.0010</u>	<u>0.5212</u>	<u>0.0089</u>	<u>13.084</u>	<u>0.2390</u>	<u>0.149</u>	<u>0.0030</u>	<u>2672</u>	<u>9</u>	<u>-1</u>
<u>N18-16C.10-4</u>	<u>587</u>	<u>20801</u>	<u>35.00</u>	<u>0.02</u>	<u>0.00</u>	<u>0.1820</u>	<u>0.0011</u>	<u>0.5089</u>	<u>0.0096</u>	<u>12.772</u>	<u>0.2570</u>	<u>0.146</u>	<u>0.0033</u>	<u>2671</u>	<u>10</u>	<u>+1</u>
<u>N18-16C.10-1</u>	<u>466</u>	<u>14728</u>	<u>32.00</u>	<u>0.10</u>	<u>0.03</u>	<u>0.1819</u>	<u>0.0011</u>	<u>0.5268</u>	<u>0.0110</u>	<u>13.210</u>	<u>0.2900</u>	<u>0.153</u>	<u>0.0039</u>	<u>2670</u>	<u>10</u>	<u>-2</u>

968  
969  
970  
971  
972  
973  
974  
975  
976  
977  
978  
979  
980  
981  
982  
983  
984  
985  
986  
987  
988  
989  
990  
991  
992  
993  
994  
995  
996  
997  
998  
999  
1000  
1001  
1002  
1003  
1004  
1005  
1006  
1007  
1008

<u>N18-06B.B-2</u>	<u>202</u>	<u>9808</u>	<u>49.00</u>	<u>0.22</u>	<u>0.04</u>	<u>0.1812</u>	<u>0.0022</u>	<u>0.5116</u>	<u>0.0094</u>	<u>12.779</u>	<u>0.2860</u>	<u>0.141</u>	<u>0.0027</u>	<u>2664</u>	<u>20</u>	<u>0</u>
<u>N18-16C.8-4</u>	<u>636</u>	<u>13910</u>	<u>22.00</u>	<u>0.02</u>	<u>0.01</u>	<u>0.1810</u>	<u>0.0010</u>	<u>0.5352</u>	<u>0.0069</u>	<u>13.353</u>	<u>0.1920</u>	<u>0.144</u>	<u>0.0030</u>	<u>2662</u>	<u>9</u>	<u>-4</u>
<u>N18-16D.13-1</u>	<u>389</u>	<u>6592</u>	<u>17.00</u>	<u>0.09</u>	<u>0.04</u>	<u>0.1808</u>	<u>0.0011</u>	<u>0.5403</u>	<u>0.0104</u>	<u>13.471</u>	<u>0.2760</u>	<u>0.155</u>	<u>0.0034</u>	<u>2661</u>	<u>10</u>	<u>-5</u>
<u>N18-06B.D-1</u>	<u>362</u>	<u>26423</u>	<u>73.00</u>	<u>0.04</u>	<u>0.00</u>	<u>0.1808</u>	<u>0.0018</u>	<u>0.4927</u>	<u>0.0099</u>	<u>12.282</u>	<u>0.2780</u>	<u>0.139</u>	<u>0.0026</u>	<u>2660</u>	<u>16</u>	<u>+3</u>
<u>N18-16C.10-3</u>	<u>557</u>	<u>15536</u>	<u>28.00</u>	<u>0.07</u>	<u>0.02</u>	<u>0.1805</u>	<u>0.0012</u>	<u>0.5212</u>	<u>0.0087</u>	<u>12.968</u>	<u>0.2360</u>	<u>0.142</u>	<u>0.0030</u>	<u>2657</u>	<u>11</u>	<u>-2</u>
<u>&gt;5% discordance and/or &gt;0.5% 4f206</u>																
<u>N18-06A.N-3</u>	<u>115</u>	<u>12090</u>	<u>105.00</u>	<u>1.31</u>	<u>0.09</u>	<u>0.1942</u>	<u>0.0046</u>	<u>0.3399</u>	<u>0.0074</u>	<u>9.100</u>	<u>0.2920</u>	<u>0.120</u>	<u>0.0024</u>	<u>2778</u>	<u>38</u>	<u>+32</u>
<u>N18-06B.A-4</u>	<u>484</u>	<u>26279</u>	<u>54.00</u>	<u>0.98</u>	<u>0.17</u>	<u>0.1903</u>	<u>0.0024</u>	<u>0.4979</u>	<u>0.0106</u>	<u>13.063</u>	<u>0.3280</u>	<u>0.134</u>	<u>0.0025</u>	<u>2745</u>	<u>21</u>	<u>+5</u>
<u>N18-06B.E-1</u>	<u>142</u>	<u>5608</u>	<u>40.00</u>	<u>2.70</u>	<u>0.69</u>	<u>0.1879</u>	<u>0.0044</u>	<u>0.5326</u>	<u>0.0107</u>	<u>13.801</u>	<u>0.4280</u>	<u>0.132</u>	<u>0.0024</u>	<u>2724</u>	<u>39</u>	<u>-1</u>
<u>N18-06B.K-1</u>	<u>440</u>	<u>31841</u>	<u>72.00</u>	<u>0.93</u>	<u>0.12</u>	<u>0.1852</u>	<u>0.0025</u>	<u>0.4438</u>	<u>0.0078</u>	<u>11.331</u>	<u>0.2530</u>	<u>0.120</u>	<u>0.0023</u>	<u>2700</u>	<u>22</u>	<u>+12</u>
<u>N18-06B.G-1</u>	<u>173</u>	<u>10873</u>	<u>63.00</u>	<u>0.06</u>	<u>0.01</u>	<u>0.1843</u>	<u>0.0025</u>	<u>0.4764</u>	<u>0.0124</u>	<u>12.104</u>	<u>0.3560</u>	<u>0.133</u>	<u>0.0027</u>	<u>2692</u>	<u>22</u>	<u>+7</u>
<u>N18-06B.B-8</u>	<u>245</u>	<u>13623</u>	<u>56.00</u>	<u>-0.03</u>	<u>-0.01</u>	<u>0.1831</u>	<u>0.0020</u>	<u>0.4666</u>	<u>0.0083</u>	<u>11.780</u>	<u>0.2490</u>	<u>0.123</u>	<u>0.0022</u>	<u>2681</u>	<u>18</u>	<u>+8</u>
<u>N18-16A.1-2</u>	<u>288</u>	<u>14906</u>	<u>52.00</u>	<u>0.08</u>	<u>0.01</u>	<u>0.1819</u>	<u>0.0015</u>	<u>0.5669</u>	<u>0.0127</u>	<u>14.220</u>	<u>0.3420</u>	<u>0.160</u>	<u>0.0036</u>	<u>2670</u>	<u>14</u>	<u>-8</u>
<u>N18-06B.A-8</u>	<u>349</u>	<u>26244</u>	<u>75.00</u>	<u>2.02</u>	<u>0.21</u>	<u>0.1818</u>	<u>0.0056</u>	<u>0.3843</u>	<u>0.0130</u>	<u>9.635</u>	<u>0.4430</u>	<u>0.122</u>	<u>0.0029</u>	<u>2670</u>	<u>51</u>	<u>+21</u>
<u>N18-06B.B-4</u>	<u>143</u>	<u>9993</u>	<u>70.00</u>	<u>0.14</u>	<u>0.02</u>	<u>0.1816</u>	<u>0.0027</u>	<u>0.4682</u>	<u>0.0095</u>	<u>11.725</u>	<u>0.2960</u>	<u>0.128</u>	<u>0.0025</u>	<u>2668</u>	<u>24</u>	<u>+7</u>
<u>N18-06B.G-8</u>	<u>220</u>	<u>14795</u>	<u>67.00</u>	<u>0.26</u>	<u>0.04</u>	<u>0.1814</u>	<u>0.0020</u>	<u>0.4741</u>	<u>0.0101</u>	<u>11.857</u>	<u>0.2890</u>	<u>0.128</u>	<u>0.0025</u>	<u>2666</u>	<u>18</u>	<u>+6</u>
<u>N18-16B.6-3</u>	<u>843</u>	<u>59533</u>	<u>71.00</u>	<u>0.07</u>	<u>0.01</u>	<u>0.1812</u>	<u>0.0010</u>	<u>0.4463</u>	<u>0.0081</u>	<u>11.152</u>	<u>0.2140</u>	<u>0.140</u>	<u>0.0030</u>	<u>2664</u>	<u>9</u>	<u>+11</u>
<u>N18-06A.N-1</u>	<u>76</u>	<u>9566</u>	<u>125.00</u>	<u>1.76</u>	<u>0.15</u>	<u>0.1811</u>	<u>0.0049</u>	<u>0.4884</u>	<u>0.0112</u>	<u>12.191</u>	<u>0.4330</u>	<u>0.110</u>	<u>0.0023</u>	<u>2663</u>	<u>45</u>	<u>+4</u>
<u>N18-06B.G-6</u>	<u>281</u>	<u>13360</u>	<u>48.00</u>	<u>0.06</u>	<u>0.01</u>	<u>0.1810</u>	<u>0.0018</u>	<u>0.4676</u>	<u>0.0182</u>	<u>11.670</u>	<u>0.4720</u>	<u>0.137</u>	<u>0.0027</u>	<u>2662</u>	<u>17</u>	<u>+7</u>

1009  
1010  
1011  
1012  
1013  
1014  
1015  
1016  
1017  
1018  
1019  
1020  
1021  
1022  
1023  
1024  
1025  
1026  
1027  
1028  
1029  
1030  
1031  
1032  
1033  
1034  
1035  
1036  
1037  
1038  
1039  
1040  
1041  
1042  
1043  
1044  
1045  
1046  
1047  
1048  
1049

362  
363

<a href="#">N18-16C.10-2</a>	<a href="#">629</a>	<a href="#">16612</a>	<a href="#">26.00</a>	<a href="#">0.12</a>	<a href="#">0.03</a>	<a href="#">0.1802</a>	<a href="#">0.0019</a>	<a href="#">0.4040</a>	<a href="#">0.0213</a>	<a href="#">10.040</a>	<a href="#">0.5400</a>	<a href="#">0.133</a>	<a href="#">0.0031</a>	<a href="#">2655</a>	<a href="#">17</a>	<a href="#">+18</a>
<a href="#">N18-06B.A-2</a>	<a href="#">814</a>	<a href="#">29448</a>	<a href="#">36.00</a>	<a href="#">1.02</a>	<a href="#">0.23</a>	<a href="#">0.1763</a>	<a href="#">0.0020</a>	<a href="#">0.4132</a>	<a href="#">0.0093</a>	<a href="#">10.042</a>	<a href="#">0.2560</a>	<a href="#">0.124</a>	<a href="#">0.0024</a>	<a href="#">2618</a>	<a href="#">19</a>	<a href="#">+15</a>
<a href="#">N18-06B.A-3</a>	<a href="#">638</a>	<a href="#">36168</a>	<a href="#">57.00</a>	<a href="#">1.50</a>	<a href="#">0.23</a>	<a href="#">0.1753</a>	<a href="#">0.0038</a>	<a href="#">0.4980</a>	<a href="#">0.0173</a>	<a href="#">12.034</a>	<a href="#">0.4960</a>	<a href="#">0.136</a>	<a href="#">0.0027</a>	<a href="#">2609</a>	<a href="#">36</a>	<a href="#">0</a>
<a href="#">N18-16G.23-1</a>	<a href="#">147</a>	<a href="#">17544</a>	<a href="#">120.00</a>	<a href="#">0.89</a>	<a href="#">0.04</a>	<a href="#">0.1270</a>	<a href="#">0.0034</a>	<a href="#">0.2374</a>	<a href="#">0.0127</a>	<a href="#">4.155</a>	<a href="#">0.2490</a>	<a href="#">0.094</a>	<a href="#">0.0021</a>	<a href="#">2056</a>	<a href="#">47</a>	<a href="#">+33</a>
<a href="#">N18-16G.23-2</a>	<a href="#">456</a>	<a href="#">36602</a>	<a href="#">80.00</a>	<a href="#">1.94</a>	<a href="#">0.08</a>	<a href="#">0.0971</a>	<a href="#">0.0042</a>	<a href="#">0.1036</a>	<a href="#">0.0017</a>	<a href="#">1.387</a>	<a href="#">0.0640</a>	<a href="#">0.067</a>	<a href="#">0.0019</a>	<a href="#">1569</a>	<a href="#">81</a>	<a href="#">+59</a>

### 3.1.34.1.3 *Penzance granite*

The CL imaging of abundant zircons from all three samples collected from different locations in a single quarry of the Penzance granite displays textures typical of metamict zircons (Figure 6). These include cavities, fractures, disruption of the original zoning and development of dark CL areas (Corfu, 2003; Kılıç, 2016).

Even when targeting zircon grains seemingly less affected by metamictisation, twenty-seven analysis were aborted throughout ~~the~~ a single analytical session due to the unacceptably high  $^{204}\text{Pb}$  content. Of the twenty-four analysis which were not aborted, only nine were <5% discordant and had less than 1% common Pb (Figure 6, [Table 2 Supplementary Material 2](#)). The U and Th contents of completed analyses (average of ~580 and ~400 ppm, respectively) were commensurate with the observed metamictisation. The nine near concordant analysis have scattered ages typical of metamict zircons, and only one of the ages is within error of the previously reported age (Geoscience Australia ~~(GA)~~, 2019). We conclude that no reliable age could be calculated from these zircon data. The average and range of Th/U from the completed SHRIMP analyses was 0.72 and 0.52-1.46, respectively.

### 3.24.2 **U-Pb SHRIMP monazite dating of the Penzance granite**

A significant number of the monazite grains were separated from the three Penzance granite samples. They have euhedral zoning textures on BSE images (Figure 7), which indicates magmatic crystallization. Recent studies (e.g.: Piechocka et al., 2017) have demonstrated the increased reliability of magmatic monazite as a geochronometer for igneous rocks with unreliable zircon age data, when subsequent metamorphic conditions remained under the Pb closure temperature of monazite. Monazite contains high U and Th and incorporates minor common Pb and, unlike zircon, is largely immune to metamictisation and radiogenic Pb loss at low temperatures (Piechocka et al., 2017).

1109  
1110  
1111 389 A total of 38 of 56 analysis from 18 grains with low common Pb ( $f_{206} < 0.5\%$ ) and low  
1112  
1113 390 discordance ( $\leq 5\%$ ) (Table 13) yield a mean  $^{207}\text{Pb}/^{206}\text{Pb}$  age of  $2681.9 \pm 4.5$  Ma (95% c1;  
1114  
1115 391 MSWD = 1.4; Figure 3). The slightly high MSWD indicates the possibility of scatter from a  
1116  
1117  
1118 392 single-age population. However, in the absence of any skewness in the age probability plot (not  
1119  
1120 393 shown), anomalous Th-U chemistry or other evidence for either inheritance or Pb-loss, and  
1121  
1122 394 given the amount of data collected ( $n=56$ ) and used ( $n=38$ ), this is considered to be the age of  
1123  
1124 395 these igneous monazites.

### 1126 396 **3.3.4.3 HF-isotopes in zircon**

#### 1129 397 *3.3.4.3.1 Teutonic Bore volcanics*

1130  
1131 398 Twenty-five zircon grains from sample 15BUDD78 – 111.60 m of the footwall rhyolite  
1132  
1133 399 (unit I) were analysed for Lu–Hf by LA-SS-ICP-MS (Table 4 Supplementary Material 3, mount  
1134  
1135 400 N18-15D, sample B78,). The calculated  $\epsilon\text{Hf}_{(t)}$ , based on the interpreted SHRIMP  $^{207}\text{Pb}/^{206}\text{Pb}$   
1136  
1137 401 age (2692.9Ma), plot in a homogeneous population with values ranging between +2.3 and +5.6  
1138  
1139 402 (Figure 8), and a mean of  $3.7 \pm 0.5$  (MSWD = 0.47,  $n = 25$ ). The low MSWD value partly  
1140  
1141 403 reflects the relatively large  $\epsilon\text{Hf}_{(t)}$  errors on individual analyses.

1142  
1143  
1144 404 Twenty-nine Lu–Hf analysis (Table 4 Supplementary Material 3, mount N18-15C, sample  
1145  
1146 405 B137) were conducted on zircons from sample 15BUDD137 – 398.60 m of the same footwall  
1147  
1148 406 rhyolite (unit I), and, once again, the  $\epsilon\text{Hf}_{(t)}$  is calculated based on the interpreted SHRIMP  
1149  
1150 407  $^{207}\text{Pb}/^{206}\text{Pb}$  age for emplacement.  $\epsilon\text{Hf}_{(t)}$  values range between -0.6 and +5.2 with a mean of 2.9  
1151  
1152 408  $\pm 0.5$  (MSWD = 0.90,  $n = 29$ , Figure 8). Combining the  $\epsilon\text{Hf}_{(t)}$  data for the both footwall rhyolite  
1153  
1154 409 samples (unit I) yields a value of  $3.27 \pm 0.33$  (MSWD = 0.79,  $n = 54$ ).

1155  
1156  
1157 410 Sixteen Lu–Hf analysis (Table 4 Supplementary Material 3, B37) were conducted on zircon  
1158  
1159 411 from both samples of transitional andesite (unit III) and the mean age of the combined SHRIMP  
1160  
1161 412 analyses of 2693.4 Ma was used to calculate  $\epsilon\text{Hf}_{(t)}$  which showed considerable scatter and  
1162  
1163 413 ranged between -11.7 and +8.6 with significant errors on individual analyses (Table

1168  
1169  
1170  
1171  
1172  
1173  
1174  
1175  
1176  
1177  
1178  
1179  
1180  
1181  
1182  
1183  
1184  
1185  
1186  
1187  
1188  
1189  
1190  
1191  
1192  
1193  
1194  
1195  
1196  
1197  
1198  
1199  
1200  
1201  
1202  
1203  
1204  
1205  
1206  
1207  
1208  
1209  
1210  
1211  
1212  
1213  
1214  
1215  
1216  
1217  
1218  
1219  
1220  
1221  
1222  
1223  
1224  
1225  
1226

[4Supplementary Material 3](#)). The lower precision is a result of the smaller spot-size necessary for the small zircons from these samples. The mean  $\epsilon\text{Hf}_{(t)}$  for the transitional andesite (unit III) is  $2.6 \pm 1.8$  (MSWD = 1.05,  $n = 16$ , Figure 8).

### ~~3.3.2.4.3.2~~ *Penzance granite*

Recent studies show that the Lu–Hf system remains relatively undisturbed within metamorphic zircon that do not undergo significant later alteration (Lenting et al., 2010). Thirty-four Lu–Hf analyses on zircon from the Penzance granite ([Table 4Supplementary Material 3](#), N18-06) show a range of  $\epsilon\text{Hf}_{(t)}$  between -1.5 to +4.7 with mean value of  $2.17 \pm 0.45$  (MSWD = 1.15,  $n = 34$ ). The  $\epsilon\text{Hf}_{(t)}$  values were calculated based on the SHRIMP monazite ages presented herein.

#### **3.4.4.4 Trace elements in zircon**

Selected trace elements were measured via LA-SS-ICP-MS ([Table 5Supplementary Material 4](#)). Figure 9 illustrates patterns for selected REEs normalized to chondrite (Anders and Grevesse, 1989) for the two samples from the footwall rhyolite (unit I), the combined samples of andesite (unit III) and the Penzance granite. ~~Despite being represented separately on Figure 9, both samples of footwall rhyolite (unit I) display consistent REE chemistry.~~

The zircons from the footwall rhyolite (unit I) and the andesite (unit III) have similar MREE and HREE content, ~~as showed on~~ (Figure 9). The mean Yb/Dy ratio is  $4.15 \pm 0.85$  and  $4.45 \pm 0.68$  ( $1\sigma$ ) for the rhyolite and andesite, respectively. The Ce anomaly is estimated by the Ce/Nd<sub>(CN)</sub> ratio (Loucks et al., 2018) to be positive in both rock types ([Tables 4Supplementary Material 4](#)), with mean Ce/Nd<sub>(CN)</sub> of  $1.04 \pm 0.58$  and  $1.30 \pm 0.75$  ( $1\sigma$ ) for the rhyolite and andesite, respectively. The zircons from the Penzance granite show a mean Ce/Nd<sub>(CN)</sub> of  $0.92 \pm 0.23$  ( $1\delta$ ), indicating a positive Ce anomaly, and Yb/Dy ratio of  $2.5 \pm 0.67$  ( $1\sigma$ ).

**Commented [61]:** If you believe that this graphical representation might be misleading provide an alternative version. To me it seems clear as it is, and I find this sentence not necessary.

**Commented [62R62]:** The unnecessary sentence was erased.

1227  
1228  
1229  
1230  
1231  
1232  
1233  
1234  
1235  
1236 438 ~~Table 5: Selected trace element contents (ppm) of zircons from the Penzance granite and~~  
1237 439 ~~the volcanic sequence at the Bentley deposit.~~

**Commented [63]:** As for Table 2 and 4, also Table 5 should be included in the ESMs. Raw data should have no place in the manuscript. If you think to be necessary provide a small summary-table of the analyses, but your figures already represent well your data.

**Commented [64R64]:** Ok

## 1240 440 **45 DISCUSSION**

### 1242 441 **4.15.1 Age constrains on the Penzance granite**

1244 442 Hollis et al. (2015) proposed a link between VHMS mineralisation at the [Teutonic Bore](#)  
1245 443 Camp and the emplacement of the HFSE-enriched Penzance granite, based on geochemical  
1246 444 similarities, the proximity and broad synchronicity between the intrusive magmatic activity  
1248 445 and the volcanism of the host sequence. These observations were underpinned by a U-Pb zircon  
1250 446 age for the volcanism ( $2692 \pm 4$  Ma; Nelson, 1995) and the age reported by Champion and  
1251 447 Cassidy (2002) of  $2679 \pm 8$  Ma, for the Kent Complex of the Penzance Supersuite. This latter  
1253 448 age was obtained by SHRIMP U-Pb zircon dating of sample ID 96969076 of Geoscience  
1254 449 Australia's database, after L.Black, AGSO (unpublished) in Champion and Cassidy (2002).

1256 450 Champion and Cassidy (2002) reported the age but not the data table. However, the  
1258 451 geochronological data, as well as location and description for sample ID 96969076, are  
1259 452 available from Geoscience Australia's Geochron Delivery database (Geoscience Australia  
1261 453 (GA), 2019). The reported age for this sample is  $2686 \pm 9$  Ma with MSWD = 1.6 and  
1262 454 probability = 0.044 (Geoscience Australia (GA), 2019), which is within error of the age  
1263 455 reported by Champion and Cassidy (2002), but not identical.

1266 456 We have reprocessed the data available from Geochron Delivery for sample 96969076 and  
1267 457 obtained an identical age of  $2686 \pm 9$  Ma, MSWD = 1.6 from 21 analysis. However, given the  
1269 458 scatter inferred by the high MSWD, we have filtered the data by only considering analysis with  
1270 459 common Pb <0.3%, deriving a more statistically robust age of  $2682 \pm 9$  Ma (n=12; MSWD =  
1272 460 1.3). More importantly, only four zircons were recovered from sample 96969076 and the 21  
1273 461 analyses and calculated age is based on analyses from only three grains, of which: one was is



1286  
1287  
1288  
1289  
1290  
1291  
1292  
1293  
1294  
1295  
1296  
1297  
1298  
1299  
1300  
1301  
1302  
1303  
1304  
1305  
1306  
1307  
1308  
1309  
1310  
1311  
1312  
1313  
1314  
1315  
1316  
1317  
1318  
1319  
1320  
1321  
1322  
1323  
1324  
1325  
1326  
1327  
1328  
1329  
1330  
1331  
1332  
1333  
1334  
1335  
1336  
1337  
1338  
1339  
1340  
1341  
1342  
1343  
1344

462 a xenocryst. Each of ~~the~~our three samples ~~we~~ collected from the same quarry had hundreds of  
463 zircon grains, and after hand-picking the clearest (least metamict) zircons and analysing the  
464 best areas based on CL-SE imaging, we only detected one analysis in the relevant time interval,  
465 and it was 7% discordant. In view of this discrepancy, we searched for other datable minerals  
466 in the Penzance granite and identified igneous monazite. The monazite age of  $2681.9 \pm 4.5$  Ma  
467 discussed above is considered to be a statistically valid age of magma crystallization for the  
468 Penzance granite, and supersedes the previous zircon age(s).

#### 469 **4.25.2 Geochronological associations**

470 The relative timing of ore formation in the ~~FB~~Teutonic Bore ~~C~~eamp is well constrained  
471 within the stratigraphic sequence at Jaguar, where substantial evidence of seafloor precipitation  
472 indicate coeval mineralisation to the development of the upper sedimentary package (unit IV).  
473 Such evidence is absent from Bentley and the ~~FB~~Teutonic Bore deposit, which indicates that  
474 they were formed at greater depths, probably by replacement of a slightly older stratigraphy  
475 (see Figure 2A).

476 The syn-ore nature of the upper sedimentary package (unit IV) at Jaguar, the deposit hosted  
477 within the youngest stratigraphic level in the ~~FB~~Teutonic Bore ~~C~~eamp, indicates that the  
478 hangingwall sequence at Jaguar post-dates ore formation and could provide a potential  
479 minimum mineralisation age. Attempts to date this sequence have proven unsuccessful to date  
480 (Das, 2018). The footwall in all three deposits, as well as the hangingwall immediately above  
481 the orebodies of the Bentley and the ~~FB~~Teutonic Bore deposits, pre-date the mineralisation and  
482 represent a maximum age of ore formation.

483 The ages obtained in this study for the footwall rhyolite (unit I -  $2691.7 \pm 2.5$  Ma and  $2696.5$   
484  $\pm 4.3$  Ma) and the transitional andesite (unit III -  $2693.4 \pm 4.1$  Ma) suggest that mineralisation  
485 at the ~~FB~~Teutonic Bore ~~C~~eamp is younger than c.a. ~~2694~~ Ma, ~~as indicated in~~ (Figure 10). The  
486 unpublished TIMS age for the footwall rhyolite sequence (unit I) of  $2692.6 \pm 1.5$  Ma (Das,

1345  
1346  
1347 487 2018) is indistinguishable from the SHRIMP age presented here for the pre-ore volcanic  
1348  
1349  
1350 488 sequence at the [FBTeutonic Bore Ceamp](#). Similarly, the previous SHRIMP age for the  
1351  
1352 489 [FBTeutonic Bore Ceamp](#) sequence ( $2692 \pm 4$  Ma; (Nelson, 1995) is similar to the age  
1353  
1354 490 determined in this study (Figure 10). Therefore, although poorly constrained in the stratigraphy,  
1355  
1356 491 it is likely that the porphyritic dacite dated by Nelson (1995) is part of the pre-ore stratigraphy  
1357  
1358 492 (units I, II, or III).

1359  
1360 493 The ages for the footwall rhyolite (unit I) of  $2696.5 \pm 4.3$  Ma and  $2691.7 \pm 2.5$  Ma are  
1361  
1362 494 within error of each other, when considering a 95% confidence interval. However, considering  
1363  
1364 495 the normal distribution tendency ([Figure 10](#)) of single-population ages obtained from multiple  
1365  
1366 496 grains ([Figure 10](#); Schoene et al., 2013), it is probable that these could also represent a long  
1367  
1368 497 duration of volcanic activity during the development of this stratigraphic facies.

1370  
1371 498 The ages for the footwall rhyolite (unit I) and the Penzance granite ( $2681.9 \pm 4.5$  Ma) do  
1372  
1373 499 not overlap (Figure 10) at the 95% confidence interval and are not, therefore, coeval.  
1374  
1375 500 Furthermore, the porphyritic dacite from Nelson (1995) and the transitional andesite (unit III)  
1376  
1377 501 do not overlap the age of the Penzance (Figure 10) at a 95% confidence interval. We infer that  
1378  
1379 502 these rocks pre-date the mineralisation and the syn-ore stratigraphy.

### 1381 503 **[4.35.3](#) Geochemical correlations**

#### 1382 504 **[4.3.15.3.1](#) Whole-rock geochemistry**

1383  
1384 505 Hollis et al. (2015) described similarities in whole-rock REE distribution between the  
1385  
1386 506 Penzance granite (Kent Complex) and the felsic volcanics that host the mineralisation at Jaguar  
1387  
1388 507 (footwall rhyolite – unit I). Based on these observations and the HFSE enrichment of both rock  
1389  
1390 508 types they suggested a possible genetic link between these rocks, proposing that the footwall  
1391  
1392 509 volcanic sequence at Jaguar would be the extrusive equivalent to the Penzance granite.  
1393  
1394

1395  
1396 510 The geochronological results presented here indicate that the crystallization of the Penzance  
1397  
1398 511 granite is not coeval to the formation of the footwall rhyolite (unit I) or the transitional andesite  
1399  
1400  
1401  
1402  
1403

1404  
1405  
1406 512 (unit III) at Bentley. However, these processes occur within a ~12 M.y. interval. Given the  
1407  
1408 513 chemical similarities between these rock types and their proximity in age it is conceivable that  
1409  
1410 514 they are both the product of a single magmatic system or had a common source.  
1411

1412  
1413 515 Additionally, based on whole-rock geochemistry observations, other stratigraphic facies  
1414  
1415 516 within the younger, syn-ore, portion of the volcanic sequence at the [TB Teutonic Bore](#) [eCamp](#)  
1416  
1417 517 are alternative candidates to be the extrusive correspondent to the Penzance granite.  
1418

1419 518 The dacite that can be observed at the sedimentary-volcanic package of the upper  
1420  
1421 519 sedimentary horizon (unit IV) in the Jaguar deposit (MPD from Belford et al., 2015) has Y/Zr  
1422  
1423 520 ratios that indicates a tholeiitic affinity (Belford et al., 2015), which is also the case for the  
1424  
1425 521 Penzance granite (ID 96969076, sampled from the same locality of the geochronological study;  
1426  
1427 522 Sedgmen et al., 2007) (Figure 11). Furthermore, the MPD dacite yields a La/Yb<sub>CN</sub> ratio of 3.4  
1428  
1429 523 – 5.5 (Belford, 2010), which indicates a significant LREE/HREE enrichment, equal to what is  
1430  
1431 524 indicated by whole-rock REE content for the Penzance granite (Hollis et al., 2015).  
1432  
1433

#### 1434 525 4.3.25.3.2 *Zircon geochemistry* 1435

1436 526 The Hf-isotopes corroborate Hollis et al. (2015)'s hypothesis of a genetic link between the  
1437  
1438 527 [TB Teutonic Bore](#) Camp volcanic sequence and the Penzance granite. All zircons (Penzance,  
1439  
1440 528 units I and III) have very similar  $\epsilon_{\text{Hf}(i)}$ , with most values between -1 and +6 (Figure 8). The  
1441  
1442 529  $\epsilon_{\text{Hf}(i)}$  values show little contribution from evolved sources ~~as shown in~~ (Figure 8). Indeed, Nd  
1443  
1444 530 and Pb isotopes indicate that the [TB Teutonic Bore](#) [eCamp](#) is located within a more juvenile  
1445  
1446 531 zone of the Yilgarn craton, the Teutonic zone (Huston et al., 2014). The  $\epsilon_{\text{Hf}(i)}$  for the zircons  
1447  
1448 532 from the Penzance granite and the volcanic rocks from the [TB Teutonic Bore](#) [eCamp](#) plot above  
1449  
1450 533 the CHUR line (Figure 8), indicating a juvenile depleted mantle source component. These  
1451  
1452 534  $\epsilon_{\text{Hf}(i)}$  are slightly higher than the  $\epsilon_{\text{Hf}(i)}$  of zircons from other granites and volcanics within  
1453  
1454 535 the Kurnalpi Terrain (Isaac, 2015; Wyche et al., 2012).  
1455  
1456  
1457  
1458  
1459  
1460  
1461  
1462

1463  
1464  
1465 536 [According to Kirkland et al. \(2015\), parental magma composition is one of four factors that](#)  
1466  
1467 537 [may contribute to variations in the Th/U of a zircon crystal.](#) Therefore, the similar Th/U ratios  
1468  
1469 538 ([Table 2 Supplementary Material 2](#)) of the Penzance (~0.7) and Bentley zircons (Unit I: ~0.6)  
1470  
1471  
1472 539 also suggest they could have a shared magma source. Furthermore, all zircons have similar  
1473  
1474 540 Ce/Nd<sub>(CN)</sub> ratios ([Table 5 Supplementary Material 4](#)), which indicates comparable redox  
1475  
1476 541 conditions, as this ratio is a proxy for the Ce anomaly (Loucks et al., 2018).  
1477

1478 542 The zircons from the Penzance granite have higher overall REE content and MREE/HREE  
1479  
1480 543 enrichment (indicated by the Yb/Dy ratio), when compared to the Bentley units I and III zircons  
1481  
1482 544 ([Table 5 Supplementary Material 4](#)). These chemical differences indicate that the Penzance  
1483  
1484 545 granite is more fractionated but do not resolve whether this is the result of igneous  
1485  
1486 546 differentiation from a common magma or magma production from a common source. The ~12  
1487  
1488  
1489 547 M.y. interval between the units I and III volcanics, and the Penzance granite suggests the latter.  
1490

#### 1491 548 **4.45.4 The Contribution to the 4D evolutionary model of the Teutonic Bore** 1492 1493 549 **Camp ore**

1494  
1495  
1496 550 [The 4D evolutionary model of the Teutonic Bore Camp is achieved by the addition of the](#)  
1497  
1498 551 [time dimension to the current understanding of the geological evolution of the deposits,](#)  
1499  
1500 552 [including stratigraphy and geochemistry \(Figure 2; Belford, 2010; Belford et al., 2015; Chen](#)  
1501  
1502 553 [et al., 2015; Das, 2018; Hallberg and Thompson, 1985; Macklin, 2010; Parker et al., 2017\).](#)  
1503  
1504 554 [The geochronology data presented in this study constrain in time several processes within the](#)  
1505  
1506 555 [Teutonic Bore Camp, including the intrusion of the Penzance granite, which could be linked to](#)  
1507  
1508 556 [the development of the mineral system.](#)  
1509

1510 557 Similarities in zircon chemistry (i.e.:  $\square \text{Hf}_{(i)}$  and Th/U ratio; see section 5.3: Geochemical  
1511  
1512 558 correlations) complemented by the geochemical correspondences between the Penzance  
1513  
1514  
1515 559 granite and the Teutonic Bore volcanics (i.e.: HFSE-enrichment and REE pattern, see  
1516  
1517  
1518  
1519  
1520  
1521

1522  
1523  
1524  
1525  
1526  
1527  
1528  
1529  
1530  
1531  
1532  
1533  
1534  
1535  
1536  
1537  
1538  
1539  
1540  
1541  
1542  
1543  
1544  
1545  
1546  
1547  
1548  
1549  
1550  
1551  
1552  
1553  
1554  
1555  
1556  
1557  
1558  
1559  
1560  
1561  
1562  
1563  
1564  
1565  
1566  
1567  
1568  
1569  
1570  
1571  
1572  
1573  
1574  
1575  
1576  
1577  
1578  
1579  
1580

section 5.3: Geochemical correlations), suggest a genetic association between the intrusive granite and the extrusive rocks that constitute the ~~FB~~Teutonic Bore Camp host sequence.

~~Additionally, there is evidence of interaction between the Penzance and the volcanic rocks that are intruded by it, such as the i~~rrregular contact between the Penzance granite and the volcanic sequence, as well as, the recognition of intrusive veins of granitoid within the volcanics, and xenoliths of volcanic rocks within the ~~intrusive~~ granite (Hallberg and Thompson, 1985) ~~indicate that the Penzance intrudes the volcanic Teutonic Bore sequence and that their proximity is not the result of subsequent tectonic processes.~~ Considering the close geographic position of the granite and the ore-bearing volcanic sequence (Figure\_1), their shared geochemical features and broad synchronicity, it is ~~probable-possible~~ that the Penzance granite was involved in the process that generated the VHMS mineralisation at the ~~FB~~Teutonic Bore ~~C~~camp.

~~The role of granites in the development of VHMS systems has been the focus of numerous studies (1-). Magmatic-hydrothermal contribution of metals is not necessary in the development~~ of VHMS deposits (Huston et al., 2011) and syn-ore intrusions do not always directly supply metal to the system, but rather act as a heating source, driving hydrothermal circulation that leaches metals from the country host rock (Lode et al., 2017). However, in a number of cases there is evidence of a significant contribution of metals and/or volatiles from the magmatic source, in addition to the supply of heat (~~e.g.:~~ Chen et al., 2015; Lode et al., 2017; ~~e.g.:~~ Yang and Scott, 1996).

Chen et al. (2015) used S-isotopes as a proxy for the hydrothermal fluid composition in the ~~FB~~Teutonic Bore Camp and interpreted that the supply of sulphur to the hydrothermal ore fluid was the result of a mixture between seawater and a hydrothermal fluid of magmatic origin. These authors did not find compelling evidence for leaching of sulphur from the host sequence into the ore fluid in the ~~FB~~Teutonic Bore Camp. Therefore, the Penzance granite is a strong

**Commented [65]:** References are required.  
**Commented [66R66]:** I simply erased the sentence. It was not necessary to the understanding of the paragraph and the studies that would be referenced are presented through the rest of the text.

1581  
1582  
1583  
1584  
1585  
1586  
1587  
1588  
1589  
1590 candidate to have acted as the probable magmatic source of sulphur to the mineralisation, and  
1591 [consequently possibly](#), metals.

#### 1593 **4.55.5 Exploration strategies**

1595 Our observations show that the HFSE-enriched Penzance granite probably played a  
1596 fundamental role in the supply of metals and heat that culminated in the development of the  
1597 replacement-type VHMS deposits of the [Teutonic Bore](#) [Camp](#). Therefore, future  
1598 exploration efforts within the camp should focus on fluid pathways from [the similar](#) granites.  
1599  
1600 The emphasis should be on mapping syn- or pre-intrusive structures that could facilitate fluid  
1601 flow from the granite to the host sequence. Fertile zones are likely to be discovered where these  
1602 fluid paths find the appropriate conditions for metal precipitation, which has been suggested  
1603 by previous studies to be sediment-rich horizons (Parker et al., 2017) and/or depositional breaks  
1604 (Belford et al., 2015).

1609 This paper supports conclusions proposed by Hollis et al. (2015), of a connection between  
1610 HFSE-enriched granites and VHMS ( $\pm$  base metals) deposits within the Yilgarn Craton.  
1611 Following the identification of fertile terrains, populated with HFSE-enriched granites,  
1612 *greenfield* exploration campaigns should employ a multi-disciplinary approach to test the  
1613 processes involved in the formation of an ore deposit. The development of 4D models ([i.e.](#)  
1614 [constrain in time of 3D geological processes](#)) allows for a better understanding of the timing  
1615 and nature of the magmatic and stratigraphical processes necessary for the development of such  
1616 ore deposits. [This is particular true in Archean replacement-type VHMS deposits, where the](#)  
1617 [syn-volcanic timing of the mineralisation is not always clear \(e.g. Barrote et al., 2019\)](#)

## 1624 **56 CONCLUSIONS**

- 1626 • Three mined VHMS orebodies in the Teutonic Bore [Camp](#) (Teutonic Bore deposit,  
1627 Jaguar and Bentley) formed at different stratigraphic levels.  
1628  
1629

**Commented [67]:** Whereas the suggestion that the Penzance granite could have acted as a sulfur source is coherent with the isotopic data discussed in Chen et al. (2015), the assumption that metals were sourced from the the granite magma needs to be supported from further evidence.

**Commented [68R68]:** We understand the reviewers concern and have re-phrased the text as to not point the reader towards unsupported affirmations.

- 1640  
1641  
1642  
1643 609 • Jaguar formed coeval with its host sequence, whereas the ore in Teutonic Bore and  
1644 Bentley replaces slightly older stratigraphy.  
1645 610  
1646  
1647 611 • The age of the host sequence at the stratigraphic level of the Bentley deposit is ca.  
1648 2693 Ma.  
1649 612  
1650  
1651 613 • The age of the ~~FB~~Teutonic Bore ~~e~~Camp mineralisation is likely-possibly coeval to  
1652 the intrusion of the Penzance granite at ca. 2682 Ma.  
1653 614  
1654  
1655 615 • Monazite has been shown to be a more reliable chronometer than high-U-Th zircons  
1656 in the HFSE-enriched Penzance granite.  
1657 616  
1658  
1659 617 • The Penzance granite possibly acted as the source of heat and potentially  
1660 fluid/metals to the ore formation at the ~~FB~~Teutonic Bore ~~C~~eamp.  
1661 618  
1662  
1663 619 • VHMS exploration in the Yilgarn Craton should focus in finding fluid pathways  
1664 between HFSE-enriched intrusives and potential host sequences to orebodies.  
1665  
1666 620  
1667  
1668

## 1669 621 **67 ACKNOWLEDGMENTS**

1672 622 The authors acknowledge: Dr Steve Bereford and Mr. Kyle Hodges from IGO for their  
1673 wisdom, access to samples, drill core and internal data; Thermo Fisher, GSWA and MRIWA  
1674 623 for financial support; and the John de Laeter Centre (JdLC) for the facilities, scientific and  
1675 technical assistance. We thank Dr. Haoyang Zhou, Dr. Nicolas Thebaud and an anonymous  
1676 624 reviewer whose comments helped improve and clarify this manuscript. JdLC facilities are  
1677 supported by a university-government consortium, ARC and AuScope via NCRIS. GeoHistory  
1678 625 Facility instruments in the John de Laeter Centre, Curtin University were funded via an  
1679 Australian Geophysical Observing System grant provided to AuScope Pty Ltd. by the AQ44  
1680 626 Australian Education Investment Fund program. The NPII multi-collector was obtained via  
1681 funding from the Australian Research Council LIEF program (LE150100013).  
1682  
1683 627  
1684  
1685 628  
1686  
1687 629  
1688  
1689 630  
1690  
1691 631  
1692  
1693  
1694  
1695  
1696  
1697  
1698

1699  
1700  
1701  
1702  
1703  
1704  
1705  
1706  
1707  
1708  
1709  
1710  
1711  
1712  
1713  
1714  
1715  
1716  
1717  
1718  
1719  
1720  
1721  
1722  
1723  
1724  
1725  
1726  
1727  
1728  
1729  
1730  
1731  
1732  
1733  
1734  
1735  
1736  
1737  
1738  
1739  
1740  
1741  
1742  
1743  
1744  
1745  
1746  
1747  
1748  
1749  
1750  
1751  
1752  
1753  
1754  
1755  
1756  
1757

632 **78 BIBLIOGRAPHY**

633 Anders, E., Grevesse, N., 1989. Abundances of the elements: Meteoritic and solar. *Geochim.*  
634 *Cosmochim. Acta* 53, 197–214. [https://doi.org/10.1016/0016-7037\(89\)90286-X](https://doi.org/10.1016/0016-7037(89)90286-X)

635 Barrett, T.J., MacLean, W.H., 1994. Chemostratigraphy and hydrothermal alteration in  
636 exploration for VHMS deposits in greenstones and younger volcanic rocks., in: Lentz,  
637 D.R. (Ed.), *Alteration and Alteration Processes Associated with Ore-Forming Systems*,  
638 *Short Course Notes / Geological Association of Canada*. Geological Assoc. of Canada,  
639 St. John's, Newfoundland, pp. 433–467.

640 [Barrote, V., Tessalina, S., McNaughton, N., Jourdan, F., Hollis, S.P., Ware, B., Zi, J.-W., 2020.](#)  
641 [4D history of the Nimbus VHMS ore deposit in the Yilgarn Craton, Western Australia.](#)  
642 [Precambrian Research 337, 105536. https://doi.org/10.1016/j.precamres.2019.105536](#)

643 Belford, S.M., 2010. Genetic and chemical characterisation of the host succession to the  
644 archean Jaguar VHMS deposit. (Doctoral dissertation). University of Tasmania, UTAS,  
645 Hobart, Tasmania, Australia.

646 Belford, S.M., Davidson, G.J., McPhie, J., Large, R.R., 2015. Architecture of the Neoproterozoic  
647 Jaguar VHMS deposit, Western Australia: Implications for prospectivity and the  
648 presence of depositional breaks. *Precambrian Res.* 260, 136–160.  
649 <https://doi.org/10.1016/j.precamres.2014.12.019>

650 [Black, L.P., Kamo, S.L., Allen, C.M., Aleinikoff, J.N., Davis, D.W., Korsch, R.J., Foudoulis,](#)  
651 [C., 2003. TEMORA 1: a new zircon standard for Phanerozoic U–Pb geochronology.](#)  
652 [Chem. Geol. 200, 155–170. https://doi.org/10.1016/S0009-2541\(03\)00165-7](#)

653 [Blichert-Toft, J., Albarède, F., 1997. The Lu–Hf isotope geochemistry of chondrites and the](#)  
654 [evolution of the mantle–crust system. Earth Planet. Sci. Lett. 148, 243–258.](#)  
655 [https://doi.org/10.1016/S0012-821X\(97\)00040-X](https://doi.org/10.1016/S0012-821X(97)00040-X)

656 Butt, C.R.M., Anand, R.R., Smith, R.E., 2017. Geology of the Australian regolith, in: Phillips,  
657 G.N. (Ed.), *Australian Ore Deposits*. The Australian Institute of Mining and  
658 Metallurgy, Melbourne, pp. 27–34.

659 Champion, D.C., Cassidy, K.F., 2002. Granites of the Northern Eastern Goldfields: their  
660 Distribution, Age, Geochemistry, Petrogenesis, Relationship with Mineralisation, and  
661 Implications for Tectonic Environment, AMIRA P482/MERIWAM281-Yilgarn  
662 Granitoids. AMIRA P482/MERIWAM281-Yilgarn Granitoids.

663 Chen, M., Campbell, I.H., Xue, Y., Tian, W., Ireland, T.R., Holden, P., Cas, R.A.F., Hayman,  
664 P.C., Das, R., 2015. Multiple Sulfur Isotope Analyses Support a Magmatic Model for  
665 the Volcanogenic Massive Sulfide Deposits of the Teutonic Bore Volcanic Complex,  
666 Yilgarn Craton, Western Australia. *Econ. Geol.* 110, 1411–1423.  
667 <https://doi.org/10.2113/econgeo.110.6.1411>

668 [Chu, N.-C., Taylor, R.N., Chavagnac, V., Nesbitt, R.W., Boella, R.M., Milton, J.A., German,](#)  
669 [C.R., Bayon, G., Burton, K., 2002. Hf isotope ratio analysis using multi-collector](#)  
670 [inductively coupled plasma mass spectrometry: an evaluation of isobaric interference](#)  
671 [corrections. J. Anal. At. Spectrom. 17, 1567–1574. https://doi.org/10.1039/b206707b](#)

672 [Claoué-Long, J.C., Compston, W., Roberts, J., Fanning, C.M., 1995. Two Carboniferous Ages:](#)  
673 [A Comparison of Shrimp Zircon Dating with Conventional Zircon Ages and <sup>40</sup>Ar/<sup>39</sup>Ar](#)  
674 [Analysis, in: Berggren, W.A., Kent, D.V., Aubry, M. P., Hardenbol, J. \(Eds.\),](#)  
675 [Geochronology, Time Scales, and Global Stratigraphic Correlation, Society for](#)  
676 [Sedimentary Geology Special Publications. SEPM \(Society for Sedimentary Geology\),](#)  
677 [pp. 3–21. https://doi.org/10.2110/pec.95.54](#)

678 [Compston, W., Williams, I.S., Meyer, C., 1984. U–Pb geochronology of zircons from lunar](#)  
679 [breccia 73217 using a sensitive high-mass-resolution ion microprobe. Proc. 14th Lunar](#)



1758  
1759  
1760  
1761  
1762  
1763  
1764  
1765  
1766  
1767  
1768  
1769  
1770  
1771  
1772  
1773  
1774  
1775  
1776  
1777  
1778  
1779  
1780  
1781  
1782  
1783  
1784  
1785  
1786  
1787  
1788  
1789  
1790  
1791  
1792  
1793  
1794  
1795  
1796  
1797  
1798  
1799  
1800  
1801  
1802  
1803  
1804  
1805  
1806  
1807  
1808  
1809  
1810  
1811  
1812  
1813  
1814  
1815  
1816

- 680 [Planet. Sci. Conf. J. Geophys. Res. Suppl 89, B525-B534.](#)  
681 <https://doi.org/10.1029/JB089iS02p0B525>
- 682 Corfu, F., 2003. Atlas of Zircon Textures. *Rev. Mineral. Geochem.* 53, 469–500.  
683 <https://doi.org/10.2113/0530469>
- 684 Czarnota, K., Champion, D.C., Goscombe, B., Blewett, R.S., Cassidy, K.F., Henson, P.A.,  
685 Groenewald, P.B., 2010. Geodynamics of the eastern Yilgarn Craton. *Precambrian Res.*  
686 183, 175–202. <https://doi.org/10.1016/j.precamres.2010.08.004>
- 687 Das, R., 2018. Understanding the Palaeovolcanological and Palaeoenvironmental setting of  
688 Archaean VMS Deposit: Stratigraphic Architecture and Volcanology of the Archaean  
689 VMS host rock succession of the Teutonic Bore, Jaguar and Bentley Mine corridor,  
690 Eastern Goldfields Province, Western Australia (Master thesis). Melbourne University,  
691 Melbourne.
- 692 ~~De Laeter, J.R., Kennedy, A.K., 1998. A double focusing mass spectrometer for~~  
693 ~~geochronology. *Int. J. Mass Spectrom.* 178, 43–50. [https://doi.org/10.1016/S1387-](https://doi.org/10.1016/S1387-3806(98)14092-7)~~  
694 ~~[3806\(98\)14092-7](https://doi.org/10.1016/S1387-3806(98)14092-7)~~
- 695 Doyle, M.G., Allen, R.L., 2003. Subsea-floor replacement in volcanic-hosted massive sulfide  
696 deposits. *Ore Geol. Rev.* 23, 183–222. [https://doi.org/10.1016/S0169-1368\(03\)00035-](https://doi.org/10.1016/S0169-1368(03)00035-0)  
697 0
- 698 Ellis, P., 2004. Geology and mineralisation of the Jaguar copper-zinc deposit, Western  
699 Australia, in: McConachy, T.F., McInnes, B.I.A. (Eds.), *Copper-Zinc Massive Sulphide*  
700 *Deposits in Western Australia*. CSIRO Exploration and Mining, Melbourne, pp. 39–46.
- 701 ~~Fletcher, I.R., McNaughton, N.J., Davis, W.J., Rasmussen, B., 2010. Matrix effects and~~  
702 ~~calibration limitations in ion probe U–Pb and Th–Pb dating of monazite. *Chem. Geol.*~~  
703 ~~270, 31–44. <https://doi.org/10.1016/j.chemgeo.2009.11.003>~~
- 704 Geoscience Australia (GA), 2019. Geochron Delivery Database. Accessed June 2019.  
705 <http://www.ga.gov.au/geochron-sapub-web/geochronology/shrimp/search.htm>.
- 706 GeoVIEW.WA, 2016. 1:500 000 State interpreted bedrock geology polygons, 2016.
- 707 Hallberg, J.A., Thompson, J.F.H., 1985. Geologic setting of the Teutonic Bore massive sulfide  
708 deposit, Archean Yilgarn Block, Western Australia. *Econ. Geol.* 80, 1953–1964.  
709 <https://doi.org/10.2113/gsecongeo.80.7.1953>
- 710 Hollis, S.P., Mole, D.R., Gillespie, P., Barnes, S.J., Tessalina, S., Cas, R.A.F., Hildrew, C.,  
711 Pumphrey, A., Goodz, M.D., Caruso, S., Yeats, C.J., Verbeeten, A., Belford, S.M.,  
712 Wyche, S., Martin, L.A.J., 2017. 2.7 Ga plume associated VHMS mineralization in the  
713 Eastern Goldfields Superterrane, Yilgarn Craton: Insights from the low temperature and  
714 shallow water, Ag-Zn-(Au) Nimbus deposit. *Precambrian Res.* 291, 119–142.  
715 <https://doi.org/10.1016/j.precamres.2017.01.002>
- 716 Hollis, S.P., Yeats, C.J., Wyche, S., Barnes, S.J., Ivanic, T.J., Belford, S.M., Davidson, G.J.,  
717 Roache, A.J., Wingate, M.T.D., 2015. A review of volcanic-hosted massive sulfide  
718 (VHMS) mineralization in the Archaean Yilgarn Craton, Western Australia: Tectonic,  
719 stratigraphic and geochemical associations. *Precambrian Res.* 260, 113–135.  
720 <https://doi.org/10.1016/j.precamres.2014.11.002>
- 721 Huston, D.L., Champion, D.C., Cassidy, K.F., 2014. Tectonic Controls on the Endowment of  
722 Neoproterozoic Cratons in Volcanic-Hosted Massive Sulfide Deposits: Evidence from  
723 Lead and Neodymium Isotopes. *Econ. Geol.* 109, 11–26.  
724 <https://doi.org/10.2113/econgeo.109.1.11>
- 725 Huston, D.L., Relvas, J.M.R.S., Gemmill, J.B., Drieberg, S., 2011. The role of granites in  
726 volcanic-hosted massive sulphide ore-forming systems: an assessment of magmatic–  
727 hydrothermal contributions. *Miner. Deposita* 46, 473–507.  
728 <https://doi.org/10.1007/s00126-010-0322-7>

1817  
1818  
1819  
1820  
1821  
1822  
1823  
1824  
1825  
1826  
1827  
1828  
1829  
1830  
1831  
1832  
1833  
1834  
1835  
1836  
1837  
1838  
1839  
1840  
1841  
1842  
1843  
1844  
1845  
1846  
1847  
1848  
1849  
1850  
1851  
1852  
1853  
1854  
1855  
1856  
1857  
1858  
1859  
1860  
1861  
1862  
1863  
1864  
1865  
1866  
1867  
1868  
1869  
1870  
1871  
1872  
1873  
1874  
1875

- 729 Independence Group NL (IGO), 2015. Annual Report 2015 (Unpublished Annual Report).  
730 Independence Group NL (IGO), Perth, W.A.
- 731 Isaac, C., 2015. Geochemistry of the north Eastern Goldfields, Western Australia: examining  
732 the processes that produce nickel sulphide camps (Masters Thesis). The University of  
733 Western Australia, Perth, W.A.
- 734 ~~Kennedy, A.K., De Laeter, J.R., 1994. The performance characteristics of the WA SHRIMP II  
735 ion microprobe., in: Abstracts Vol., U.S. Geological Survey Circular. Presented at the  
736 Eighth International Conference on Geochronology, Cosmochronology and Isotope  
737 Geology, Berkeley, USA, p. 166. Kirkland, C.L., Smithies, R.H., Taylor, R.J.M., Evans,  
738 N., McDonald, B., 2015. Zircon Th/U ratios in magmatic environs. Lithos 212–215,  
739 397–414. <https://doi.org/10.1016/j.lithos.2014.11.021>~~
- 740 Kılıç, A.D., 2016. Investigation of zircon by CL (Cathodoluminescence) and Raman  
741 Spectroscopy. IOP Conf. Ser. Earth Environ. Sci. 44, 042006.  
742 <https://doi.org/10.1088/1755-1315/44/4/042006>
- 743 Lenting, C., Geisler, T., Gerdes, A., Kooijman, E., Scherer, E.E., Zeh, A., 2010. The behavior  
744 of the Hf isotope system in radiation-damaged zircon during experimental  
745 hydrothermal alteration. Am. Mineral. 95, 1343–1348.  
746 <https://doi.org/10.2138/am.2010.3521>
- 747 ~~Li, X.-H., Long, W.-G., Li, Q.-L., Liu, Y., Zheng, Y.-F., Yang, Y.-H., Chamberlain, K.R.,  
748 Wan, D.-F., Guo, C.-H., Wang, X.-C., Tao, H., 2010. Penglai Zircon Mega-crystals: A  
749 Potential New Working Reference Material for Microbeam Determination of Hf-O  
750 Isotopes and U-Pb Age. Geostand. Geoanalytical Res. 34, 117–134.  
751 <https://doi.org/10.1111/j.1751-908X.2010.00036.x>~~
- 752 Lode, S., Piercey, S.J., Layne, G.D., Piercey, G., Cloutier, J., 2017. Multiple sulphur and lead  
753 sources recorded in hydrothermal exhalites associated with the Lemarchant  
754 volcanogenic massive sulphide deposit, central Newfoundland, Canada. Miner.  
755 Deposita 52, 105–128. <https://doi.org/10.1007/s00126-016-0652-1>
- 756 Loucks, R.R., Fiorentini, M.L., Rohrlach, B.D., 2018. Divergent T–fO<sub>2</sub> paths during  
757 crystallisation of H<sub>2</sub>O-rich and H<sub>2</sub>O-poor magmas as recorded by Ce and U in zircon,  
758 with implications for TitanQ and TitanZ geothermometry. Contrib. Mineral. Petrol.  
759 173. <https://doi.org/10.1007/s00410-018-1529-3>
- 760 ~~Ludwig, K.R., 2011. User's manual for Isoplot 4.15: a geochronological toolkit for Microsoft  
761 Excel, Berkeley Geochronology Center Special Publication.~~
- 762 ~~Ludwig, K.R., 2009. Squid 2.50, A User's Manual, Berkeley Geochronology Centre Special  
763 Publication.~~
- 764 Macklin, D., 2010. Alteration at the Teutonic Bore (VHMS) Deposit, Western Australia (B.Sc  
765 with honours thesis). University of Tasmania, UTAS.
- 766 McConachy, T.F., McInnes, B.I.A., Carr, G.R., 2004. Is Western Australia intrinsically  
767 impoverished in volcanogenic massive sulphide deposits, or under explored?, in:  
768 McConachy, T.F., McInnes, B.I.A. (Eds.), Copper-Zinc Massive Sulphide Deposits in  
769 Western Australia. CSIRO Exploration and Mining, Melbourne, pp. 15–32.
- 770 ~~Morel, M.L.A., Nebel, O., Nebel-Jacobsen, Y.J., Miller, J.S., Vroon, P.Z., 2008. Hafnium  
771 isotope characterization of the GJ-1 zircon reference material by solution and laser-  
772 ablation—MC-ICPMS. Chem. Geol. 255, 231–235.  
773 <https://doi.org/10.1016/j.chemgeo.2008.06.040>~~
- 774 ~~Nasdala, L., Hofmeister, W., Norberg, N., Martinson, J.M., Corfu, F., Dörr, W., Kamo, S.L.,  
775 Kennedy, A.K., Kronz, A., Reiners, P.W., Frei, D., Kosler, J., Wan, Y., Götze, J.,  
776 Häger, T., Kröner, A., Valley, J.W., 2008. Zircon M257—a Homogeneous Natural  
777 Reference Material for the Ion Microprobe U-Pb Analysis of Zircon. Geostand.  
778 Geoanalytical Res. 32, 247–265. <https://doi.org/10.1111/j.1751-908X.2008.00914.x>~~

1876  
1877  
1878  
1879  
1880  
1881  
1882  
1883  
1884  
1885  
1886  
1887  
1888  
1889  
1890  
1891  
1892  
1893  
1894  
1895  
1896  
1897  
1898  
1899  
1900  
1901  
1902  
1903  
1904  
1905  
1906  
1907  
1908  
1909  
1910  
1911  
1912  
1913  
1914  
1915  
1916  
1917  
1918  
1919  
1920  
1921  
1922  
1923  
1924  
1925  
1926  
1927  
1928  
1929  
1930  
1931  
1932  
1933  
1934

- 779 Nelson, D.R., 1995. Compilation of SHIRMP U-Pb zircon geochronology data, 1994, Record  
780 / Geological Survey of Western Australia. Geological Survey of Western Australia,  
781 Perth.
- 782 Parker, P., Belford, S.M., Maier, R., Lynn, S., Stewart, W., 2017. Teutonic Bore - Jaguar -  
783 Bentley volcanogenic massive sulfide field, in: Phillips, G.N. (Ed.), Australian Ore  
784 Deposits. The Australian Institute of Mining and Metallurgy, Melbourne, pp. 167–172.
- 785 ~~Patchett, P.J., Tatsumoto, M., 1980. Hafnium isotope variations in oceanic basalts. Geophys.~~  
786 ~~Res. Lett. 7, 1077–1080. <https://doi.org/10.1029/GL007i012p01077>~~
- 787 ~~Paton, C., Hellstrom, J., Paul, B., Woodhead, J., Hergt, J., 2011. Iolite: Freeware for the~~  
788 ~~visualisation and processing of mass spectrometric data. J. Anal. At. Spectrom. 26,~~  
789 ~~2508. <https://doi.org/10.1039/c1ja10172b>~~
- 790 Piechocka, A.M., Gregory, C.J., Zi, J.-W., Sheppard, S., Wingate, M.T.D., Rasmussen, B.,  
791 2017. Monazite trumps zircon: applying SHRIMP U–Pb geochronology to  
792 systematically evaluate emplacement ages of leucocratic, low-temperature granites in  
793 a complex Precambrian orogen. Contrib. Mineral. Petrol. 172.  
794 <https://doi.org/10.1007/s00410-017-1386-5>
- 795 ~~Scherer, E., 2001. Calibration of the Lutetium-Hafnium Clock. Science 293, 683–687.~~  
796 ~~<https://doi.org/10.1126/science.1061372>~~
- 797 Schoene, B., Condon, D.J., Morgan, L., McLean, N., 2013. Precision and Accuracy in  
798 Geochronology. Elements 9, 19–24. <https://doi.org/10.2113/gselements.9.1.19>
- 799 Sedgmen, A., Hazell, M.S., Budd, A.R., Champion, D.C., 2007. OZCHEM National Whole  
800 Rock Geochemistry Dataset.
- 801 ~~Sláma, J., Košler, J., Condon, D.J., Crowley, J.L., Gerdes, A., Hanchar, J.M., Horstwood,~~  
802 ~~M.S.A., Morris, G.A., Nasdala, L., Norberg, N., Schaltegger, U., Schoene, B., Tubrett,~~  
803 ~~M.N., Whitehouse, M.J., 2008. Plešovice zircon — A new natural reference material~~  
804 ~~for U–Pb and Hf isotopic microanalysis. Chem. Geol. 249, 1–35.~~  
805 ~~<https://doi.org/10.1016/j.chemgeo.2007.11.005>~~
- 806 ~~Stern, R.A., Bodorkos, S., Kamo, S.L., Hickman, A.H., Corfu, F., 2009. Measurement of SIMS~~  
807 ~~Instrumental Mass Fractionation of Pb Isotopes During Zircon Dating. Geostand.~~  
808 ~~Geoanalytical Res. 33, 145–168. <https://doi.org/10.1111/j.1751-908X.2009.00023.x>~~
- 809 ~~Thirlwall, M.F., Anczkiewicz, R., 2004. Multidynamic isotope ratio analysis using MC-ICP-~~  
810 ~~MS and the causes of secular drift in Hf, Nd and Pb isotope ratios. Int. J. Mass~~  
811 ~~Spectrom. 235, 59–81. <https://doi.org/10.1016/j.ijms.2004.04.002>~~
- 812 ~~Williams, I.S., 1998. Geochronology by Ion Microprobe, in: McKibben, M.A., Shanks, W.C.,~~  
813 ~~Ridley, W.I. (Eds.), Applications of Microanalytical Techniques to Understanding~~  
814 ~~Mineralizing Processes, Reviews in Economic Geology. pp. 1–35.~~
- 815 ~~Woodhead, J., Hergt, J., Shelley, M., Eggins, S., Kemp, R., 2004. Zircon Hf isotope analysis~~  
816 ~~with an excimer laser, depth profiling, ablation of complex geometries, and~~  
817 ~~concomitant age estimation. Chem. Geol. 209, 121–135.~~  
818 ~~<https://doi.org/10.1016/j.chemgeo.2004.04.026>~~
- 819 ~~Woodhead, J.D., Hergt, J.M., 2005. A Preliminary Appraisal of Seven Natural Zircon~~  
820 ~~Reference Materials for In Situ Hf Isotope Determination. Geostand. Geoanalytical~~  
821 ~~Res. 29, 183–195. <https://doi.org/10.1111/j.1751-908X.2005.tb00891.x>~~
- 822 Wyche, S., Kirkland, C.L., Riganti, A., Pawley, M.J., Belousova, E., Wingate, M.T.D., 2012.  
823 Isotopic constraints on stratigraphy in the central and eastern Yilgarn Craton, Western  
824 Australia. Aust. J. Earth Sci. 59, 657–670.  
825 <https://doi.org/10.1080/08120099.2012.697677>
- 826 Yang, K., Scott, S.D., 1996. Possible contribution of a metal-rich magmatic fluid to a sea-floor  
827 hydrothermal system. Nature 383, 420–423.  
828 <https://doi.org/10.1038/383420a0>  
<https://doi.org/10.1038/383420a0>

Table 2: SHRIMP isotopic data for zircons in samples 15BUDD78 (mount N18-15D), 15BUDD138 (mount N18-15C), 15BUDD120-226.04 (mount N19-07, 08), 15BUDD120-228.42 (mount N19-09, 10) and Penzance granite (mount N18-06).

15BUDD78 (mount N18-15D)														
Mount grain-spot	ppm U	ppm Th	$^{232}\text{Th}/^{238}\text{U}$	%com 206Pb	$^{207}\text{Pb}^*/^{206}\text{Pb}^*$	% 1 $\sigma$ err	$^{207}\text{Pb}^*/^{235}\text{U}$	% 1 $\sigma$ err	$^{206}\text{Pb}^*/^{238}\text{U}$	% 1 $\sigma$ err	err corr	$^{207}\text{Pb}/^{206}\text{Pb}$ Age (Ma)	1 $\sigma$ err	% Disc.
$\leq 3\%$ discordance														
N18-15D.11-1	126	72	0.59	0.01	0.1860	0.38	13.46	3.0	0.525	3.0	0.992	2707	6	-1
N18-15D.2-1	65	29	0.46	0.04	0.1858	0.54	13.58	3.4	0.530	3.4	0.987	2705	9	-2
N18-15D.9-1	75	33	0.45	-0.11	0.1856	1.04	13.44	3.3	0.525	3.1	0.948	2703	17	-1
N18-15D.8-1	71	33	0.48	-0.07	0.1854	0.55	13.56	3.3	0.531	3.2	0.986	2701	9	-2
N18-15D.7-1	214	129	0.62	0.05	0.1853	0.49	13.36	2.9	0.523	2.9	0.986	2700	8	-1
N18-15D.1-1	182	123	0.70	0.03	0.1850	0.32	13.42	3.2	0.526	3.2	0.995	2698	5	-1
N18-15D.14-1	185	129	0.72	0.03	0.1849	0.33	13.48	3.2	0.529	3.2	0.995	2697	5	-2
N18-15D.10-1	85	54	0.65	0.02	0.1845	0.46	13.30	3.0	0.523	3.0	0.988	2693	8	-1
N18-15D.13-1	148	101	0.70	0.04	0.1841	0.37	13.55	3.0	0.534	3.0	0.993	2690	6	-3
N18-15D.12-1	75	48	0.66	0.21	0.1840	0.57	13.48	2.9	0.531	2.9	0.981	2690	9	-3
N18-15D.3-1	73	38	0.53	0.11	0.1837	0.54	13.05	3.2	0.515	3.1	0.985	2686	9	+0
N18-15D.6-1	77	48	0.65	0.21	0.1827	0.62	13.22	3.5	0.525	3.4	0.984	2678	10	-2
$> 3\%$ discordance														
N18-15D.4-1	125	74	0.62	0.00	0.1857	0.42	14.52	3.3	0.567	3.2	0.992	2705	7	-9
N18-15D.5-1	175	124	0.73	0.07	0.1848	0.71	14.32	3.1	0.562	3.0	0.973	2696	12	-8
15BUDD138 (mount N18-15C)														

1976  
1977  
1978  
1979  
1980  
1981  
1982  
1983  
1984  
1985  
1986  
1987  
1988  
1989  
1990  
1991  
1992  
1993  
1994  
1995  
1996  
1997  
1998  
1999  
2000  
2001  
2002  
2003  
2004  
2005  
2006  
2007  
2008  
2009  
2010  
2011  
2012  
2013  
2014  
2015  
2016

Mount grain-spot	ppm U	ppm Th	<sup>232</sup> Th/ <sup>238</sup> U	%com 206Pb	<sup>207</sup> Pb*/ <sup>206</sup> Pb*	% 1σ err	<sup>207</sup> Pb*/ <sup>235</sup> U	% 1σ err	<sup>206</sup> Pb*/ <sup>238</sup> U	% 1σ err	err corr	<sup>207</sup> Pb/ <sup>206</sup> Pb Age (Ma)	1σ err	% Disc.
<5% discordance and <0.3% common Pb														
N18-15C.22-1	136	83	0.63	0.04	0.1857	0.37	13.15	3.0	0.513	2.9	0.992	2705	6	+2
N18-15C.26-1	174	128	0.76	0.04	0.1853	0.32	13.64	3.3	0.534	3.3	0.995	2701	5	-3
N18-15C.3-1	103	78	0.78	0.07	0.1851	0.44	13.27	3.5	0.520	3.5	0.992	2699	7	0
N18-15C.17-1	175	120	0.71	0.03	0.1849	0.34	13.44	3.2	0.527	3.2	0.994	2698	6	-1
N18-15C.6-1	250	173	0.71	0.02	0.1849	0.28	13.03	3.2	0.511	3.2	0.996	2697	5	+2
N18-15C.21-1	85	39	0.47	-0.03	0.1847	0.48	13.40	3.0	0.526	3.0	0.987	2696	8	-1
N18-15C.4-1	35	15	0.44	0.23	0.1846	0.85	12.77	3.5	0.502	3.4	0.969	2694	14	+3
N18-15C.7-1	189	113	0.61	0.08	0.1845	0.33	13.35	3.4	0.525	3.3	0.995	2694	5	-1
N18-15C.9-1	91	51	0.58	0.10	0.1845	0.49	13.92	3.3	0.547	3.3	0.989	2694	8	-5
N18-15C.10-1	89	48	0.55	0.02	0.1845	0.49	13.67	3.6	0.537	3.5	0.990	2694	8	-4
N18-15C.16-1	178	111	0.64	0.02	0.1843	0.35	12.64	3.6	0.498	3.6	0.995	2692	6	+4
N18-15C.14-1	181	123	0.70	0.03	0.1842	0.32	12.86	3.0	0.506	2.9	0.994	2691	5	+2
N18-15C.15-1	65	29	0.47	0.12	0.1841	0.57	13.08	3.3	0.515	3.2	0.99	2690	9	1
N18-15C.18-1	238	180	0.78	0.01	0.1840	0.28	13.16	3.1	0.519	3.0	0.996	2689	5	0
N18-15C.5-1	264	195	0.77	0.01	0.1840	0.27	13.10	3.1	0.516	3.0	0.996	2689	4	0
N18-15C.20-1	53	21	0.41	0.040	0.184	0.63	13.42	3	0.529	2.9	0.98	2689	10	-2
N18-15C.1-1	84	38	0.47	0.02	0.1839	0.46	13.08	2.9	0.516	2.8	0.987	2688	8	0
N18-15C.11-1	165	98	0.61	0.09	0.1839	0.36	13.30	3.4	0.525	3.4	0.994	2688	6	-1
N18-15C.8-1	169	98	0.60	0.05	0.1838	0.35	13.33	3.0	0.526	2.9	0.993	2688	6	-2
N18-15C.24-1	91	74	0.84	0.00	0.1838	0.42	13.17	3.0	0.520	3.0	0.990	2687	7	-1
N18-15C.12-1	102	59	0.60	0.04	0.1837	0.82	13.36	3.3	0.528	3.2	0.968	2686	14	-2
N18-15C.19-1	304	264	0.90	0.06	0.1836	0.27	12.95	3.2	0.511	3.2	0.997	2686	4	+1
N18-15C.23-1	60	24	0.42	0.09	0.1833	0.59	13.00	2.9	0.514	2.9	0.980	2683	10	0
N18-15C.25-1	94	66	0.73	0.12	0.1828	0.47	13.08	3.0	0.519	3.0	0.988	2678	8	-1
N18-15C.13-1	51	25	0.50	0.24	0.1822	0.68	12.82	3.0	0.510	2.9	0.973	2673	11	+1

2017  
2018  
2019  
2020  
2021  
2022  
2023  
2024  
2025  
2026  
2027  
2028  
2029  
2030  
2031  
2032  
2033  
2034  
2035  
2036  
2037  
2038  
2039  
2040  
2041  
2042  
2043  
2044  
2045  
2046  
2047  
2048  
2049  
2050  
2051  
2052  
2053  
2054  
2055  
2056  
2057

<b>&gt;5% discordance or &gt;0.3% common Pb</b>														
N18-15C.2-1	52	21	0.43	1.77	0.1869	2.85	13.19	4.2	0.512	3.1	0.739	2715	47	+2
N18-15C.27-1	192	171	0.92	0.12	0.1826	0.36	12.12	3.6	0.481	3.6	0.995	2676	6	+6
<b>15BUDD120-226.04 (mount N19-07, 08)</b>														
Mount grain-spot	ppm U	ppm Th	<sup>232</sup> Th/ <sup>238</sup> U	%com 206Pb	<sup>207</sup> Pb*/ <sup>206</sup> Pb*	% 1σ err	<sup>207</sup> Pb*/ <sup>235</sup> U	% 1σ err	<sup>206</sup> Pb*/ <sup>238</sup> U	% 1σ err	err eorr	<sup>207</sup> Pb/ <sup>206</sup> Pb Age (Ma)	1σ err	% Disc.
<b>&lt;5% discordance</b>														
N19-08.K.1-1	156	163	1.08	0.070	0.1859	0.51	13.25	2.8	0.517	2.7	0.98	2707	8	1
N19-07.G.1-1	107	85	0.82	0.09	0.1857	0.61	13.39	3.3	0.523	3.2	0.982	2704	10	0
N19-08.I.1-1	149	158	1.10	0.13	0.1853	0.57	12.86	2.7	0.504	2.7	0.978	2701	9	+3
N19-07.C.1-1	298	445	1.55	0.16	0.1844	0.36	12.80	2.4	0.504	2.4	0.989	2692	6	+3
N19-08.A.1-1	134	110	0.84	0.10	0.1843	0.58	12.66	4.0	0.498	3.9	0.989	2692	10	+4
N19-07.B.1-1	107	75	0.73	0.07	0.1841	0.65	13.05	2.5	0.514	2.4	0.965	2690	11	+1
N19-07.L.1-2	60	23	0.39	0.08	0.1840	0.79	12.87	3.3	0.507	3.2	0.971	2689	13	+2
N19-07.L.1-1	83	46	0.58	-0.04	0.1835	0.70	12.84	3.1	0.507	3.0	0.974	2685	12	+2
N19-07.H.1-1	115	85	0.76	0.09	0.1834	0.60	13.08	3.2	0.517	3.1	0.982	2684	10	0
N19-07.C.2-1	126	93	0.76	0.37	0.1828	0.65	12.91	2.6	0.512	2.5	0.968	2678	11	+1
N19-07.J.1-1#	153	156	1.05	0.19	0.1804	0.64	12.75	2.4	0.512	2.3	0.962	2657	11	0
N19-08.H.1-1#	177	205	1.20	0.11	0.1789	1.04	11.99	3.9	0.486	3.7	0.963	2643	17	+4
N19-07.C.2-2#	120	88	0.76	0.10	0.1779	1.29	11.87	2.7	0.484	2.3	0.875	2633	21	+4
<b>&gt;5% discordance</b>														
N19-03B.1-1	497	1322	2.75	0.39	0.2230	0.72	7.37	4.9	0.240	4.9	0.989	3003	12	+60
N19-07.J.2-2	130	131	1.04	0.11	0.1848	0.62	10.74	5.0	0.422	5.0	0.992	2697	10	+19
N19-07.C.2-3	196	171	0.9	0.200	0.1839	0.57	11.96	2.9	0.472	2.8	0.98	2688	9	9
N19-08.G.1-1	124	113	0.94	0.09	0.1833	0.57	13.76	1.4	0.544	1.3	0.918	2683	9	-5
N19-07.A.1-2	107	98	0.95	0.14	0.1832	0.95	12.03	2.9	0.476	2.7	0.944	2682	16	+8
N19-07.K.1-1	128	115	0.93	0.26	0.1832	0.62	12.14	2.6	0.481	2.6	0.972	2682	10	+7
N19-08.C.1-1	344	359	1.08	0.03	0.1826	0.57	12.21	3.5	0.485	3.4	0.987	2676	9	+6

2058  
2059  
2060  
2061  
2062  
2063  
2064  
2065  
2066  
2067  
2068  
2069  
2070  
2071  
2072  
2073  
2074  
2075  
2076  
2077  
2078  
2079  
2080  
2081  
2082  
2083  
2084  
2085  
2086  
2087  
2088  
2089  
2090  
2091  
2092  
2093  
2094  
2095  
2096  
2097  
2098

N19-08.J.1-1	113	77	0.70	0.23	0.1779	1.21	11.47	3.1	0.468	2.8	0.918	2633	20	+7
N19-07.A.1-1	430	422	1.01	0.18	0.1777	0.63	11.23	5.0	0.458	5.0	0.992	2632	10	+9
N19-08.E.1-1	186	148	0.82	0.17	0.1740	0.95	10.91	4.8	0.455	4.7	0.980	2597	16	+8
N19-07.J.2-1	136	134	1.01	0.41	0.1725	1.48	9.66	5.4	0.406	5.2	0.962	2582	25	+18

**15BUDD120 – 228.42 (mount N19-09, 10)**

Mount grain-spot	ppm U	ppm Th	<sup>232</sup> Th/ <sup>238</sup> U	%com 206Pb	<sup>207</sup> Pb*/ <sup>206</sup> Pb*	% 1σ err	<sup>207</sup> Pb*/ <sup>235</sup> U	% 1σ err	<sup>206</sup> Pb*/ <sup>238</sup> U	% 1σ err	err corr	<sup>207</sup> Pb/ <sup>206</sup> Pb Age (Ma)	1σ err	% Disc.
<b>&lt;5% discordant and common Pb &lt;0.1%</b>														
N19-09.C.1-1	107	76	0.73	0.00	0.1852	0.64	12.99	1.9	0.509	1.8	0.940	2700	11	+2
N19-09.G.2-1	178	184	1.06	0.01	0.1850	0.9	13.1	2.1	0.514	1.9	0.9	2698	15	1
N19-10.D.2-1	162	181	1.16	-0.03	0.1849	0.50	12.77	2.3	0.501	2.3	0.980	2697	8	+4
N19-10.I.1-3	252	210	0.86	-0.04	0.1849	0.50	12.76	1.3	0.501	1.2	0.920	2697	8	+4
N19-09.G.1-1	215	273	1.31	0.050	0.1846	0.47	12.96	2	0.509	1.9	0.97	2695	8	2
N19-10.I.1-1	226	181	0.83	0.05	0.1842	0.47	13.15	1.6	0.518	1.5	0.960	2691	8	0
N19-10.F.1-1	139	122	0.90	0.00	0.1842	0.60	12.92	1.8	0.509	1.7	0.940	2691	10	+2
N19-09.F.1-1	128	113	0.91	0.03	0.1840	0.62	13.35	2.8	0.526	2.8	0.980	2689	10	-2
N19-10.G.1-1	177	164	0.96	0.08	0.1836	0.56	12.93	1.7	0.511	1.6	0.940	2686	9	+1
<b>&gt;5% discordant or common Pb &gt;0.1%</b>														
N19-10.H.1-1	132	109	0.85	-0.03	0.1884	0.61	13.05	1.5	0.502	1.3	0.910	2728	10	+5
N19-10.D.1-1	49	33	0.70	-0.14	0.1875	1.06	12.36	2.3	0.478	2.0	0.890	2721	17	+9
N19-10.I.1-2	305	289	0.98	0.33	0.1868	1.39	12.66	2.8	0.491	2.4	0.870	2715	23	+6
N19-10.E.1-1	152	138	0.93	0.02	0.1854	0.59	12.55	2.7	0.491	2.6	0.980	2701	10	+6
N19-10.C.1-1	143	150	1.08	-0.02	0.1842	0.59	12.14	2.2	0.478	2.1	0.960	2691	10	+8
N19-09.H.1-1	146	133	0.94	0.09	0.1823	0.57	12.23	2.3	0.486	2.2	0.970	2674	9	+5
N19-10.A.1-1	108	86	0.82	0.61	0.1815	0.92	12.33	1.6	0.493	1.4	0.830	2666	15	+4
N19-10.B.1-1	115	86	0.77	0.07	0.1799	1.2	11.33	8.5	0.457	8.4	0.99	2652	20	10
N19-10.J.1-1	223	247	1.14	0.17	0.1789	0.46	12.01	2.5	0.487	2.4	0.980	2643	8	+4

**Penzance granite (mount N18-06)**

2099  
2100  
2101  
2102  
2103  
2104  
2105  
2106  
2107  
2108  
2109  
2110  
2111  
2112  
2113  
2114  
2115  
2116  
2117  
2118  
2119  
2120  
2121  
2122  
2123  
2124  
2125  
2126  
2127  
2128  
2129  
2130  
2131  
2132  
2133  
2134  
2135  
2136  
2137  
2138  
2139

Mount grain-spot	ppm U	ppm Th	<sup>232</sup> Th / <sup>238</sup> U	%com 206Pb	<sup>207</sup> Pb* / <sup>206</sup> Pb*	% 1σ err	<sup>207</sup> Pb* / <sup>235</sup> U	% 1σ err	<sup>206</sup> Pb* / <sup>238</sup> U	% 1σ err	err coeff	<sup>207</sup> Pb/ <sup>206</sup> Pb Age (Ma)	1σ err	% Disc.
N18-06B.16-1	476	378	0.82	0.43	0.1830	0.34	12.10	1.1	0.480	1.1	0.960	2676	6	+7
N18-06A.4-1	534	246	0.48	0.11	0.1790	0.25	13.20	1.1	0.536	1.1	0.970	2640	4	-6
N18-06C.9-1	462	381	0.85	0.75	0.1750	0.56	10.90	1.2	0.454	1.1	0.890	2602	9	+9
N18-06C.1-1	513	335	0.68	0.24	0.1750	0.29	12.20	1.1	0.509	1.1	0.970	2601	5	-2
N18-06A.7-1	475	250	0.54	0.46	0.1740	0.36	11.10	1.2	0.465	1.1	0.950	2593	6	+6
N18-06A.10-1	502	252	0.52	0.67	0.1730	0.37	11.30	1.1	0.475	1.1	0.950	2589	6	+4
N18-06C.12-1	542	451	0.86	0.28	0.1730	0.31	11.00	1.1	0.463	1.1	0.960	2583	5	+6
N18-06A.3-1	401	295	0.76	0.64	0.1700	0.61	11.00	1.3	0.469	1.1	0.870	2554	10	+3
N18-06B.8-1	641	350	0.56	0.31	0.1680	0.28	11.30	1.1	0.486	1.1	0.970	2541	5	-1
N18-06A.3-2	535	555	1.07	0.97	0.1610	0.43	9.50	1.3	0.429	1.2	0.940	2463	7	+8
N18-06C.5-1	594	344	0.60	0.20	0.1610	0.66	9.90	1.3	0.449	1.1	0.850	2463	11	+4
N18-06C.2-1	540	313	0.60	0.38	0.1550	0.85	8.80	1.6	0.414	1.3	0.840	2401	14	+8
N18-06B.2-1	556	356	0.66	0.38	0.1510	0.35	8.6	1.1	0.413	1.1	0.95	2352	6	6
N18-06A.19-1	601	363	0.62	0.95	0.1460	0.44	8.00	1.2	0.394	1.1	0.930	2304	8	+8
N18-06C.6-1	622	445	0.74	0.50	0.1410	0.41	7.50	1.2	0.383	1.1	0.930	2243	7	+8
N18-06A.8-1	568	354	0.64	1.910	0.141	0.58	8.1	1.2	0.416	1.1	0.88	2237	10	0
N18-06A.14-1	591	360	0.63	0.96	0.1410	0.48	7.70	1.2	0.395	1.1	0.910	2234	8	+5
N18-06B.12-1	605	339	0.58	0.54	0.1380	0.38	7.50	1.1	0.393	1.1	0.940	2198	7	+3
N18-06A.2-1	623	442	0.73	1.87	0.1370	1.43	6.70	1.8	0.357	1.0	0.580	2190	25	+12
N18-06B.11-1	601	850	1.46	0.94	0.1370	0.47	7.30	1.2	0.387	1.1	0.920	2185	8	+4
N18-06C.8-1	652	442	0.70	0.61	0.1330	0.42	6.80	1.1	0.369	1.1	0.930	2138	7	+6
N18-06B.9-1	676	514	0.79	0.86	0.1320	0.44	6.80	1.2	0.374	1.1	0.920	2127	8	+4
N18-06A.1-1	830	539	0.67	2.80	0.1200	1.62	5.70	1.9	0.347	1.0	0.530	1951	29	+2
N18-06B.13-1	801	567	0.73	0.74	0.1180	0.70	5.30	1.4	0.324	1.2	0.860	1934	12	+7

# young outlier: omitted from age calculation



2140  
2141  
2142  
2143  
2144  
2145  
2146  
2147  
2148  
2149  
2150  
2151  
2152  
2153  
2154  
2155  
2156  
2157  
2158  
2159  
2160  
2161  
2162  
2163  
2164  
2165  
2166  
2167  
2168  
2169  
2170  
2171  
2172  
2173  
2174  
2175  
2176  
2177  
2178  
2179  
2180

831  
832  
833

Table 3: SHRIMP isotopic data for monazite from the Penzance granite (mounts N18-06, 16)

Penzance granite (mount N18-06, 16)																
Mount grain-spot	ppm U	ppm Th	<sup>232</sup> Th/ <sup>238</sup> U	4f206 (%)	4f208 (%)	<sup>207</sup> Pb*/ <sup>206</sup> Pb±	±1σ err	<sup>206</sup> Pb*/ <sup>238</sup> U	±1σ err	<sup>207</sup> Pb*/ <sup>235</sup> U	±1σ err	<sup>208</sup> Pb*/ <sup>232</sup> Th	±1σ err	<sup>207</sup> Pb/ <sup>206</sup> Pb	±1σ err	% Disc.
≤5% discordance and <0.5% 4f206																
N18-06B-B-5	207	12986	63.00	-0.02	0.00	0.1865	0.0022	0.5074	0.0114	13.044	0.3320	0.137	0.0026	2711	19	+2
N18-16C-8-3	629	12531	20.00	-0.01	-0.01	0.1863	0.0010	0.5232	0.0101	13.435	0.2720	0.148	0.0032	2709	9	0
N18-16A-1-6	508	15332	30.00	-0.06	-0.02	0.1862	0.0014	0.5092	0.0069	13.075	0.2050	0.142	0.0030	2709	12	+2
N18-06B-G-2	215	14282	66.00	0.02	0.00	0.1855	0.0022	0.5170	0.0097	13.224	0.2950	0.141	0.0026	2703	19	+1
N18-06B-A-6	789	32172	41.00	0.00	0.00	0.1853	0.0015	0.5092	0.0090	13.010	0.2560	0.140	0.0029	2701	13	+2
N18-16A-1-1	448	11587	26.00	0.00	0.00	0.1852	0.0026	0.5288	0.0091	13.499	0.3020	0.152	0.0032	2700	23	-1
N18-06B-B-7	310	11884	38.00	-0.04	-0.01	0.1851	0.0018	0.5140	0.0088	13.119	0.2620	0.138	0.0028	2699	16	+1
N18-06B-G-5	345	16469	48.00	-0.06	-0.01	0.1847	0.0019	0.4933	0.0085	12.563	0.2540	0.136	0.0024	2696	17	+4
N18-06B-A-5	573	19934	35.00	0.43	0.11	0.1844	0.0017	0.5213	0.0094	13.257	0.2710	0.144	0.0028	2693	15	0
N18-06B-K-2	1134	74444	66.00	0.34	0.04	0.1842	0.0016	0.4894	0.0085	12.430	0.2430	0.136	0.0027	2691	14	+5
N18-16B-6-2	926	62647	68.00	0.05	0.01	0.1842	0.0010	0.4854	0.0078	12.327	0.2130	0.142	0.0030	2691	9	+5

2181  
 2182  
 2183  
 2184  
 2185  
 2186  
 2187  
 2188  
 2189  
 2190  
 2191  
 2192  
 2193  
 2194  
 2195  
 2196  
 2197  
 2198  
 2199  
 2200  
 2201  
 2202  
 2203  
 2204  
 2205  
 2206  
 2207  
 2208  
 2209  
 2210  
 2211  
 2212  
 2213  
 2214  
 2215  
 2216  
 2217  
 2218  
 2219  
 2220  
 2221

<del>N18-16D.15-1</del>	602	14098	23.00	0.02	0.01	0.1841	0.0009	0.5092	0.0083	12.929	0.2250	0.147	0.0030	2690	8	+1
<del>N18-16C.8-5</del>	664	14242	21.00	-0.05	-0.02	0.1841	0.0012	0.5198	0.0080	13.193	0.2240	0.141	0.0030	2690	11	0
<del>N18-16C.8-6</del>	466	11320	24.00	0.01	0.00	0.1840	0.0013	0.4927	0.0118	12.502	0.3140	0.144	0.0029	2689	12	+4
<del>N18-16D.16-1</del>	1039	19243	19.00	0.03	0.01	0.1839	0.0007	0.5021	0.0120	12.729	0.3110	0.147	0.0033	2688	6	+2
<del>N18-16G.18-1</del>	1002	69393	69.00	0.32	0.04	0.1838	0.0009	0.4905	0.0102	12.430	0.2690	0.149	0.0035	2687	8	+4
<del>N18-06B.A-7</del>	1097	38290	35.00	0.01	0.00	0.1835	0.0014	0.5314	0.0097	13.442	0.2700	0.146	0.0029	2685	13	-2
<del>N18-06B.G-7</del>	216	12340	57.00	0.07	0.01	0.1832	0.0020	0.5244	0.0095	13.249	0.2840	0.143	0.0028	2682	18	-1
<del>N18-16D.14-1</del>	129	6945	54.00	-0.03	-0.01	0.1832	0.0019	0.5022	0.0137	12.685	0.3700	0.152	0.0032	2682	17	+2
<del>N18-16A.1-4</del>	279	15220	54.00	-0.01	0.00	0.1831	0.0016	0.5303	0.0114	13.390	0.3120	0.152	0.0032	2681	14	-2
<del>N18-06B.B-6</del>	308	10496	34.00	0.03	0.01	0.1830	0.0018	0.4883	0.0107	12.323	0.2980	0.137	0.0028	2681	16	+4
<del>N18-06B.G-4</del>	178	11404	64.00	0.04	0.01	0.1828	0.0023	0.4965	0.0095	12.515	0.2870	0.139	0.0026	2679	20	+3
<del>N18-06B.K-3</del>	895	38759	43.00	0.02	0.00	0.1827	0.0015	0.4817	0.0083	12.135	0.2340	0.136	0.0026	2678	13	+5
<del>N18-16A.1-3</del>	515	14308	28.00	-0.01	0.00	0.1827	0.0010	0.5205	0.0105	13.111	0.2760	0.147	0.0032	2677	9	-1
<del>N18-16C.8-1</del>	638	13479	21.00	0.00	0.00	0.1824	0.0014	0.5182	0.0072	13.035	0.2110	0.147	0.0032	2675	13	-1
<del>N18-06B.A-1</del>	863	31292	36.00	-0.02	0.00	0.1824	0.0015	0.5070	0.0088	12.750	0.2490	0.149	0.0030	2675	14	+1
<del>N18-06B.B-3</del>	296	11665	39.00	-0.09	-0.02	0.1823	0.0020	0.5334	0.0095	13.405	0.2850	0.144	0.0029	2674	18	-3
<del>N18-06B.B-1</del>	188	10313	55.00	0.05	0.01	0.1821	0.0023	0.5124	0.0099	12.868	0.2980	0.144	0.0026	2672	21	0
<del>N18-06B.G-3</del>	475	24369	51.00	-0.03	-0.01	0.1821	0.0017	0.4923	0.0083	12.363	0.2420	0.136	0.0026	2672	15	+3
<del>N18-16A.6-1</del>	1052	69743	66.00	-0.01	0.00	0.1821	0.0007	0.5010	0.0077	12.581	0.2020	0.150	0.0033	2672	6	+2

2222  
 2223  
 2224  
 2225  
 2226  
 2227  
 2228  
 2229  
 2230  
 2231  
 2232  
 2233  
 2234  
 2235  
 2236  
 2237  
 2238  
 2239  
 2240  
 2241  
 2242  
 2243  
 2244  
 2245  
 2246  
 2247  
 2248  
 2249  
 2250  
 2251  
 2252  
 2253  
 2254  
 2255  
 2256  
 2257  
 2258  
 2259  
 2260  
 2261  
 2262

<del>N18-16C.8-2</del>	605	11778	19.00	0.00	0.00	0.1821	0.0010	0.5212	0.0089	13.084	0.2390	0.149	0.0030	2672	9	-1
<del>N18-16C.10-4</del>	587	20801	35.00	0.02	0.00	0.1820	0.0011	0.5089	0.0096	12.772	0.2570	0.146	0.0033	2671	10	+1
<del>N18-16C.10-1</del>	466	14728	32.00	0.10	0.03	0.1819	0.0011	0.5268	0.0110	13.210	0.2900	0.153	0.0039	2670	10	-2
<del>N18-06B.B-2</del>	202	9808	49.00	0.22	0.04	0.1812	0.0022	0.5116	0.0094	12.779	0.2860	0.141	0.0027	2664	20	0
<del>N18-16C.8-4</del>	636	13910	22.00	0.02	0.01	0.1810	0.0010	0.5352	0.0069	13.353	0.1920	0.144	0.0030	2662	9	-4
<del>N18-16D.13-1</del>	389	6592	17.00	0.09	0.04	0.1808	0.0011	0.5403	0.0104	13.471	0.2760	0.155	0.0034	2661	10	-5
<del>N18-06B.D-1</del>	362	26423	73.00	0.04	0.00	0.1808	0.0018	0.4927	0.0099	12.282	0.2780	0.139	0.0026	2660	16	+3
<del>N18-16C.10-3</del>	557	15536	28.00	0.07	0.02	0.1805	0.0012	0.5212	0.0087	12.968	0.2360	0.142	0.0030	2657	11	-2
≥5% discordance and/or ≥0.5% 4f206																
<del>N18-06A.N-3</del>	115	12090	105.00	1.31	0.09	0.1942	0.0046	0.3399	0.0074	9.100	0.2920	0.120	0.0024	2778	38	+32
<del>N18-06B.A-4</del>	484	26279	54.00	0.98	0.17	0.1903	0.0024	0.4979	0.0106	13.063	0.3280	0.134	0.0025	2745	21	+5
<del>N18-06B.E-1</del>	142	5608	40.00	2.70	0.69	0.1879	0.0044	0.5326	0.0107	13.801	0.4280	0.132	0.0024	2724	39	-1
<del>N18-06B.K-1</del>	440	31841	72.00	0.93	0.12	0.1852	0.0025	0.4438	0.0078	11.331	0.2530	0.120	0.0023	2700	22	+12
<del>N18-06B.G-1</del>	173	10873	63.00	0.06	0.01	0.1843	0.0025	0.4764	0.0124	12.104	0.3560	0.133	0.0027	2692	22	+7
<del>N18-06B.B-8</del>	245	13623	56.00	-0.03	-0.01	0.1831	0.0020	0.4666	0.0083	11.780	0.2490	0.123	0.0022	2681	18	+8
<del>N18-16A.1-2</del>	288	14906	52.00	0.08	0.01	0.1819	0.0015	0.5669	0.0127	14.220	0.3420	0.160	0.0036	2670	14	-8
<del>N18-06B.A-8</del>	349	26244	75.00	2.02	0.21	0.1818	0.0056	0.3843	0.0130	9.635	0.4430	0.122	0.0029	2670	51	+21
<del>N18-06B.B-4</del>	143	9993	70.00	0.14	0.02	0.1816	0.0027	0.4682	0.0095	11.725	0.2960	0.128	0.0025	2668	24	+7
<del>N18-06B.G-8</del>	220	14795	67.00	0.26	0.04	0.1814	0.0020	0.4741	0.0101	11.857	0.2890	0.128	0.0025	2666	18	+6

2263  
2264  
2265  
2266  
2267  
2268  
2269  
2270  
2271  
2272  
2273  
2274  
2275  
2276  
2277  
2278  
2279  
2280  
2281  
2282  
2283  
2284  
2285  
2286  
2287  
2288  
2289  
2290  
2291  
2292  
2293  
2294  
2295  
2296  
2297  
2298  
2299  
2300  
2301  
2302  
2303

<del>N18-16B-6-3</del>	843	59533	71.00	0.07	0.01	0.1812	0.0010	0.4463	0.0081	11.152	0.2140	0.140	0.0030	2664	9	+11
<del>N18-06A-N-1</del>	76	9566	125.00	1.76	0.15	0.1811	0.0049	0.4884	0.0112	12.191	0.4330	0.110	0.0023	2663	45	+4
<del>N18-06B-G-6</del>	281	13360	48.00	0.06	0.01	0.1810	0.0018	0.4676	0.0182	11.670	0.4720	0.137	0.0027	2662	17	+7
<del>N18-16C-10-2</del>	629	16612	26.00	0.12	0.03	0.1802	0.0019	0.4040	0.0213	10.040	0.5400	0.133	0.0031	2655	17	+18
<del>N18-06B-A-2</del>	814	29448	36.00	1.02	0.23	0.1763	0.0020	0.4132	0.0093	10.042	0.2560	0.124	0.0024	2618	19	+15
<del>N18-06B-A-3</del>	638	36168	57.00	1.50	0.23	0.1753	0.0038	0.4980	0.0173	12.034	0.4960	0.136	0.0027	2609	36	0
<del>N18-16G-23-1</del>	147	17544	120.00	0.89	0.04	0.1270	0.0034	0.2374	0.0127	4.155	0.2490	0.094	0.0021	2056	47	+33
<del>N18-16G-23-2</del>	456	36602	80.00	1.94	0.08	0.0971	0.0042	0.1036	0.0017	1.387	0.0640	0.067	0.0019	1569	81	+59

2304  
2305  
2306  
2307  
2308  
2309  
2310  
2311  
2312  
2313  
2314  
2315  
2316  
2317  
2318  
2319  
2320  
2321  
2322  
2323  
2324  
2325  
2326  
2327  
2328  
2329  
2330  
2331  
2332  
2333  
2334  
2335  
2336  
2337  
2338  
2339  
2340  
2341  
2342  
2343  
2344  
2345  
2346  
2347  
2348  
2349  
2350  
2351  
2352  
2353  
2354  
2355  
2356  
2357  
2358  
2359  
2360  
2361  
2362

835 Figure 1: Location of the ~~FB~~[Teutonic Bore](#) Camp on a map showing the major subdivisions  
836 of the Eastern Goldfields Superterrane, Yilgarn Craton, Western Australia. [The town of](#)  
837 [Leonora is indicated by a black diamond.](#) ~~Also~~ [The inset map shows](#) the location of the three  
838 deposits (Teutonic Bore, Jaguar and Bentley) and the sampled Penzance granite on the 1:500  
839 000 State interpreted bedrock geological map from the GSWA online database GeoVIEW.WA  
840 (2016).

841

2363  
2364  
2365  
2366  
2367  
2368  
2369  
2370  
2371  
2372  
2373  
2374  
2375  
2376  
2377  
2378  
2379  
2380  
2381  
2382  
2383  
2384  
2385  
2386  
2387  
2388  
2389  
2390  
2391  
2392  
2393  
2394  
2395  
2396  
2397  
2398  
2399  
2400  
2401  
2402  
2403  
2404  
2405  
2406  
2407  
2408  
2409  
2410  
2411  
2412  
2413  
2414  
2415  
2416  
2417  
2418  
2419  
2420  
2421

842 Figure 2: A) Schematic geological model for the [TB Teutonic Bore](#) Camp showing the  
843 position of each deposit within the stratigraphic sequence and illustrating the sub-seafloor  
844 replacement feature of the VHMS mineralisation and possible relationship of the host  
845 stratigraphy and the intrusive leucogranite described by Hallberg and Thompson (1985). B)  
846 Simplified stratigraphic sequence and stratigraphical subdivisions for each of the three deposits  
847 within the [TB Teutonic Bore](#) Camp (Belford, 2010; Belford et al., 2015; Chen et al., 2015; Das,  
848 2018 and complemented by this study; stratigraphic sequence modified from Hallberg and  
849 Thompson, 1985; Macklin, 2010; Parker et al., 2017). The U-Pb zircon age, drillhole and depth  
850 for the dacite are from Nelson (1995).

851

2422  
2423  
2424  
2425  
2426  
2427  
2428  
2429  
2430  
2431  
2432  
2433  
2434  
2435  
2436  
2437  
2438  
2439  
2440  
2441  
2442  
2443  
2444  
2445  
2446  
2447  
2448  
2449  
2450  
2451  
2452  
2453  
2454  
2455  
2456  
2457  
2458  
2459  
2460  
2461  
2462  
2463  
2464  
2465  
2466  
2467  
2468  
2469  
2470  
2471  
2472  
2473  
2474  
2475  
2476  
2477  
2478  
2479  
2480

852 Figure 3: U-Pb Concordia diagram showing the SHRIMP spot analyses and mean  
853  $^{207}\text{Pb}/^{206}\text{Pb}$  ages for: A) Footwall rhyolite (unit I) – Bentley footwall zircons (sample  
854 15BUDD78; mount N18-15D). B) Footwall rhyolite (unit I) – Bentley footwall zircons (sample  
855 15BUDD138; mount N18-15C). C) Transitional andesite (unit III) – Bentley hangingwall  
856 zircons (sample 15BUDD120 - 226.04m; mount N19-07, 08). D) Transitional andesite (unit  
857 III) – Bentley hangingwall zircons (sample 15BUDD120 - 228.42m; mount N19-09, 10). E)  
858 Penzance granite zircons (mount N18-06, 16). F) Penzance granite monazites (mounts N18-  
859 06, N18-16). Error ellipses are  $\pm 1\sigma$ .

860

2481  
2482  
2483  
2484  
2485  
2486  
2487  
2488  
2489  
2490  
2491  
2492  
2493  
2494  
2495  
2496  
2497  
2498  
2499  
2500  
2501  
2502  
2503  
2504  
2505  
2506  
2507  
2508  
2509  
2510  
2511  
2512  
2513  
2514  
2515  
2516  
2517  
2518  
2519  
2520  
2521  
2522  
2523  
2524  
2525  
2526  
2527  
2528  
2529  
2530  
2531  
2532  
2533  
2534  
2535  
2536  
2537  
2538  
2539

861 Figure 4: Cathodoluminescence electron microscope images of zircon grains separated  
862 from the footwall rhyolite (unit I) at the Bentley deposit, and analysed with SHRIMP and/or  
863 LA-SS-ICPMS. The location of the spots are indicated within each grain as well as the name  
864 (and  $^{207}\text{Pb}/^{206}\text{Pb}$  age for SHRIMP spots).

865



2540  
2541  
2542  
2543  
2544  
2545  
2546  
2547  
2548  
2549  
2550  
2551  
2552  
2553  
2554  
2555  
2556  
2557  
2558  
2559  
2560  
2561  
2562  
2563  
2564  
2565  
2566  
2567  
2568  
2569  
2570  
2571  
2572  
2573  
2574  
2575  
2576  
2577  
2578  
2579  
2580  
2581  
2582  
2583  
2584  
2585  
2586  
2587  
2588  
2589  
2590  
2591  
2592  
2593  
2594  
2595  
2596  
2597  
2598

866 Figure 5: Cathodoluminescence electron microscope images of zircon grains separated  
867 from the transitional andesite (unit III) at the Bentley deposit, and analysed with SHRIMP or  
868 LA-SS-ICPMS. The location of the spots are indicated within each grain as well as the name  
869 (and  $^{207}\text{Pb}/^{206}\text{Pb}$  age and discordance for SHRIMP spots).

870

2599  
2600  
2601  
2602  
2603  
2604  
2605  
2606  
2607  
2608  
2609  
2610  
2611  
2612  
2613  
2614  
2615  
2616  
2617  
2618  
2619  
2620  
2621  
2622  
2623  
2624  
2625  
2626  
2627  
2628  
2629  
2630  
2631  
2632  
2633  
2634  
2635  
2636  
2637  
2638  
2639  
2640  
2641  
2642  
2643  
2644  
2645  
2646  
2647  
2648  
2649  
2650  
2651  
2652  
2653  
2654  
2655  
2656  
2657

871           Figure 6: Cathodoluminescence images of zircon grains separated from the Penzance  
872 granite, and analysed with SHRIMP and/or LA-SS-ICPMS. The location of the spots are  
873 indicated within each grain as well as the name (and  $^{207}\text{Pb}/^{206}\text{Pb}$  age and discordance for  
874 SHRIMP spots). The zircons exhibit cavities, fractures, disruption of the original zoning and/or  
875 development of dark CL areas.

876

2658  
2659  
2660  
2661  
2662  
2663  
2664  
2665  
2666  
2667  
2668  
2669  
2670  
2671  
2672  
2673  
2674  
2675  
2676  
2677  
2678  
2679  
2680  
2681  
2682  
2683  
2684  
2685  
2686  
2687  
2688  
2689  
2690  
2691  
2692  
2693  
2694  
2695  
2696  
2697  
2698  
2699  
2700  
2701  
2702  
2703  
2704  
2705  
2706  
2707  
2708  
2709  
2710  
2711  
2712  
2713  
2714  
2715  
2716

877            Figure 7: Backscatter electron images of four monazite grains separated from the Penzance  
878 granite, and analysed with SHRIMP. The location of the spots are indicated within each grain  
879 as well as the name,  $^{207}\text{Pb}/^{206}\text{Pb}$  ages and discordance. Most crystals present visible regular  
880 euhedral zoning, typical of magmatic monazite.

881

2717  
2718  
2719  
2720  
2721  
2722  
2723  
2724  
2725  
2726  
2727  
2728  
2729  
2730  
2731  
2732  
2733  
2734  
2735  
2736  
2737  
2738  
2739  
2740  
2741  
2742  
2743  
2744  
2745  
2746  
2747  
2748  
2749  
2750  
2751  
2752  
2753  
2754  
2755  
2756  
2757  
2758  
2759  
2760  
2761  
2762  
2763  
2764  
2765  
2766  
2767  
2768  
2769  
2770  
2771  
2772  
2773  
2774  
2775

882 Figure 8:  $\epsilon\text{Hf}_{(i)}$  (CHUR) vs.  $^{207}\text{Pb}/^{206}\text{Pb}$  age (Ma) plot for zircon from the Penzance granite,  
883 the volcanic sequence at Bentley and zircons from other magmatic rocks within the Kurnalpi  
884 Terrane (Wyche et al., 2012). The errors for  $\epsilon\text{Hf}_{(i)}$  are  $1\sigma$ . The zircon data from this study are  
885 plotted with the interpreted  $^{207}\text{Pb}/^{206}\text{Pb}$  magmatic age for each sample, which is also used in  
886 the calculation of the  $\epsilon\text{Hf}_{(i)}$ . The thick black line labelled DM represents  $\epsilon\text{Hf}$  of depleted mantle  
887 over time.

888

2776  
2777  
2778  
2779  
2780  
2781  
2782  
2783  
2784  
2785  
2786  
2787  
2788  
2789  
2790  
2791  
2792  
2793  
2794  
2795  
2796  
2797  
2798  
2799  
2800  
2801  
2802  
2803  
2804  
2805  
2806  
2807  
2808  
2809  
2810  
2811  
2812  
2813  
2814  
2815  
2816  
2817  
2818  
2819  
2820  
2821  
2822  
2823  
2824  
2825  
2826  
2827  
2828  
2829  
2830  
2831  
2832  
2833  
2834

889            Figure 9: MREE and HREE patterns for zircon from the Penzance granite and the volcanic  
890 sequence at Bentley, normalized to chondrite (Anders and Grevesse, 1989). The lower graph  
891 is a compilation of the four results.

892

2835  
2836  
2837  
2838  
2839  
2840  
2841  
2842  
2843  
2844  
2845  
2846  
2847  
2848  
2849  
2850  
2851  
2852  
2853  
2854  
2855  
2856  
2857  
2858  
2859  
2860  
2861  
2862  
2863  
2864  
2865  
2866  
2867  
2868  
2869  
2870  
2871  
2872  
2873  
2874  
2875  
2876  
2877  
2878  
2879  
2880  
2881  
2882  
2883  
2884  
2885  
2886  
2887  
2888  
2889  
2890  
2891  
2892  
2893

893 Figure 10: Graph of probability density, assuming a normal distribution, for the zircon  
894  $^{207}\text{Pb}/^{206}\text{Pb}$  mean ages obtained in this study and the previous age from Nelson (1995), with the  
895 mean age indicated by a dashed line for each sample. Each age is represented both by the  
896 probability plot and by a graph bar. In both cases, the different shades represent  $1\sigma$  or  $2\sigma$  for  
897 each age, as indicated in the legend. The thick red line marks the maximum age of the  
898 mineralisation. The unpublished TIMS age of the footwall rhyolite (unit I) (Das, 2018) is  
899 represented only in bar graph form.

900

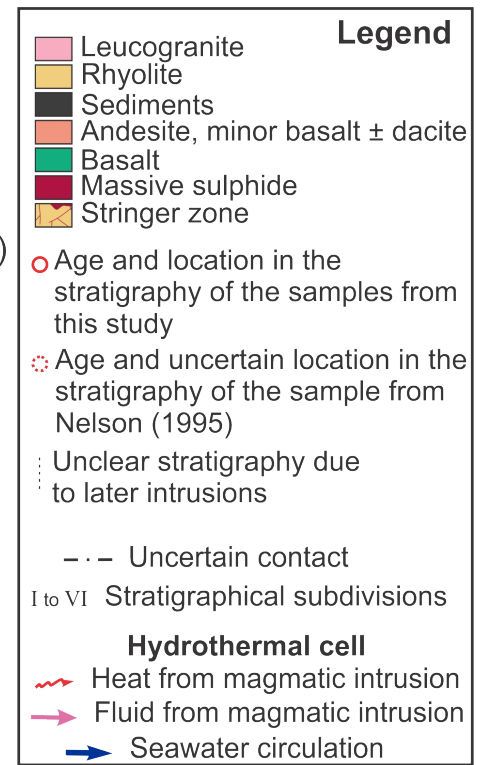
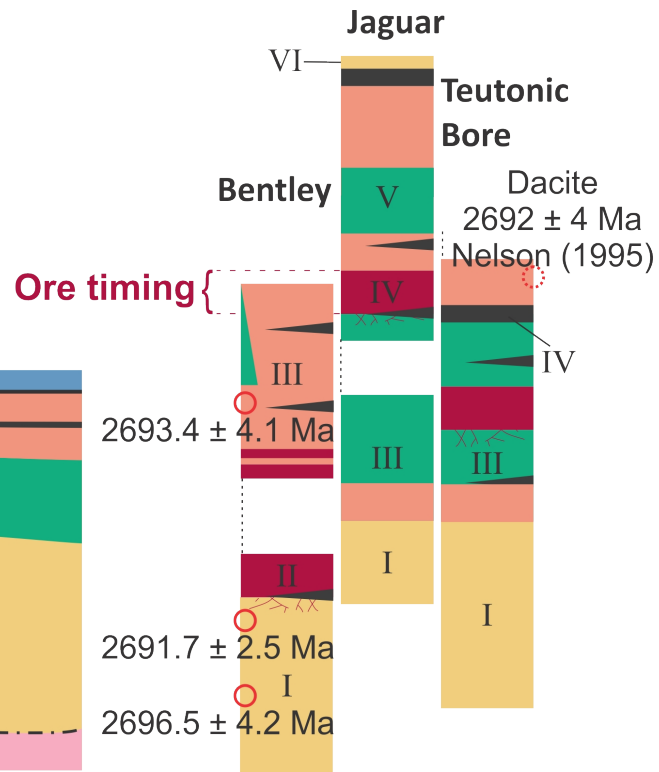
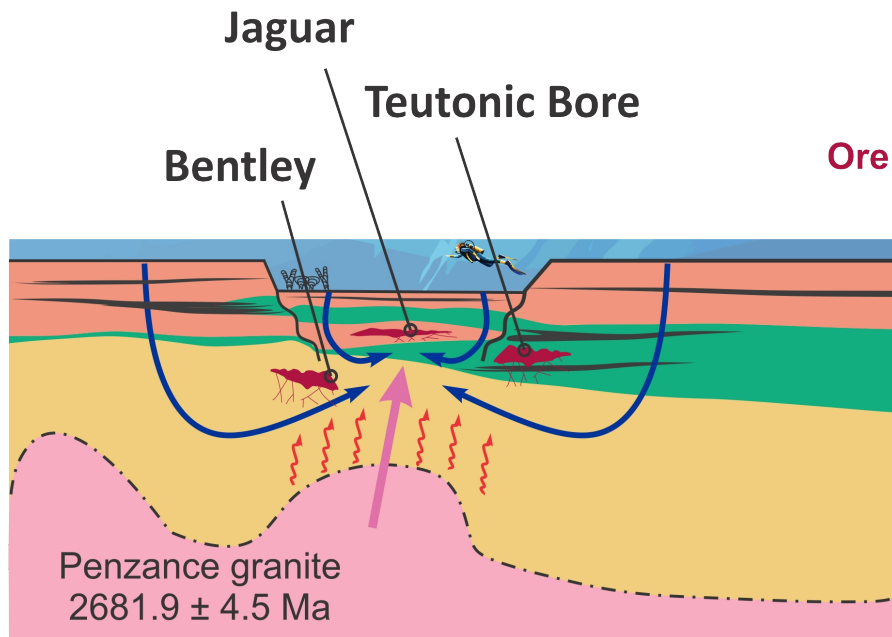
2894  
2895  
2896  
2897  
2898  
2899  
2900  
2901  
2902  
2903  
2904  
2905  
2906  
2907  
2908  
2909  
2910  
2911  
2912  
2913  
2914  
2915  
2916  
2917  
2918  
2919  
2920  
2921  
2922  
2923  
2924  
2925  
2926  
2927  
2928  
2929  
2930  
2931  
2932  
2933  
2934  
2935  
2936  
2937  
2938  
2939  
2940  
2941  
2942  
2943  
2944  
2945  
2946  
2947  
2948  
2949  
2950  
2951  
2952

901           Figure 11: Zr vs Y plot for the volcanic rocks that host the Jaguar deposit (Belford et al.,  
902 2015) and two samples from the Penzance granite from Geoscience Australia's OZCHEM  
903 database (Sedgmen et al., 2007). The filled square represents a sample collected from the same  
904 quarry that was sampled for the geochemical studies (Sample id 96969076). The roman  
905 numerals indicates the stratigraphical subdivisions from this study and their correspondence to  
906 the facies described by Belford et al. (2015). The boundaries and indicated Zr/Y ratios that  
907 define tholeiitic, transitional and calc-alkaline fields are from Barrett and MacLean (1994).

908

- The Teutonic Bore volcanics are broadly coeval to the Penzance granite
- The age of the Penzance granite is ca. 2682 Ma
- The Jaguar volcanics and the ore at the Teutonic Bore camp are  $\leq$  ca. 2693 Ma
- The Penzance granite possibly supplied heat and metals to the mineralisation
- Exploration in the EGS should focus on fluid pathways of HFSE-enriched granites





# The 4D evolution of the Teutonic Bore Camp VHMS deposits, Yilgarn Craton, Western Australia

Vitor R. Barrote<sup>1,2,3</sup>, Neal J. McNaughton<sup>1</sup>, Svetlana G. Tessalina<sup>1</sup>, Noreen J. Evans<sup>1,2</sup>, Cristina Talavera<sup>1,4</sup>, Jian-Wei Zi<sup>1,5</sup>, Bradley J. McDonald<sup>1,2</sup>

1- John de Laeter Centre and The Institute for Geoscience Research (TIGeR), Curtin University, Kent St, Bentley, WA 6102, Australia

2- School of Earth and Planetary Sciences, Curtin University, Kent St, Bentley, WA 6102, Australia

3- School of Earth, Atmosphere and Environment, Monash University, Clayton, Victoria 3800, Australia

4- School of Geosciences, University of Edinburgh, The King's Building, James Hutton Road, EH9 3FE, Edinburgh, UK

5- State Key Lab of Geological Processes and Mineral Resources, China University of Geosciences

Declarations of interest: none

## ABSTRACT

The Teutonic Bore Camp, comprised of the Teutonic Bore, Jaguar and Bentley deposits, is one of the most significant volcanic-hosted massive sulphide (VHMS) camps in Western Australia. Despite being extensively studied, only recently there have been advances in the understanding of the mechanism that drove the formation of mineralisation. It has been recognized by recent studies that the volcanic-hosted deposits from the Teutonic Bore Camp represent replacement-type VHMS systems, with significant input of fluids and metals from a magmatic source. This paper tests the existing hypothesis that the nearby Penzance granite acted as the metals source and/or thermal engine driving the development of these ore deposits.

60  
61  
62 26 New age constraints on the formation of the host volcanic sequence at the Bentley deposit  
63  
64 27 and the crystallization of the Penzance granite allows for the construction of a 4D evolutionary  
65  
66 28 model for the ore system. A new U-Pb SHRIMP monazite age of  $2681.9 \pm 4.5$  Ma indicates  
67  
68 29 that the Penzance granite post-dates the host stratigraphy at Bentley (ca. 2693 Ma) and is  
69  
70 30 probably coeval with mineralisation. All zircons (Penzance, Bentley units I and III) have very  
71  
72 31 similar  $\epsilon_{\text{Hf}(i)}$ , with most values between -1 and +6, slightly higher than the  $\epsilon_{\text{Hf}(i)}$  of zircons  
73  
74 32 from other granites and volcanics within the Kurnalpi Terrain, and indicative of juvenile  
75  
76 33 sources. The mean Th/U ratios are  $\sim 0.7$  and  $\sim 0.6$  for the Penzance and Bentley zircons,  
77  
78 34 respectively. All zircons have similar Ce/Nd<sub>(CN)</sub> ratios. The chemical similarities between the  
79  
80 35 zircons from the granite and the volcanic rocks at Bentley support a shared magmatic source  
81  
82 36 between the Penzance and the Teutonic Bore Camp sequence. The Penzance granite is the  
83  
84 37 likely source of heat, and potentially metals, which drove the VHMS mineralisation at the  
85  
86 38 Teutonic Bore Camp.  
87  
88

89  
90 39 Keywords: Penzance; Teutonic Bore; Volcanic-hosted massive sulphide; Archean;  
91  
92 40 Geochronology; 4D modelling  
93  
94

## 95 41 **1 INTRODUCTION**

96  
97  
98 42 Using an extensive database of compiled whole-rock geochemistry and U-Pb  
99  
100 43 geochronology, Hollis et al (2015) proposed a link between VHMS mineralisation and the  
101  
102 44 emplacement of HFSE-enriched syn-volcanic intrusions, throughout the Archean Yilgarn  
103  
104 45 Craton, including the Eastern Goldfield Superterrane. Despite the apparent geographical and  
105  
106 46 broadly coeval association between VHMS ores and HFSE-enriched intrusions, the  
107  
108 47 identification of a genetic link would benefit from further geochronological and isotopic  
109  
110 48 evidence.  
111

112  
113 49 The number of significant VHMS occurrences in the Yilgarn Craton is small compared to  
114  
115 50 other Archean terrains with similar characteristics such as the Superior Province of Canada  
116  
117  
118

119  
120  
121  
122  
123  
124  
125  
126  
127  
128  
129  
130  
131  
132  
133  
134  
135  
136  
137  
138  
139  
140  
141  
142  
143  
144  
145  
146  
147  
148  
149  
150  
151  
152  
153  
154  
155  
156  
157  
158  
159  
160  
161  
162  
163  
164  
165  
166  
167  
168  
169  
170  
171  
172  
173  
174  
175  
176  
177

51 (Hollis et al., 2015). Previous studies suggested that this could be due to under-exploration and  
52 the use of techniques inappropriate for mineral prospecting in the Yilgarn Craton (Butt et al.,  
53 2017; Ellis, 2004; Hollis et al., 2017, 2015; McConachy et al., 2004). Unlike classic VHMS  
54 systems, replacement-type VHMS systems, such as those in the Eastern Goldfield Superterrane,  
55 do not precipitate onto the seafloor and although some stratigraphic control can be observed  
56 within replacement-type mineralisation, it is not an inevitable feature (Doyle and Allen, 2003).

57 Historically, exploration for VHMS occurrences within the Teutonic Bore area was focused  
58 on key stratigraphic horizons. However, the known deposits formed at different stratigraphic  
59 positions and show significant differences in the geometry of mineralisation, compared to  
60 Teutonic Bore (Chen et al., 2015; Parker et al., 2017). This led to a significant time gap between  
61 the discoveries of the Teutonic Bore deposit in 1976, and the Jaguar and Bentley deposits in  
62 2004 and 2008, respectively (Ellis, 2004; Parker et al., 2017).

63 To better understand this lack of stratigraphic control on the position of orebodies at the  
64 Teutonic Bore Camp, and a possible link between high-field-strength-elements (HFSE)-  
65 enriched granite emplacement and ore precipitation, this work re-examines and expands the  
66 database of geochronology and isotopic/geochemical fingerprints for the igneous rock units.  
67 This includes re-assessment of the geochronological data from the nearby HFSE-enriched  
68 granite, the Penzance granite (Champion and Cassidy, 2002; Geoscience Australia, 2019), and  
69 the volcanic sequence from the Teutonic Bore Camp (Nelson, 1995), with additional U-Pb  
70 Sensitive High-Resolution Ion Microprobe (SHRIMP) dating of zircon and monazite.

71 These geochronological studies are complemented by zircon Hf-isotope and trace element  
72 analyses from the Bentley volcanic sequence and Penzance granite, and compilation of detailed  
73 stratigraphy, whole-rock geochemistry and sulphur isotope data from previous studies (Belford  
74 et al., 2015; Chen et al., 2015; Das, 2018; Isaac, 2015; Sedgmen et al., 2007). The present work  
75 combines the improved geochronological constrains presented here to the current 3D

178  
179  
180 76 understanding of the geological processes at place, to develop a 4D evolutionary model of the  
181  
182 77 deposits at the Teutonic Bore Camp.

184 78 Reliable and precise ages for magmatism and ore-hosting volcanism, combined with  
185  
186 79 traditional and isotopic geochemistry, allows testing of the hypothesis of a genetic relationship  
187  
188 80 between the HFSE-rich Penzance granite and the Teutonic Bore Camp deposits. The results  
189  
190 81 could have implications for future exploration for Precambrian VHMS deposits, not only in the  
191  
192 82 well-established Teutonic Bore Camp, but also in *greenfields* throughout the Eastern Goldfield  
193  
194 83 Superterrane and, potentially, elsewhere in the Yilgarn Craton.

## 198 84 **2 GEOLOGICAL BACKGROUND**

### 201 85 **2.1 Geology of the Teutonic Bore Camp**

203 86 The Teutonic Bore, Jaguar and Bentley VHMS deposits, along with several other smaller  
204  
205 87 occurrences, form the Teutonic Bore Camp (Independence Group NL (IGO), 2015). The  
206  
207 88 Teutonic Bore Camp is located near the town of Leonora, within the Kurnalpi Terrane of the  
208  
209 89 Eastern Goldfield Superterrane, Yilgarn Craton (Figure 1). The deposits in the Teutonic Bore  
210  
211 90 Camp are hosted by the Teutonic Bore volcanic complex, which comprises pillow basalt,  
212  
213 91 overlain and interlayered with volcanoclastic units, coherent rhyolite, andesite and thin  
214  
215 92 sedimentary units (Belford et al., 2015; Parker et al., 2017 and references therein). The prefix  
216  
217 93 “meta” is assumed but omitted when addressing the Archean stratigraphic sequence of the  
218  
219 94 Yilgarn Craton, because all rocks are metamorphosed to some extent (Czarnota et al., 2010).

222 95 The volcanic stratigraphy and the distribution of the three deposits, as well as other known  
223  
224 96 uneconomic ore bodies, have a NW-SE trend (Figure 1). This trend coincides with the general  
225  
226 97 alignment of regional structures, such as the fault that bounds the Teutonic Bore volcanic  
227  
228 98 complex to the west (Hallberg and Thompson, 1985; Parker et al., 2017).

237  
238  
239  
240  
241  
242  
243  
244  
245  
246  
247  
248  
249  
250  
251  
252  
253  
254  
255  
256  
257  
258  
259  
260  
261  
262  
263  
264  
265  
266  
267  
268  
269  
270  
271  
272  
273  
274  
275  
276  
277  
278  
279  
280  
281  
282  
283  
284  
285  
286  
287  
288  
289  
290  
291  
292  
293  
294  
295

99 The stratigraphy at the Teutonic Bore Camp comprises a predominantly laterally  
100 continuous lithofacies association between the three deposits (Figure 2A). Therefore, the  
101 volcanic sequence that hosts the mineralisation can be broadly subdivided in six units as follow  
102 from bottom to top (Figure 2B; Belford et al., 2015; Parker et al., 2017):

I. Footwall Rhyolite: from 200 m to over 1 km thick. Mainly coherent, either massive  
or flow-banded, with minor breccia (Parker et al., 2017), and with calc-alkaline to  
transitional magmatic affinity (Belford et al., 2015). This package is footwall to all  
three deposits.

II. Sedimentary rocks partly derived from the rhyolite, locally coarse but grading to  
arenite, siltstone and shale. This is the host unit to the Bentley deposit. The thickness  
range from 0 to 70 m according to Parker et al. (2017)

III. Transitional to tholeiitic basalt/ transitional andesite with thickness between 30 and  
170 m, with massive or pillowed habit, commonly intercalated with shale rich  
sediments (Parker et al., 2017). This package is host to the Teutonic Bore deposit  
and upper lens at Bentley (e.g.: Flying Spur, Brooklands, Comet: Independence  
Group NL (IGO), 2015) and overlays the lower orebody at the Bentley deposit  
(Arnage: Independence Group NL (IGO), 2015). Belford et al. (2015) names this  
unit Footwall Andesite (FA) and Footwall Basalt (FB), relative to their position to  
the mineralised zone at Jaguar.

IV. Upper sedimentary horizon (mineralised package from Belford et al., 2015) consists  
of a complex assemblage of intercalated dacite (called MPD by Belford et al., 2015),  
conglomerate, pumice-rich breccia, laminated sediment, laminated chert and  
massive sulphide (Belford et al., 2015). Unit IV marks a geochemical break in  
magmatic affinity, from tholeiitic/transitional of the underlying basalts/andesites to

296  
297  
298  
299  
300  
301  
302  
303  
304  
305  
306  
307  
308  
309  
310  
311  
312  
313  
314  
315  
316  
317  
318  
319  
320  
321  
322  
323  
324  
325  
326  
327  
328  
329  
330  
331  
332  
333  
334  
335  
336  
337  
338  
339  
340  
341  
342  
343  
344  
345  
346  
347  
348  
349  
350  
351  
352  
353  
354

123 calc-alkaline in the overlying lavas. The thickness is typically within 20 to 40 m  
124 (Parker et al., 2017).

125 V. Upper basalt and andesite of calc-alkaline affinity consists of massive and pillowed  
126 basalt and andesite lavas with minor volcanic breccias, and intercalated with mostly  
127 carbonaceous shales (Belford et al., 2015). The total thickness of this unit ranges  
128 between about 200 to 700 m (Parker et al., 2017).

129 VI. Hangingwall rhyolite: uppermost stratigraphic unit, described by Belford et al.  
130 (2015) from a single drillhole. The thickness of this unit is estimated to be between  
131 100 to 500m according to Parker et al. (2017).

132 The Teutonic Bore volcanic sequence is bounded to the east by a large composite batholith  
133 (Figure 1) named the Kent Complex by Champion and Cassidy (2002) and part of the Penzance  
134 Supersuite (Hollis et al., 2015). The Penzance Supersuite consists of HFSE-enriched granites  
135 with biotite and/or amphibole in quartz and feldspar rich rocks. These granites are characterised  
136 by variably elevated total Fe, MgO, Y, LREE, Zr, coupled with low to moderate Al<sub>2</sub>O<sub>3</sub>, K<sub>2</sub>O,  
137 Rb, Sr and moderate Na<sub>2</sub>O (Champion and Cassidy, 2002).

138 The relationship between the Penzance granite and the volcanic sequence in the Teutonic  
139 Bore Camp area remains unclear. Earlier studies (e.g.: Hallberg and Thompson, 1985) suggest  
140 an irregular contact between the granite and the volcanic rocks, with anastomosing veins of  
141 granitoid extending into adjacent extrusive rocks and a number of xenoliths of volcanic rocks  
142 within the intrusive granite. The Penzance granite is one of several HFSE-enriched intrusions  
143 in the Yilgarn Craton that occurs in close proximity to VHMS deposits or occurrences hosted  
144 by equally HFSE-enriched volcanics (Hollis et al., 2015).

145 The Jaguar deposit was classified as a replacement-type VHMS deposit by Belford (2010).  
146 This classification relied on evidence including replacement front texture, absence of chimney  
147 structures, and rapid emplacement of the host volcanic sequence, according to the criteria

355  
356  
357 148 proposed by Doyle and Allen (2003). Later studies (Chen et al., 2015; Das, 2018; Parker et al.,  
358  
359 149 2017) have identified similar textures in Bentley and other smaller occurrences and,  
360  
361 150 consequently, the replacement-type VHMS model is accepted within the Teutonic Bore Camp.  
362

363  
364 151 Despite the predominance of sub-seafloor replacement processes, Belford (2010) observed  
365  
366 152 features that indicate possible above seafloor activity. The development of thin beds of  
367  
368 153 translucent chert with colloform intergrowths of chert and sulphide is interpreted as products  
369  
370 154 of a waning hydrothermal system that had vented fluid to the sediment–water interface and  
371  
372 155 deposited precipitates onto the seafloor (Belford et al., 2015). Massive sulphides conformably  
373  
374 156 overlain by, and gradational upwards into, narrow beds of laminated chert intercalated with  
375  
376 157 finely-bedded sulphide-rich mudstone, support the idea of a progressive disruption of the  
377  
378 158 mineral activity and indicate that some sulphide precipitation might have taken place very near  
379  
380 159 or at seafloor (Belford et al., 2015).  
381

382  
383 160 The occurrence of massive sulphide clasts in the surrounding breccias and conglomerates,  
384  
385 161 which were the result of rapid erosion and mass flow, indicates that the sulphide body was  
386  
387 162 formed contemporaneously with the deposition of the upper sedimentary horizon (IV) (Belford  
388  
389 163 et al., 2015). Similar features have not been observed in either the Bentley or the Teutonic Bore  
390  
391 164 deposits.  
392

## 393 165 **2.2 Geochronology of the Teutonic Bore sequence and the Penzance granite**

394  
395  
396 166 The SHRIMP zircon age of  $2692 \pm 4$  Ma (Nelson, 1995) is the only published age for the  
397  
398 167 volcanic sequence at the Teutonic Bore Camp and comes from a porphyric dacite with unclear  
399  
400 168 stratigraphic position (Belford et al., 2015). Additionally, Das (2018) reported an ID-TIMS U-  
401  
402 169 Pb age of  $2692 \pm 1.5$  Ma for a sample of coherent Footwall Rhyolite (unit IV) from Jaguar.  
403  
404 170 These analysis remain unpublished and no data table or sample characterization is provided by  
405  
406 171 Das (2018).  
407  
408  
409  
410  
411  
412  
413



414  
415  
416 172 The reported ages for the Penzance granite are  $2679 \pm 8\text{Ma}$  (Champion and Cassidy, 2002)  
417  
418 173 and  $2686 \pm 9\text{Ma}$  (Geoscience Australia, 2019, sample ID 96969076). The two ages are derived  
419  
420 174 from the same analyses and calculated from a single dataset for sample ID 96969076. No  
421  
422  
423 175 explanation is provided by either references as to the reason behind the difference in age  
424  
425 176 calculation from a single set of analysis.

## 427 428 177 **3 SAMPLES AND METHODS**

### 429 430 431 178 **3.1 Penzance samples**

432  
433 179 Samples from the Penzance granite were collected from three different positions within  
434  
435 180 the same quarry (Lat. -28.264050, Long. 121.077888, Penzance Quarry in Figure 1). They were  
436  
437 181 collected from the same quarry as sample ID 96969076 from the Geochron Delivery database  
438  
439 182 of Geoscience Australia (2019). Each one of the three samples was processed separately and  
440  
441 183 treated as different samples, the analyses were combined only in the data processing phase of  
442  
443 184 each technique.

### 444 445 446 185 **3.2 Bentley samples**

447  
448 186 Two samples were collected from different positions within the footwall rhyolite (unit I) in  
449  
450 187 the Bentley deposit. Sample 15BUDD78 – 111.60 m was collected from drillhole 15BUDD78  
451  
452 188 at 111.60 meters depth, from a distal position to the ore. Sample 15BUDD137 – 398.60 m was  
453  
454 189 collected from a higher stratigraphic position within the sequence, a stringer zone to the lower  
455  
456 190 massive sulphide lens, from a different drillhole (15BUDD137).

457  
458  
459 191 Two samples (15BUDD120 - 228.42 and 15BUDD120 - 226.04) of the transitional andesite  
460  
461 192 (unit III), were collected from a single drillhole (15BUDD120), within two meters of each  
462  
463 193 other. The transitional andesite at the sampled point is hangingwall to the lower lens (Arnage),  
464  
465 194 but it is in the stringer zone for the upper lens, marked by the occurrence of disseminated  
466  
467 195 sulphides.

### 196 3.3 Analytical techniques

197 Zircon and Monazites were analysed on the SHRIMP II at the John de Laeter Centre,  
198 Curtin University (JdLC). Additionally, Zircon Lu–Hf isotopes and rare earth element (REE)  
199 abundances were measured over two analytical sessions using laser ablation split stream  
200 inductively coupled plasma mass spectrometry (LA-SS-ICPMS). The analyses were conducted  
201 in zircons from the same samples that were analysed by SHRIMP, but not necessarily on the  
202 same grain or over the same spot as the SHRIMP analysis. Detailed description of the  
203 conditions and procedures are provided in Supplementary Material 1.

## 204 4 RESULTS

### 205 4.1 U-Pb SHRIMP Zircon dating

#### 206 4.1.1 Footwall rhyolite (unit I) – Bentley Footwall

207 Fourteen analyses on 14 zircons from sample 15BUDD78 – 111.60 m were performed  
208 (Supplementary Material 2). Using only analyses within 3% of concordant yields a mean  
209  $^{207}\text{Pb}/^{206}\text{Pb}$  age of  $2696.5 \pm 4.2$  Ma (95% c.l., n=12; mean square weighted deviation,  
210 MSWD=1.04, Figure 3). The average and range of Th/U ratio from the most concordant  
211 SHRIMP analyses for this sample are 0.60 and 0.45-0.72, respectively.

212 A second sample from unit I was dated, twenty-seven analyses from 27 zircons from sample  
213 15BUDD137 – 398.60 m were collected (Supplementary Material 2). The mean  $^{207}\text{Pb}/^{206}\text{Pb}$   
214 age obtained for analyses within 4% of concordant and with <0.3% common Pb was  $2691.7 \pm$   
215  $2.5$  Ma (95% c.l.; n=25; MSWD=0.95, Figure 3). The average and range of Th/U ratio from  
216 the most concordant SHRIMP analyses are 0.63 and 0.41-0.84, respectively.

217 The CL images of zircons from the two unit I, footwall rhyolite samples show grains with  
218 continuous oscillatory zoning and no discernible core and/or rims, with sizes ranging from  
219 about 50 to 100  $\mu\text{m}$  (Figure 4). Their morphologies, Th/U and ages are indistinguishable, and

532  
533  
534 220 combining the most concordant data, the resulting age of  $2692.9 \pm 2.1$  Ma (95% cl; n=37;  
535  
536 221 MSWD=1.05) is our best estimate of the age of the footwall rhyolite at Bentley.

#### 538 539 222 *4.1.2 Transitional andesite (unit III) – Bentley Hangingwall*

540  
541 223 The samples from the transitional andesite were treated as two separate samples for the  
542  
543 224 geochronology portion of this study. However, these samples were taken 2 meters apart, from  
544  
545 225 the same drillcore (15BUDD120), and were within the same stratigraphic facies. The CL  
546  
547 226 images show zircons with continuous oscillatory zoning, and ranging from 15 to 30  $\mu\text{m}$  in  
548  
549 227 diameter (Figure 5).

550  
551 228 Sample 15BUDD120 – 226.04 m yielded 24 dates from 20 zircons. Considering only the  
552  
553 229 13 results with <5% discordance (Supplementary Material 2), the MSWD is 2.7 and indicates  
554  
555 230 an age spread not consistent with a single age population. Omitting the three youngest ages as  
556  
557 231 statistical outliers probably influenced by diffusional Pb-loss, the remaining population yields  
558  
559 232 a mean age of  $2693.2 \pm 5.8$  Ma (95% cl; n= 10; MSWD=0.88, Figure 3). The average and range  
560  
561 233 of Th/U from the SHRIMP analyses of the more concordant zircons from this sample is 0.90  
562  
563 234 and 0.39-1.55, respectively.

564  
565 235 Sample 15BUDD120 – 228.42 has 18 dates from 16 grains. The ages <5% discordant and  
566  
567 236 <0.1% common Pb yield a mean  $^{207}\text{Pb}/^{206}\text{Pb}$  age of  $2693.6 \pm 6.0$  Ma (95% cl, n=9;  
568  
569 237 MSWD=0.24, Figure 3; Supplementary Material 2). The average and range of Th/U of the  
570  
571 238 more concordant zircons is 0.95 and 0.73-1.31, respectively.

572  
573 239 The ages obtained for the two adjacent samples from the same stratigraphical facies agree  
574  
575 240 within error. Hence, the data can be combined to obtain a mean  $^{207}\text{Pb}/^{206}\text{Pb}$  age for the  
576  
577 241 Transitional Andesite (unit III) of  $2693.4 \pm 4.1$  Ma (95% c.l., n=19; MSWD=0.55). The average  
578  
579 242 Th/U from the zircons used in this mean age calculation was 0.92.

580  
581  
582  
583 243  
584  
585  
586  
587  
588  
589  
590

591  
592  
593 244  
594  
595 245  
596  
597 246  
598  
599 247  
600  
601 248  
602  
603 249  
604  
605 250  
606  
607 251  
608  
609 252  
610  
611 253  
612  
613 254  
614  
615 255  
616  
617 256  
618  
619 257  
620  
621 258  
622  
623 259  
624  
625 260  
626  
627 261  
628  
629 262  
630  
631 263  
632  
633 264  
634  
635 265  
636  
637 266  
638  
639 267  
640  
641 268  
642  
643  
644  
645  
646  
647  
648  
649

### 4.1.3 *Penzance granite*

The CL imaging of abundant zircons from all three samples collected from different locations in a single quarry of the Penzance granite displays textures typical of metamict zircons (Figure 6). These include cavities, fractures, disruption of the original zoning and development of dark CL areas (Corfu, 2003; Kılıç, 2016).

Even when targeting zircon grains seemingly less affected by metamictisation, twenty-seven analysis were aborted throughout a single analytical session due to the unacceptably high  $^{204}\text{Pb}$  content. Of the twenty-four analysis which were not aborted, only nine were <5% discordant and had less than 1% common Pb (Figure 6, Supplementary Material 2). The U and Th contents of completed analyses (average of ~580 and ~400 ppm, respectively) were commensurate with the observed metamictisation. The nine near concordant analysis have scattered ages typical of metamict zircons, and only one of the ages is within error of the previously reported age (Geoscience Australia, 2019). We conclude that no reliable age could be calculated from these zircon data. The average and range of Th/U from the completed SHRIMP analyses was 0.72 and 0.52-1.46, respectively.

## 4.2 **U-Pb SHRIMP monazite dating of the Penzance granite**

A significant number of the monazite grains were separated from the three Penzance granite samples. They have euhedral zoning textures on BSE images (Figure 7), which indicates magmatic crystallization. Recent studies (e.g.: Piechocka et al., 2017) have demonstrated the increased reliability of magmatic monazite as a geochronometer for igneous rocks with unreliable zircon age data, when subsequent metamorphic conditions remained under the Pb closure temperature of monazite. Monazite contains high U and Th and incorporates minor common Pb and, unlike zircon, is largely immune to metamictisation and radiogenic Pb loss at low temperatures (Piechocka et al., 2017).

650  
651  
652 269 A total of 38 of 56 analysis from 18 grains with low common Pb ( $f_{206} < 0.5\%$ ) and low  
653  
654 270 discordance ( $\leq 5\%$ ) (Table 1) yield a mean  $^{207}\text{Pb}/^{206}\text{Pb}$  age of  $2681.9 \pm 4.5$  Ma (95% c1; MSWD  
655  
656 271 = 1.4; Figure 3). The slightly high MSWD indicates the possibility of scatter from a single-age  
657  
658 272 population. However, in the absence of any skewness in the age probability plot (not shown),  
659  
660 273 anomalous Th-U chemistry or other evidence for either inheritance or Pb-loss, and given the  
661  
662 274 amount of data collected ( $n=56$ ) and used ( $n=38$ ), this is considered to be the age of these  
663  
664 275 igneous monazite.  
665  
666

### 667 276 **4.3 HF-isotopes in zircon**

#### 669 277 *4.3.1 Teutonic Bore volcanics*

670 278 Twenty-five zircon grains from sample 15BUDD78 – 111.60 m of the footwall rhyolite  
671  
672 279 (unit I) were analysed for Lu–Hf by LA-SS-ICP-MS (Supplementary Material 3, mount N18-  
673  
674 280 15D, sample B78,). The calculated  $\epsilon_{\text{Hf}(i)}$ , based on the interpreted SHRIMP  $^{207}\text{Pb}/^{206}\text{Pb}$  age  
675  
676 281 ( $2692.9\text{Ma}$ ), plot in a homogeneous population with values ranging between  $+2.3$  and  $+5.6$   
677  
678 282 (Figure 8), and a mean of  $3.7 \pm 0.5$  (MSWD = 0.47,  $n = 25$ ). The low MSWD value partly  
679  
680 283 reflects the relatively large  $\epsilon_{\text{Hf}(i)}$  errors on individual analyses.  
681  
682  
683  
684

685 284 Twenty-nine Lu–Hf analysis (Supplementary Material 3, mount N18-15C, sample B137)  
686  
687 285 were conducted on zircons from sample 15BUDD137 – 398.60 m of the same footwall rhyolite  
688  
689 286 (unit I), and, once again, the  $\epsilon_{\text{Hf}(i)}$  is calculated based on the interpreted SHRIMP  $^{207}\text{Pb}/^{206}\text{Pb}$   
690  
691 287 age for emplacement.  $\epsilon_{\text{Hf}(i)}$  values range between  $-0.6$  and  $+5.2$  with a mean of  $2.9 \pm 0.5$   
692  
693 288 (MSWD = 0.90,  $n = 29$ , Figure 8). Combining the  $\epsilon_{\text{Hf}(i)}$  data for the both footwall rhyolite  
694  
695 289 samples (unit I) yields a value of  $3.27 \pm 0.33$  (MSWD = 0.79,  $n = 54$ ).  
696  
697

698 290 Sixteen Lu–Hf analysis (Supplementary Material 3, B37) were conducted on zircon from  
699  
700 291 both samples of transitional andesite (unit III) and the mean age of the combined SHRIMP  
701  
702 292 analyses of  $2693.4$  Ma was used to calculate  $\epsilon_{\text{Hf}(i)}$  which showed considerable scatter and  
703  
704 293 ranged between  $-11.7$  and  $+8.6$  with significant errors on individual analyses (Supplementary  
705  
706  
707  
708

709  
710  
711 294 Material 3). The lower precision is a result of the smaller spot-size necessary for the small  
712  
713 295 zircons from these samples. The mean  $\epsilon\text{Hf}_{(i)}$  for the transitional andesite (unit III) is  $2.6 \pm 1.8$   
714  
715  
716 296 (MSWD = 1.05, n = 16, Figure 8).  
717

#### 718 297 4.3.2 *Penzance granite*

720 298 Recent studies show that the Lu–Hf system remains relatively undisturbed within metamorphic  
721  
722 299 zircon that do not undergo significant later alteration (Lenting et al., 2010). Thirty-four Lu–Hf  
723  
724 300 analyses on zircon from the Penzance granite (Supplementary Material 3, N18-06) show a  
725  
726 301 range of  $\epsilon\text{Hf}_{(i)}$  between -1.5 to +4.7 with mean value of  $2.17 \pm 0.45$  (MSWD = 1.15, n = 34).  
727  
728  
729 302 The  $\epsilon\text{Hf}_{(i)}$  values were calculated based on the SHRIMP monazite ages presented herein.  
730

#### 731 303 4.4 Trace elements in zircon

733 304 Selected trace elements were measured via LA-SS-ICP-MS (Supplementary Material 4).  
734  
735 305 Figure 9 illustrates patterns for selected REEs normalized to chondrite (Anders and Grevesse,  
736  
737 306 1989) for the two samples from the footwall rhyolite (unit I), the combined samples of andesite  
738  
739 307 (unit III) and the Penzance granite.  
740  
741

742 308 The zircons from the footwall rhyolite (unit I) and the andesite (unit III) have similar MREE  
743  
744 309 and HREE content (Figure 9). The mean Yb/Dy ratio is  $4.15 \pm 0.85$  and  $4.45 \pm 0.68$  ( $1\sigma$ ) for  
745  
746 310 the rhyolite and andesite, respectively. The Ce anomaly is estimated by the Ce/Nd<sub>(CN)</sub> ratio  
747  
748 311 (Loucks et al., 2018) to be positive in both rock types (Supplementary Material 4), with mean  
749  
750 312 Ce/Nd<sub>(CN)</sub> of  $1.04 \pm 0.58$  and  $1.30 \pm 0.75$  ( $1\sigma$ ) for the rhyolite and andesite, respectively. The  
751  
752 313 zircons from the Penzance granite show a mean Ce/Nd<sub>(CN)</sub> of  $0.92 \pm 0.23$  ( $1\delta$ ), indicating a  
753  
754 314 positive Ce anomaly, and Yb/Dy ratio of  $2.5 \pm 0.67$  ( $1\sigma$ ).  
755  
756  
757  
758  
759  
760  
761  
762  
763  
764  
765  
766  
767

768  
769  
770  
771 315 **5 DISCUSSION**  
772

773 316 **5.1 Age constrains on the Penzance granite**  
774

775 317 Hollis et al. (2015) proposed a link between VHMS mineralisation at the Teutonic Bore  
776 318 Camp and the emplacement of the HFSE-enriched Penzance granite, based on geochemical  
779 319 similarities, the proximity and broad synchronicity between the intrusive magmatic activity  
781 320 and the volcanism of the host sequence. These observations were underpinned by a U-Pb zircon  
782 321 age for the volcanism ( $2692 \pm 4$  Ma; Nelson, 1995) and the age reported by Champion and  
783 322 Cassidy (2002) of  $2679 \pm 8$  Ma, for the Kent Complex of the Penzance Supersuite. This latter  
784 323 age was obtained by SHRIMP U-Pb zircon dating of sample ID 96969076 of Geoscience  
785 324 Australia's database, after L.Black, AGSO (unpublished) in Champion and Cassidy (2002).

792 325 Champion and Cassidy (2002) reported the age but not the data table. However, the  
793 326 geochronological data, as well as location and description for sample ID 96969076, are  
794 327 available from Geoscience Australia's Geochron Delivery database (Geoscience Australia,  
798 328 2019). The reported age for this sample is  $2686 \pm 9$  Ma with MSWD = 1.6 and probability =  
799 329 0.044 (Geoscience Australia, 2019), which is within error of the age reported by Champion and  
800 330 Cassidy (2002), but not identical.

805 331 We have reprocessed the data available from Geochron Delivery for sample 96969076 and  
806 332 obtained an identical age of  $2686 \pm 9$  Ma, MSWD = 1.6 from 21 analysis. However, given the  
807 333 scatter inferred by the high MSWD, we have filtered the data by only considering analysis with  
808 334 common Pb <0.3%, deriving a more statistically robust age of  $2682 \pm 9$  Ma (n=12; MSWD =  
809 335 1.3). More importantly, only four zircons were recovered from sample 96969076 and the 21  
810 336 analyses and calculated age is based on analyses from only three grains, of which one is a  
811 337 xenocryst. Each of our three samples collected from the same quarry had hundreds of zircon  
812 338 grains, and after hand-picking the clearest (least metamict) zircons and analysing the best areas  
813 339 based on CL-SE imaging, we only detected one analysis in the relevant time interval, and it  
814  
815  
816  
817  
818  
819  
820  
821  
822  
823  
824  
825  
826

827  
828  
829 340 was 7% discordant. In view of this discrepancy, we searched for other datable minerals in the  
830  
831 341 Penzance granite and identified igneous monazite. The monazite age of  $2681.9 \pm 4.5$  Ma  
832  
833 342 discussed above is considered to be a statistically valid age of magma crystallization for the  
834  
835 343 Penzance granite, and supersedes the previous zircon age(s).  
836  
837

## 838 344 **5.2 Geochronological associations**

839

840 345 The relative timing of ore formation in the Teutonic Bore Camp is well constrained within  
841  
842 346 the stratigraphic sequence at Jaguar, where substantial evidence of seafloor precipitation  
843  
844 347 indicate coeval mineralisation to the development of the upper sedimentary package (unit IV).  
845  
846 348 Such evidence is absent from Bentley and the Teutonic Bore deposit, which indicates that they  
847  
848 349 were formed at greater depths, probably by replacement of a slightly older stratigraphy (see  
849  
850 350 Figure 2A).  
851  
852

853 351 The syn-ore nature of the upper sedimentary package (unit IV) at Jaguar, the deposit hosted  
854  
855 352 within the youngest stratigraphic level in the Teutonic Bore Camp, indicates that the  
856  
857 353 hangingwall sequence at Jaguar post-dates ore formation and could provide a potential  
858  
859 354 minimum mineralisation age. Attempts to date this sequence have proven unsuccessful to date  
860  
861 355 (Das, 2018). The footwall in all three deposits, as well as the hangingwall immediately above  
862  
863 356 the orebodies of the Bentley and the Teutonic Bore deposits, pre-date the mineralisation and  
864  
865 357 represent a maximum age of ore formation.  
866  
867

868 358 The ages obtained in this study for the footwall rhyolite (unit I -  $2691.7 \pm 2.5$  Ma and  $2696.5$   
869  
870 359  $\pm 4.3$  Ma) and the transitional andesite (unit III -  $2693.4 \pm 4.1$  Ma) suggest that mineralisation  
871  
872 360 at the Teutonic Bore Camp is younger than c.a. 2694 Ma (Figure 10). The unpublished TIMS  
873  
874 361 age for the footwall rhyolite sequence (unit I) of  $2692.6 \pm 1.5$  Ma (Das, 2018) is  
875  
876 362 indistinguishable from the SHRIMP age presented here for the pre-ore volcanic sequence at  
877  
878 363 the Teutonic Bore Camp. Similarly, the previous SHRIMP age for the Teutonic Bore Camp  
879  
880 364 sequence ( $2692 \pm 4$  Ma; (Nelson, 1995) is similar to the age determined in this study (Figure  
881  
882  
883  
884  
885



886  
887  
888 365 10). Therefore, although poorly constrained in the stratigraphy, it is likely that the porphyritic  
889  
890 366 dacite dated by Nelson (1995) is part of the pre-ore stratigraphy (units I, II, or III).

892 367 The ages for the footwall rhyolite (unit I) of  $2696.5 \pm 4.3$  Ma and  $2691.7 \pm 2.5$  Ma are  
893  
894 368 within error of each other, when considering a 95% confidence interval. However, considering  
895  
896 369 the normal distribution tendency of single-population ages obtained from multiple grains  
897  
898 370 (Figure 10; Schoene et al., 2013), it is probable that these could also represent a long duration  
899  
900 371 of volcanic activity during the development of this stratigraphic facies.

903 372 The ages for the footwall rhyolite (unit I) and the Penzance granite ( $2681.9 \pm 4.5$  Ma) do  
904  
905 373 not overlap (Figure 10) at the 95% confidence interval and are not, therefore, coeval.  
906  
907 374 Furthermore, the porphyritic dacite from Nelson (1995) and the transitional andesite (unit III)  
908  
909 375 do not overlap the age of the Penzance (Figure 10) at a 95% confidence interval. We infer that  
910  
911 376 these rocks pre-date the mineralisation and the syn-ore stratigraphy.

### 914 377 **5.3 Geochemical correlations**

#### 916 378 *5.3.1 Whole-rock geochemistry*

918 379 Hollis et al. (2015) described similarities in whole-rock REE distribution between the  
919  
920 380 Penzance granite (Kent Complex) and the felsic volcanics that host the mineralisation at Jaguar  
921  
922 381 (footwall rhyolite – unit I). Based on these observations and the HFSE enrichment of both rock  
923  
924 382 types they suggested a possible genetic link between these rocks, proposing that the footwall  
925  
926 383 volcanic sequence at Jaguar would be the extrusive equivalent to the Penzance granite.

929 384 The geochronological results presented here indicate that the crystallization of the Penzance  
930  
931 385 granite is not coeval to the formation of the footwall rhyolite (unit I) or the transitional andesite  
932  
933 386 (unit III) at Bentley. However, these processes occur within a ~12 M.y. interval. Given the  
934  
935 387 chemical similarities between these rock types and their proximity in age it is conceivable that  
936  
937 388 they are both the product of a single magmatic system or had a common source.

945  
946  
947 389 Additionally, based on whole-rock geochemistry observations, other stratigraphic facies  
948  
949 390 within the younger, syn-ore, portion of the volcanic sequence at the Teutonic Bore Camp are  
950  
951 391 alternative candidates to be the extrusive correspondent to the Penzance granite.  
952

953  
954 392 The dacite that can be observed at the sedimentary-volcanic package of the upper  
955  
956 393 sedimentary horizon (unit IV) in the Jaguar deposit (MPD from Belford et al., 2015) has Y/Zr  
957  
958 394 ratios that indicates a tholeiitic affinity (Belford et al., 2015), which is also the case for the  
959  
960 395 Penzance granite (ID 96969076, sampled from the same locality of the geochronological study;  
961  
962 396 Sedgmen et al., 2007) (Figure 11). Furthermore, the MPD dacite yields a La/Yb<sub>CN</sub> ratio of 3.4  
963  
964 397 – 5.5 (Belford, 2010), which indicates a significant LREE/HREE enrichment, equal to what is  
965  
966 398 indicated by whole-rock REE content for the Penzance granite (Hollis et al., 2015).  
967

### 968 969 399 *5.3.2 Zircon geochemistry* 970

971 400 The Hf-isotopes corroborate Hollis et al. (2015)'s hypothesis of a genetic link between the  
972  
973 401 Teutonic Bore Camp volcanic sequence and the Penzance granite. All zircons (Penzance, units  
974  
975 402 I and III) have very similar  $\epsilon_{\text{Hf}(i)}$ , with most values between -1 and +6 (Figure 8). The  $\epsilon_{\text{Hf}(i)}$   
976  
977 403 values show little contribution from evolved sources (Figure 8). Indeed, Nd and Pb isotopes  
978  
979 404 indicate that the Teutonic Bore Camp is located within a more juvenile zone of the Yilgarn  
980  
981 405 craton, the Teutonic zone (Huston et al., 2014). The  $\epsilon_{\text{Hf}(i)}$  for the zircons from the Penzance  
982  
983 406 granite and the volcanic rocks from the Teutonic Bore Camp plot above the CHUR line (Figure  
984  
985 407 8), indicating a juvenile depleted mantle source component. These  $\epsilon_{\text{Hf}(i)}$  are slightly higher  
986  
987 408 than the  $\epsilon_{\text{Hf}(i)}$  of zircons from other granites and volcanics within the Kurnalpi Terrain (Isaac,  
988  
989 409 2015; Wyche et al., 2012).  
990

991  
992 410 According to Kirkland et al. (2015), parental magma composition is one of four factors that  
993  
994 411 may contribute to variations in the Th/U of a zircon crystal. Therefore, the similar Th/U ratios  
995  
996 412 (Supplementary Material 2) of the Penzance (~0.7) and Bentley zircons (Unit I: ~0.6) also  
997  
998 413 suggest they could have a shared magma source. Furthermore, all zircons have similar  
999

1004  
1005  
1006  
1007  
1008  
1009  
1010  
1011  
1012  
1013  
1014  
1015  
1016  
1017  
1018  
1019  
1020  
1021  
1022  
1023  
1024  
1025  
1026  
1027  
1028  
1029  
1030  
1031  
1032  
1033  
1034  
1035  
1036  
1037  
1038  
1039  
1040  
1041  
1042  
1043  
1044  
1045  
1046  
1047  
1048  
1049  
1050  
1051  
1052  
1053  
1054  
1055  
1056  
1057  
1058  
1059  
1060  
1061  
1062

414 Ce/Nd<sub>(CN)</sub> ratios (Supplementary Material 4), which indicates comparable redox conditions, as  
415 this ratio is a proxy for the Ce anomaly (Loucks et al., 2018).

416 The zircons from the Penzance granite have higher overall REE content and MREE/HREE  
417 enrichment (indicated by the Yb/Dy ratio), when compared to the Bentley units I and III zircons  
418 (Supplementary Material 4). These chemical differences indicate that the Penzance granite is  
419 more fractionated but do not resolve whether this is the result of igneous differentiation from a  
420 common magma or magma production from a common source. The ~12 M.y. interval between  
421 the units I and III volcanics, and the Penzance granite suggests the latter.

#### 422 **5.4 Contribution to the 4D evolutionary model of the Teutonic Bore Camp ore**

423 The 4D evolutionary model of the Teutonic Bore Camp is achieved by the addition of the  
424 time dimension to the current understanding of the geological evolution of the deposits,  
425 including stratigraphy and geochemistry (Figure 2; Belford, 2010; Belford et al., 2015; Chen  
426 et al., 2015; Das, 2018; Hallberg and Thompson, 1985; Macklin, 2010; Parker et al., 2017).  
427 The geochronology data presented in this study constrain in time several processes within the  
428 Teutonic Bore Camp, including the intrusion of the Penzance granite, which could be linked to  
429 the development of the mineral system.

430 Similarities in zircon chemistry (i.e.:  $\square\text{Hf}_{(i)}$  and Th/U ratio; see section 5.3: Geochemical  
431 correlations) complemented by the geochemical correspondences between the Penzance  
432 granite and the Teutonic Bore volcanics (i.e.: HFSE-enrichment and REE pattern, see section  
433 5.3: Geochemical correlations), suggest a genetic association between the intrusive granite and  
434 the extrusive rocks that constitute the Teutonic Bore Camp host sequence.

435 Irregular contact between the Penzance granite and the volcanic sequence, as well as, the  
436 recognition of intrusive veins of granitoid within the volcanics, and xenoliths of volcanic rocks  
437 within the granite (Hallberg and Thompson, 1985) indicate that the Penzance intrudes the  
438 volcanic Teutonic Bore sequence and that their proximity is not the result of subsequent

1063  
1064  
1065  
1066  
1067  
1068  
1069  
1070  
1071  
1072  
1073  
1074  
1075  
1076  
1077  
1078  
1079  
1080  
1081  
1082  
1083  
1084  
1085  
1086  
1087  
1088  
1089  
1090  
1091  
1092  
1093  
1094  
1095  
1096  
1097  
1098  
1099  
1100  
1101  
1102  
1103  
1104  
1105  
1106  
1107  
1108  
1109  
1110  
1111  
1112  
1113  
1114  
1115  
1116  
1117  
1118  
1119  
1120  
1121

439 tectonic processes. Considering the close geographic position of the granite and the ore-bearing  
440 volcanic sequence (Figure 1), their shared geochemical features and broad synchronicity, it is  
441 possible that the Penzance granite was involved in the process that generated the VHMS  
442 mineralisation at the Teutonic Bore Camp.

443 Magmatic-hydrothermal contribution of metals is not necessary in the development of  
444 VHMS deposits (Huston et al., 2011) and syn-ore intrusions do not always directly supply  
445 metal to the system, but rather act as a heating source, driving hydrothermal circulation that  
446 leaches metals from the country host rock (Lode et al., 2017). However, in a number of cases  
447 there is evidence of a significant contribution of metals and/or volatiles from the magmatic  
448 source, in addition to the supply of heat (e.g.: Chen et al., 2015; Lode et al., 2017; Yang and  
449 Scott, 1996).

450 Chen et al. (2015) used S-isotopes as a proxy for the hydrothermal fluid composition in the  
451 Teutonic Bore Camp and interpreted that the supply of sulphur to the hydrothermal ore fluid  
452 was the result of a mixture between seawater and a hydrothermal fluid of magmatic origin.  
453 These authors did not find compelling evidence for leaching of sulphur from the host sequence  
454 into the ore fluid in the Teutonic Bore Camp. Therefore, the Penzance granite is a strong  
455 candidate to have acted as the probable magmatic source of sulphur to the mineralisation, and  
456 possibly, metals.

### 5.5 Exploration strategies

458 Our observations show that the HFSE-enriched Penzance granite probably played a  
459 fundamental role in the supply of metals and heat that culminated in the development of the  
460 replacement-type VHMS deposits of the Teutonic Bore Camp. Therefore, future exploration  
461 efforts within the camp should focus on fluid pathways from similar granites. The emphasis  
462 should be on mapping syn- or pre-intrusive structures that could facilitate fluid flow from the  
463 granite to the host sequence. Fertile zones are likely to be discovered where these fluid paths

1122  
1123  
1124 464 find the appropriate conditions for metal precipitation, which has been suggested by previous  
1125  
1126 465 studies to be sediment-rich horizons (Parker et al., 2017) and/or depositional breaks (Belford  
1127  
1128 et al., 2015).  
1129 466

1130  
1131 467 This paper supports conclusions proposed by Hollis et al. (2015), of a connection between  
1132  
1133 468 HFSE-enriched granites and VHMS ( $\pm$  base metals) deposits within the Yilgarn Craton.  
1134  
1135 469 Following the identification of fertile terrains, populated with HFSE-enriched granites,  
1136  
1137 470 *greenfield* exploration campaigns should employ a multi-disciplinary approach to test the  
1138  
1139 471 processes involved in the formation of an ore deposit. The development of 4D models (i.e.  
1140  
1141 472 constrain in time of 3D geological processes) allows for a better understanding of the timing  
1142  
1143 473 and nature of the magmatic and stratigraphical processes necessary for the development of such  
1144  
1145 474 ore deposits. This is particular true in Archean replacement-type VHMS deposits, where the  
1146  
1147 475 syn-volcanic timing of the mineralisation is not always clear (e.g. Barrote et al., 2019)  
1148  
1149  
1150

## 1151 476 **6 CONCLUSIONS**

1152

- 1153 477 • Three mined VHMS orebodies in the Teutonic Bore Camp (Teutonic Bore deposit,  
1154 478 Jaguar and Bentley) formed at different stratigraphic levels.
  - 1155 479 • Jaguar formed coeval with its host sequence, whereas the ore in Teutonic Bore and  
1156 480 Bentley replaces slightly older stratigraphy.
  - 1157 481 • The age of the host sequence at the stratigraphic level of the Bentley deposit is ca.  
1158 482 2693 Ma.
  - 1159 483 • The age of the Teutonic Bore Camp mineralisation is possibly coeval to the  
1160 484 intrusion of the Penzance granite at ca. 2682 Ma.
  - 1161 485 • Monazite has been shown to be a more reliable chronometer than high-U-Th zircons  
1162 486 in the HFSE-enriched Penzance granite.
- 1163  
1164  
1165  
1166  
1167  
1168  
1169  
1170  
1171  
1172  
1173  
1174  
1175  
1176  
1177  
1178  
1179  
1180

1181  
1182  
1183  
1184  
1185  
1186  
1187  
1188  
1189  
1190  
1191  
1192  
1193  
1194  
1195  
1196  
1197  
1198  
1199  
1200  
1201  
1202  
1203  
1204  
1205  
1206  
1207  
1208  
1209  
1210  
1211  
1212  
1213  
1214  
1215  
1216  
1217  
1218  
1219  
1220  
1221  
1222  
1223  
1224  
1225  
1226  
1227  
1228  
1229  
1230  
1231  
1232  
1233  
1234  
1235  
1236  
1237  
1238  
1239

- 487 • The Penzance granite possibly acted as the source of heat and potentially  
488 fluid/metals to the ore formation at the Teutonic Bore Camp.
- 489 • VHMS exploration in the Yilgarn Craton should focus in finding fluid pathways  
490 between HFSE-enriched intrusives and potential host sequences to orebodies.

## 7 ACKNOWLEDGMENTS

492 The authors acknowledge: Dr Steve Bereford and Mr. Kyle Hodges from IGO for their  
493 wisdom, access to samples, drill core and internal data; Thermo Fisher, GSWA and MRIWA  
494 for financial support; and the John de Laeter Centre (JdLC) for the facilities, scientific and  
495 technical assistance. We thank Dr. Haoyang Zhou, Dr. Nicolas Thebaud and an anonymous  
496 reviewer whose comments helped improve and clarify this manuscript. JdLC facilities are  
497 supported by a university-government consortium, ARC and AuScope via NCRIS. GeoHistory  
498 Facility instruments in the John de Laeter Centre, Curtin University were funded via an  
499 Australian Geophysical Observing System grant provided to AuScope Pty Ltd. by the AQ44  
500 Australian Education Investment Fund program. The NPII multi-collector was obtained via  
501 funding from the Australian Research Council LIEF program (LE150100013).

## 8 BIBLIOGRAPHY

503 Anders, E., Grevesse, N., 1989. Abundances of the elements: Meteoritic and solar. *Geochim.*  
504 *Cosmochim. Acta* 53, 197–214. [https://doi.org/10.1016/0016-7037\(89\)90286-X](https://doi.org/10.1016/0016-7037(89)90286-X)

505 Barrett, T.J., MacLean, W.H., 1994. Chemostratigraphy and hydrothermal alteration in  
506 exploration for VHMS deposits in greenstones and younger volcanic rocks., in: Lentz,  
507 D.R. (Ed.), *Alteration and Alteration Processes Associated with Ore-Forming Systems*,  
508 *Short Course Notes / Geological Association of Canada*. Geological Assoc. of Canada,  
509 St. John's, Newfoundland, pp. 433–467.

510 Barrote, V., Tessalina, S., McNaughton, N., Jourdan, F., Hollis, S.P., Ware, B., Zi, J.-W., 2020.  
511 4D history of the Nimbus VHMS ore deposit in the Yilgarn Craton, Western Australia.  
512 *Precambrian Research* 337, 105536. <https://doi.org/10.1016/j.precamres.2019.105536>

513 Belford, S.M., 2010. Genetic and chemical characterisation of the host succession to the  
514 archean Jaguar VHMS deposit. (Doctoral dissertation). University of Tasmania, UTAS,  
515 Hobart, Tasmania, Australia.

516 Belford, S.M., Davidson, G.J., McPhie, J., Large, R.R., 2015. Architecture of the Neoproterozoic  
517 Jaguar VHMS deposit, Western Australia: Implications for prospectivity and the

1240  
1241  
1242  
1243  
1244  
1245  
1246  
1247  
1248  
1249  
1250  
1251  
1252  
1253  
1254  
1255  
1256  
1257  
1258  
1259  
1260  
1261  
1262  
1263  
1264  
1265  
1266  
1267  
1268  
1269  
1270  
1271  
1272  
1273  
1274  
1275  
1276  
1277  
1278  
1279  
1280  
1281  
1282  
1283  
1284  
1285  
1286  
1287  
1288  
1289  
1290  
1291  
1292  
1293  
1294  
1295  
1296  
1297  
1298

- 518 presence of depositional breaks. *Precambrian Res.* 260, 136–160.  
519 <https://doi.org/10.1016/j.precamres.2014.12.019>
- 520 Butt, C.R.M., Anand, R.R., Smith, R.E., 2017. Geology of the Australian regolith, in: Phillips,  
521 G.N. (Ed.), *Australian Ore Deposits*. The Australian Institute of Mining and  
522 Metallurgy, Melbourne, pp. 27–34.
- 523 Champion, D.C., Cassidy, K.F., 2002. Granites of the Northern Eastern Goldfields: their  
524 Distribution, Age, Geochemistry, Petrogenesis, Relationship with Mineralisation, and  
525 Implications for Tectonic Environment, AMIRA P482/MERIWAM281-Yilgarn  
526 Granitoids. AMIRA P482/MERIWAM281-Yilgarn Granitoids.
- 527 Chen, M., Campbell, I.H., Xue, Y., Tian, W., Ireland, T.R., Holden, P., Cas, R.A.F., Hayman,  
528 P.C., Das, R., 2015. Multiple Sulfur Isotope Analyses Support a Magmatic Model for  
529 the Volcanogenic Massive Sulfide Deposits of the Teutonic Bore Volcanic Complex,  
530 Yilgarn Craton, Western Australia. *Econ. Geol.* 110, 1411–1423.  
531 <https://doi.org/10.2113/econgeo.110.6.1411>
- 532 Corfu, F., 2003. Atlas of Zircon Textures. *Rev. Mineral. Geochem.* 53, 469–500.  
533 <https://doi.org/10.2113/0530469>
- 534 Czarnota, K., Champion, D.C., Goscombe, B., Blewett, R.S., Cassidy, K.F., Henson, P.A.,  
535 Groenewald, P.B., 2010. Geodynamics of the eastern Yilgarn Craton. *Precambrian Res.*  
536 183, 175–202. <https://doi.org/10.1016/j.precamres.2010.08.004>
- 537 Das, R., 2018. Understanding the Palaeovolcanological and Palaeoenvironmental setting of  
538 Archaean VMS Deposit: Stratigraphic Architecture and Volcanology of the Archaean  
539 VMS host rock succession of the Teutonic Bore, Jaguar and Bentley Mine corridor,  
540 Eastern Goldfields Province, Western Australia (Master thesis). Melbourne University,  
541 Melbourne.
- 542 Doyle, M.G., Allen, R.L., 2003. Subsea-floor replacement in volcanic-hosted massive sulfide  
543 deposits. *Ore Geol. Rev.* 23, 183–222. [https://doi.org/10.1016/S0169-1368\(03\)00035-0](https://doi.org/10.1016/S0169-1368(03)00035-0)
- 544
- 545 Ellis, P., 2004. Geology and mineralisation of the Jaguar copper-zinc deposit, Western  
546 Australia, in: McConachy, T.F., McInnes, B.I.A. (Eds.), *Copper-Zinc Massive Sulphide*  
547 *Deposits in Western Australia*. CSIRO Exploration and Mining, Melbourne, pp. 39–46.
- 548 Geoscience Australia, 2019. Geochron Delivery Database. Accessed June 2019.  
549 <http://www.ga.gov.au/geochron-sapub-web/geochronology/shrimp/search.htm>.
- 550 GeoVIEW.WA, 2016. 1:500 000 State interpreted bedrock geology polygons, 2016.
- 551 Hallberg, J.A., Thompson, J.F.H., 1985. Geologic setting of the Teutonic Bore massive sulfide  
552 deposit, Archean Yilgarn Block, Western Australia. *Econ. Geol.* 80, 1953–1964.  
553 <https://doi.org/10.2113/gsecongeo.80.7.1953>
- 554 Hollis, S.P., Mole, D.R., Gillespie, P., Barnes, S.J., Tesselina, S., Cas, R.A.F., Hildrew, C.,  
555 Pumphrey, A., Goodz, M.D., Caruso, S., Yeats, C.J., Verbeeten, A., Belford, S.M.,  
556 Wyche, S., Martin, L.A.J., 2017. 2.7 Ga plume associated VHMS mineralization in the  
557 Eastern Goldfields Superterrane, Yilgarn Craton: Insights from the low temperature and  
558 shallow water, Ag-Zn-(Au) Nimbus deposit. *Precambrian Res.* 291, 119–142.  
559 <https://doi.org/10.1016/j.precamres.2017.01.002>
- 560 Hollis, S.P., Yeats, C.J., Wyche, S., Barnes, S.J., Ivanic, T.J., Belford, S.M., Davidson, G.J.,  
561 Roache, A.J., Wingate, M.T.D., 2015. A review of volcanic-hosted massive sulfide  
562 (VHMS) mineralization in the Archaean Yilgarn Craton, Western Australia: Tectonic,  
563 stratigraphic and geochemical associations. *Precambrian Res.* 260, 113–135.  
564 <https://doi.org/10.1016/j.precamres.2014.11.002>
- 565 Huston, D.L., Champion, D.C., Cassidy, K.F., 2014. Tectonic Controls on the Endowment of  
566 Neoproterozoic Cratons in Volcanic-Hosted Massive Sulfide Deposits: Evidence from

1299  
1300  
1301  
1302  
1303  
1304  
1305  
1306  
1307  
1308  
1309  
1310  
1311  
1312  
1313  
1314  
1315  
1316  
1317  
1318  
1319  
1320  
1321  
1322  
1323  
1324  
1325  
1326  
1327  
1328  
1329  
1330  
1331  
1332  
1333  
1334  
1335  
1336  
1337  
1338  
1339  
1340  
1341  
1342  
1343  
1344  
1345  
1346  
1347  
1348  
1349  
1350  
1351  
1352  
1353  
1354  
1355  
1356  
1357

- 567 Lead and Neodymium Isotopes. *Econ. Geol.* 109, 11–26.  
568 <https://doi.org/10.2113/econgeo.109.1.11>
- 569 Huston, D.L., Relvas, J.M.R.S., Gemmel, J.B., Driberg, S., 2011. The role of granites in  
570 volcanic-hosted massive sulphide ore-forming systems: an assessment of magmatic–  
571 hydrothermal contributions. *Miner. Deposita* 46, 473–507.  
572 <https://doi.org/10.1007/s00126-010-0322-7>
- 573 Independence Group NL (IGO), 2015. Annual Report 2015 (Unpublished Annual Report).  
574 Independence Group NL (IGO), Perth, W.A.
- 575 Isaac, C., 2015. Geochemistry of the north Eastern Goldfields, Western Australia: examining  
576 the processes that produce nickel sulphide camps (Masters Thesis). The University of  
577 Western Australia, Perth, W.A.
- 578 Kirkland, C.L., Smithies, R.H., Taylor, R.J.M., Evans, N., McDonald, B., 2015. Zircon Th/U  
579 ratios in magmatic environs. *Lithos* 212–215, 397–414.  
580 <https://doi.org/10.1016/j.lithos.2014.11.021>
- 581 Kılıç, A.D., 2016. Investigation of zircon by CL (Cathodoluminescence) and Raman  
582 Spectroscopy. *IOP Conf. Ser. Earth Environ. Sci.* 44, 042006.  
583 <https://doi.org/10.1088/1755-1315/44/4/042006>
- 584 Lenting, C., Geisler, T., Gerdes, A., Kooijman, E., Scherer, E.E., Zeh, A., 2010. The behavior  
585 of the Hf isotope system in radiation-damaged zircon during experimental  
586 hydrothermal alteration. *Am. Mineral.* 95, 1343–1348.  
587 <https://doi.org/10.2138/am.2010.3521>
- 588 Lode, S., Piercey, S.J., Layne, G.D., Piercey, G., Cloutier, J., 2017. Multiple sulphur and lead  
589 sources recorded in hydrothermal exhalites associated with the Lemarchant  
590 volcanogenic massive sulphide deposit, central Newfoundland, Canada. *Miner.*  
591 *Deposita* 52, 105–128. <https://doi.org/10.1007/s00126-016-0652-1>
- 592 Loucks, R.R., Fiorentini, M.L., Rohrlach, B.D., 2018. Divergent T–fO<sub>2</sub> paths during  
593 crystallisation of H<sub>2</sub>O-rich and H<sub>2</sub>O-poor magmas as recorded by Ce and U in zircon,  
594 with implications for TitaniQ and TitaniZ geothermometry. *Contrib. Mineral. Petrol.*  
595 173. <https://doi.org/10.1007/s00410-018-1529-3>
- 596 Macklin, D., 2010. Alteration at the Teutonic Bore (VHMS) Deposit, Western Australia (B.Sc  
597 with honours thesis). University of Tasmania, UTAS.
- 598 McConachy, T.F., McInnes, B.I.A., Carr, G.R., 2004. Is Western Australia intrinsically  
599 impoverished in volcanogenic massive sulphide deposits, or under explored?, in:  
600 McConachy, T.F., McInnes, B.I.A. (Eds.), *Copper-Zinc Massive Sulphide Deposits in*  
601 *Western Australia*. CSIRO Exploration and Mining, Melbourne, pp. 15–32.
- 602 Nelson, D.R., 1995. Compilation of SHRIMP U–Pb zircon geochronology data, 1994, Record  
603 / Geological Survey of Western Australia. Geological Survey of Western Australia,  
604 Perth.
- 605 Parker, P., Belford, S.M., Maier, R., Lynn, S., Stewart, W., 2017. Teutonic Bore - Jaguar -  
606 Bentley volcanogenic massive sulfide field, in: Phillips, G.N. (Ed.), *Australian Ore*  
607 *Deposits*. The Australian Institute of Mining and Metallurgy, Melbourne, pp. 167–172.
- 608 Piechocka, A.M., Gregory, C.J., Zi, J.-W., Sheppard, S., Wingate, M.T.D., Rasmussen, B.,  
609 2017. Monazite trumps zircon: applying SHRIMP U–Pb geochronology to  
610 systematically evaluate emplacement ages of leucocratic, low-temperature granites in  
611 a complex Precambrian orogen. *Contrib. Mineral. Petrol.* 172.  
612 <https://doi.org/10.1007/s00410-017-1386-5>
- 613 Schoene, B., Condon, D.J., Morgan, L., McLean, N., 2013. Precision and Accuracy in  
614 Geochronology. *Elements* 9, 19–24. <https://doi.org/10.2113/gselements.9.1.19>
- 615 Sedgmen, A., Hazell, M.S., Budd, A.R., Champion, D.C., 2007. OZCHEM National Whole  
616 Rock Geochemistry Dataset.



1358  
1359  
1360  
1361  
1362  
1363  
1364  
1365  
1366  
1367  
1368  
1369  
1370  
1371  
1372  
1373  
1374  
1375  
1376  
1377  
1378  
1379  
1380  
1381  
1382  
1383  
1384  
1385  
1386  
1387  
1388  
1389  
1390  
1391  
1392  
1393  
1394  
1395  
1396  
1397  
1398  
1399  
1400  
1401  
1402  
1403  
1404  
1405  
1406  
1407  
1408  
1409  
1410  
1411  
1412  
1413  
1414  
1415  
1416

617 Wyche, S., Kirkland, C.L., Riganti, A., Pawley, M.J., Belousova, E., Wingate, M.T.D., 2012.  
618 Isotopic constraints on stratigraphy in the central and eastern Yilgarn Craton, Western  
619 Australia. *Aust. J. Earth Sci.* 59, 657–670.  
620 <https://doi.org/10.1080/08120099.2012.697677>  
621 Yang, K., Scott, S.D., 1996. Possible contribution of a metal-rich magmatic fluid to a sea-floor  
622 hydrothermal system. *Nature* 383, 420–423. <https://doi.org/10.1038/383420a>

1  
2  
3  
4 Figure 1: Location of the Teutonic Bore Camp on a map showing the major subdivisions  
5 of the Eastern Goldfields Superterrane, Yilgarn Craton, Western Australia. The town of  
6 Leonora is indicated by a black diamond. The inset map shows the location of the three deposits  
7 (Teutonic Bore, Jaguar and Bentley) and the sampled Penzance granite on the 1:500 000 State  
8 interpreted bedrock geological map from the GSWA online database GeoVIEW.WA (2016).  
9  
10  
11  
12  
13  
14  
15  
16  
17  
18  
19  
20  
21  
22  
23  
24  
25  
26  
27  
28  
29  
30  
31  
32  
33  
34  
35  
36  
37  
38  
39  
40  
41  
42  
43  
44  
45  
46  
47  
48  
49  
50  
51  
52  
53  
54  
55  
56  
57  
58  
59

60  
61  
62  
63 Figure 2: A) Schematic geological model for the Teutonic Bore Camp showing the position  
64 of each deposit within the stratigraphic sequence and illustrating the sub-seafloor replacement  
65 feature of the VHMS mineralisation and possible relationship of the host stratigraphy and the  
66 intrusive leucogranite described by Hallberg and Thompson (1985). B) Simplified stratigraphic  
67 sequence and stratigraphical subdivisions for each of the three deposits within the Teutonic  
68 Bore Camp (Belford, 2010; Belford et al., 2015; Chen et al., 2015; Das, 2018 and  
69 complemented by this study; stratigraphic sequence modified from Hallberg and Thompson,  
70 1985; Macklin, 2010; Parker et al., 2017). The U-Pb zircon age, drillhole and depth for the  
71 dacite are from Nelson (1995).  
72  
73  
74  
75  
76  
77  
78  
79  
80  
81  
82  
83  
84  
85  
86  
87  
88  
89  
90  
91  
92  
93  
94  
95  
96  
97  
98  
99  
100  
101  
102  
103  
104  
105  
106  
107  
108  
109  
110  
111  
112  
113  
114  
115  
116  
117  
118

119  
120  
121 Figure 3: U-Pb Concordia diagram showing the SHRIMP spot analyses and mean  
122  $^{207}\text{Pb}/^{206}\text{Pb}$  ages for: A) Footwall rhyolite (unit I) – Bentley footwall zircons (sample  
123 15BUDD78; mount N18-15D). B) Footwall rhyolite (unit I) – Bentley footwall zircons (sample  
124 15BUDD138; mount N18-15C). C) Transitional andesite (unit III) – Bentley hangingwall  
125 zircons (sample 15BUDD120 - 226.04m; mount N19-07, 08). D) Transitional andesite (unit  
126 III) – Bentley hangingwall zircons (sample 15BUDD120 - 228.42m; mount N19-09, 10). E)  
127 Penzance granite zircons (mount N18-06, 16). F) Penzance granite monazite (mounts N18-06,  
128 N18-16). Error ellipses are  $\pm 1\sigma$ .  
129  
130  
131  
132  
133  
134  
135  
136  
137  
138  
139  
140  
141  
142  
143  
144  
145  
146  
147  
148  
149  
150  
151  
152  
153  
154  
155  
156  
157  
158  
159  
160  
161  
162  
163  
164  
165  
166  
167  
168  
169  
170  
171  
172  
173  
174  
175  
176  
177

178  
179  
180  
181 Figure 4: Cathodoluminescence electron microscope images of zircon grains separated  
182 from the footwall rhyolite (unit I) at the Bentley deposit, and analysed with SHRIMP and/or  
183 LA-SS-ICPMS. The location of the spots are indicated within each grain as well as the name  
184  
185  
186  
187 (and  $^{207}\text{Pb}/^{206}\text{Pb}$  age for SHRIMP spots).  
188  
189  
190  
191  
192  
193  
194  
195  
196  
197  
198  
199  
200  
201  
202  
203  
204  
205  
206  
207  
208  
209  
210  
211  
212  
213  
214  
215  
216  
217  
218  
219  
220  
221  
222  
223  
224  
225  
226  
227  
228  
229  
230  
231  
232  
233  
234  
235  
236

237  
238  
239 Figure 5: Cathodoluminescence electron microscope images of zircon grains separated  
240 from the transitional andesite (unit III) at the Bentley deposit, and analysed with SHRIMP or  
241 LA-SS-ICPMS. The location of the spots are indicated within each grain as well as the name  
242 (and  $^{207}\text{Pb}/^{206}\text{Pb}$  age and discordance for SHRIMP spots).  
243  
244  
245  
246  
247  
248  
249  
250  
251  
252  
253  
254  
255  
256  
257  
258  
259  
260  
261  
262  
263  
264  
265  
266  
267  
268  
269  
270  
271  
272  
273  
274  
275  
276  
277  
278  
279  
280  
281  
282  
283  
284  
285  
286  
287  
288  
289  
290  
291  
292  
293  
294  
295

296  
297  
298  
299  
300  
301  
302  
303  
304  
305  
306  
307  
308  
309  
310  
311  
312  
313  
314  
315  
316  
317  
318  
319  
320  
321  
322  
323  
324  
325  
326  
327  
328  
329  
330  
331  
332  
333  
334  
335  
336  
337  
338  
339  
340  
341  
342  
343  
344  
345  
346  
347  
348  
349  
350  
351  
352  
353  
354

Figure 6: Cathodoluminescence images of zircon grains separated from the Penzance granite, and analysed with SHRIMP and/or LA-SS-ICPMS. The location of the spots are indicated within each grain as well as the name (and  $^{207}\text{Pb}/^{206}\text{Pb}$  age and discordance for SHRIMP spots). The zircons exhibit cavities, fractures, disruption of the original zoning and/or development of dark CL areas.

355  
356  
357 Figure 7: Backscatter electron images of four monazite grains separated from the Penzance  
358 granite, and analysed with SHRIMP. The location of the spots are indicated within each grain  
359 as well as the name,  $^{207}\text{Pb}/^{206}\text{Pb}$  ages and discordance. Most crystals present visible regular  
360 euohedral zoning, typical of magmatic monazite.  
361  
362  
363  
364  
365  
366  
367  
368  
369  
370  
371  
372  
373  
374  
375  
376  
377  
378  
379  
380  
381  
382  
383  
384  
385  
386  
387  
388  
389  
390  
391  
392  
393  
394  
395  
396  
397  
398  
399  
400  
401  
402  
403  
404  
405  
406  
407  
408  
409  
410  
411  
412  
413



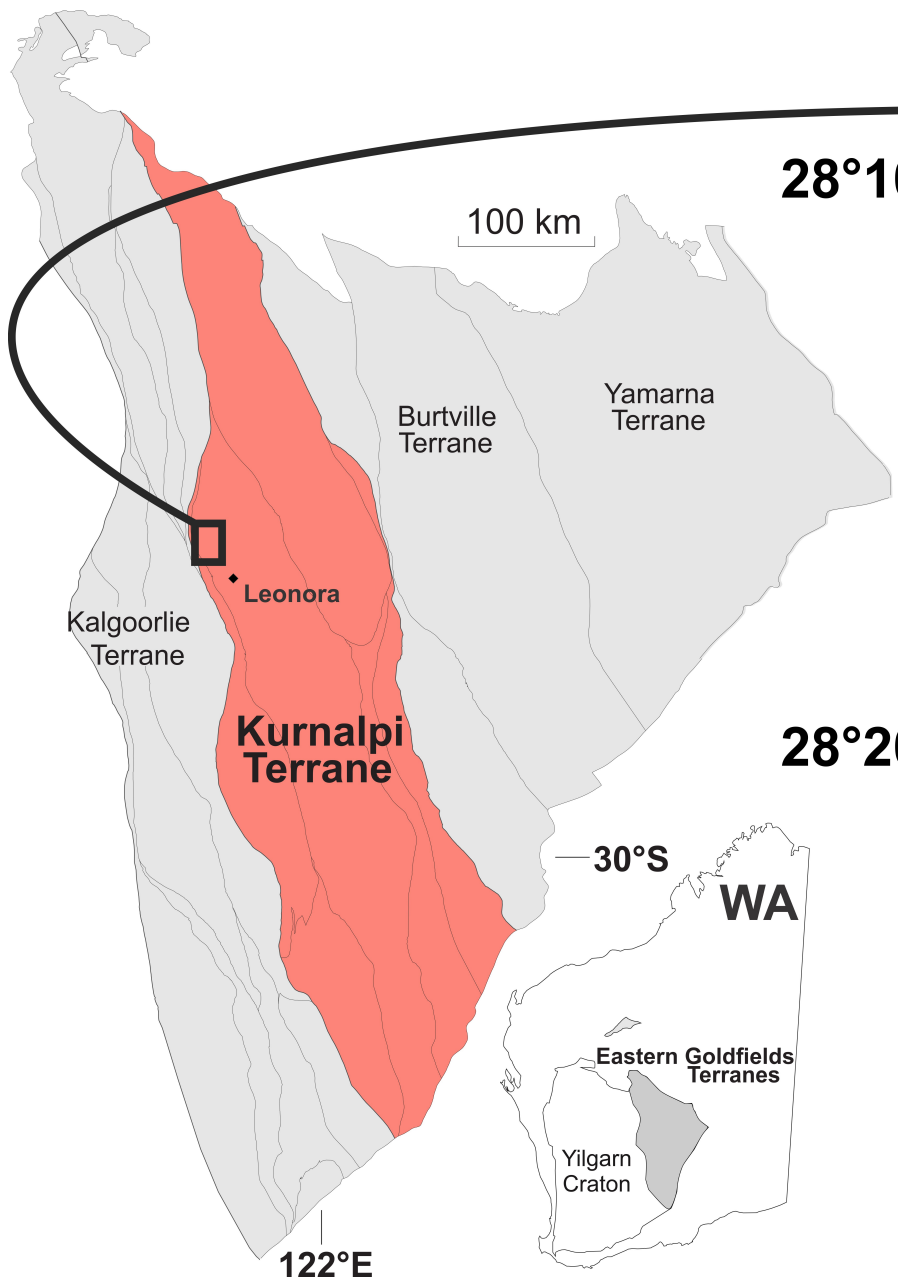
414  
415  
416 Figure 8:  $\epsilon_{\text{Hf}(i)}$  (CHUR) vs.  $^{207}\text{Pb}/^{206}\text{Pb}$  age (Ma) plot for zircon from the Penzance granite,  
417  
418 the volcanic sequence at Bentley and zircons from other magmatic rocks within the Kurnalpi  
419  
420 Terrane (Wyche et al., 2012). The errors for  $\epsilon_{\text{Hf}(i)}$  are  $1\sigma$ . The zircon data from this study are  
421  
422 plotted with the interpreted  $^{207}\text{Pb}/^{206}\text{Pb}$  magmatic age for each sample, which is also used in  
423  
424 the calculation of the  $\epsilon_{\text{Hf}(i)}$ . The thick black line labelled DM represents  $\epsilon_{\text{Hf}}$  of depleted mantle  
425  
426  
427 over time.  
428  
429  
430  
431  
432  
433  
434  
435  
436  
437  
438  
439  
440  
441  
442  
443  
444  
445  
446  
447  
448  
449  
450  
451  
452  
453  
454  
455  
456  
457  
458  
459  
460  
461  
462  
463  
464  
465  
466  
467  
468  
469  
470  
471  
472

473  
474  
475 Figure 9: MREE and HREE patterns for zircon from the Penzance granite and the volcanic  
476 sequence at Bentley, normalized to chondrite (Anders and Grevesse, 1989). The lower graph  
477 is a compilation of the four results.  
478  
479  
480  
481  
482  
483  
484  
485  
486  
487  
488  
489  
490  
491  
492  
493  
494  
495  
496  
497  
498  
499  
500  
501  
502  
503  
504  
505  
506  
507  
508  
509  
510  
511  
512  
513  
514  
515  
516  
517  
518  
519  
520  
521  
522  
523  
524  
525  
526  
527  
528  
529  
530  
531

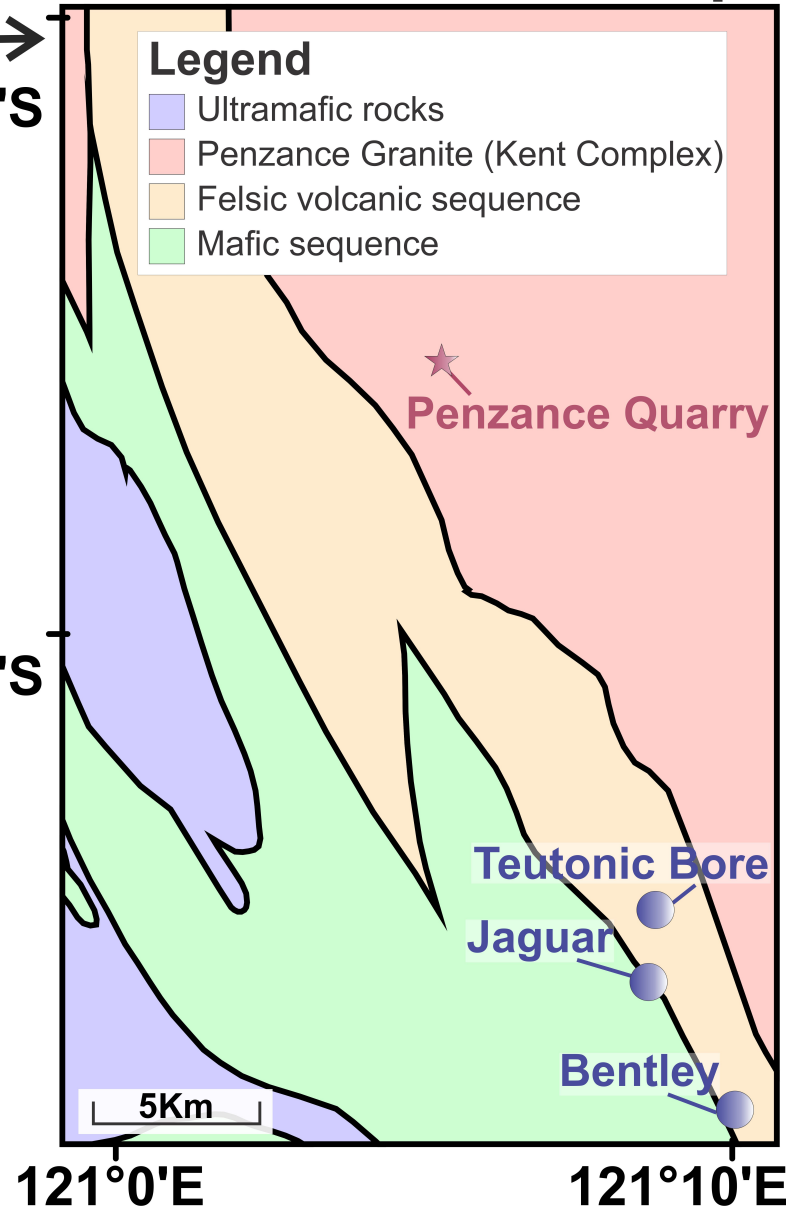
532  
533  
534 Figure 10: Graph of probability density, assuming a normal distribution, for the zircon  
535  $^{207}\text{Pb}/^{206}\text{Pb}$  mean ages obtained in this study and the previous age from Nelson (1995), with the  
536 mean age indicated by a dashed line for each sample. Each age is represented both by the  
537 probability plot and by a graph bar. In both cases, the different shades represent  $1\sigma$  or  $2\sigma$  for  
538 each age, as indicated in the legend. The thick red line marks the maximum age of the  
539 mineralisation. The unpublished TIMS age of the footwall rhyolite (unit I) (Das, 2018) is  
540 represented only in bar graph form.  
541  
542  
543  
544  
545  
546  
547  
548  
549  
550  
551  
552  
553  
554  
555  
556  
557  
558  
559  
560  
561  
562  
563  
564  
565  
566  
567  
568  
569  
570  
571  
572  
573  
574  
575  
576  
577  
578  
579  
580  
581  
582  
583  
584  
585  
586  
587  
588  
589  
590

591  
592  
593 Figure 11: Zr vs Y plot for the volcanic rocks that host the Jaguar deposit (Belford et al.,  
594 2015) and two samples from the Penzance granite from Geoscience Australia's OZCHEM  
595 database (Sedgmen et al., 2007). The filled square represents a sample collected from the same  
596 quarry that was sampled for the geochemical studies (Sample id 96969076). The roman  
597 numerals indicates the stratigraphical subdivisions from this study and their correspondence to  
598 the facies described by Belford et al. (2015). The boundaries and indicated Zr/Y ratios that  
599 define tholeiitic, transitional and calc-alkaline fields are from Barrett and MacLean (1994).  
600  
601  
602  
603  
604  
605  
606  
607  
608  
609  
610  
611  
612  
613  
614  
615  
616  
617  
618  
619  
620  
621  
622  
623  
624  
625  
626  
627  
628  
629  
630  
631  
632  
633  
634  
635  
636  
637  
638  
639  
640  
641  
642  
643  
644  
645  
646  
647  
648  
649

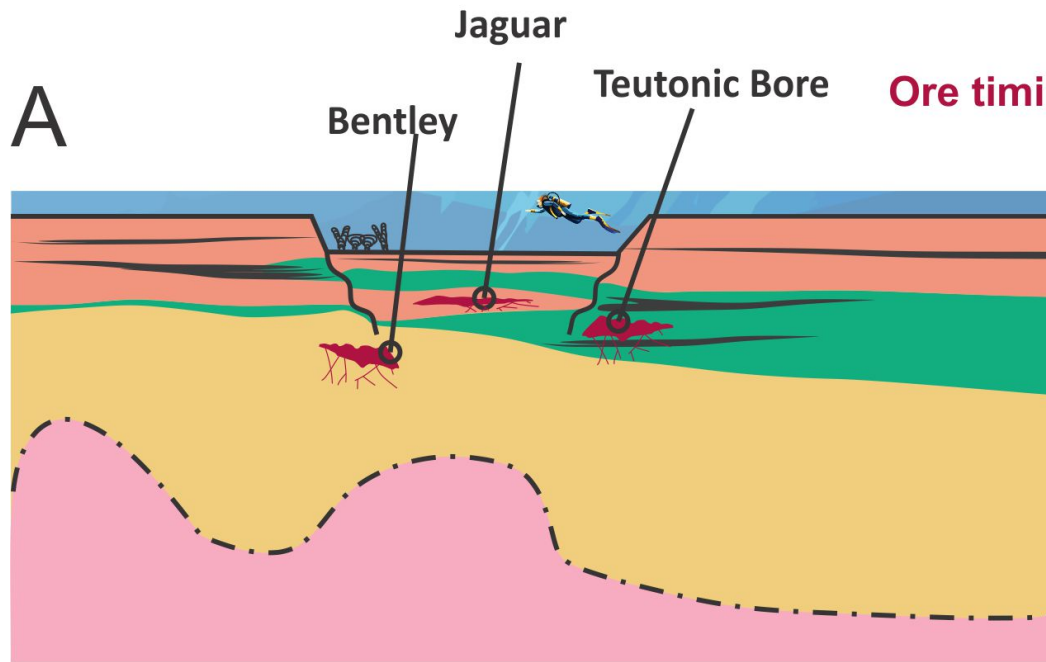
1  
2  
3  
4  
5  
6  
7  
8  
9  
10  
11  
12  
13  
14  
15  
16  
17  
18  
19  
20  
21  
22  
23  
24  
25  
26  
27  
28  
29  
30  
31  
32  
33  
34  
35  
36



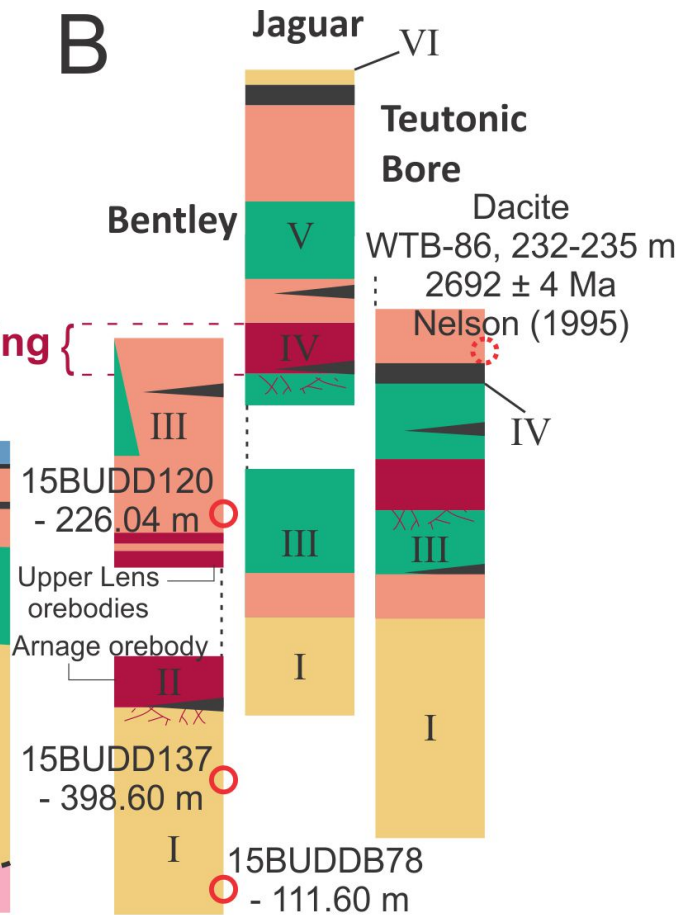
# Teutonic Bore camp



A



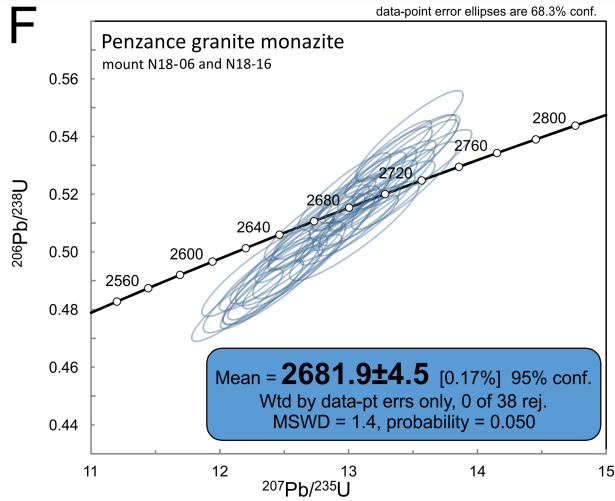
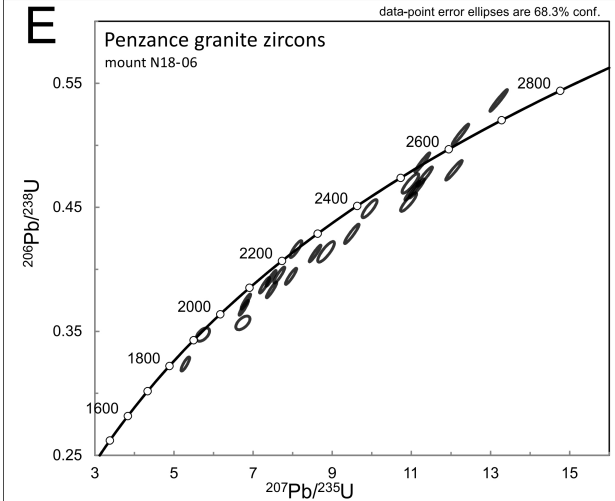
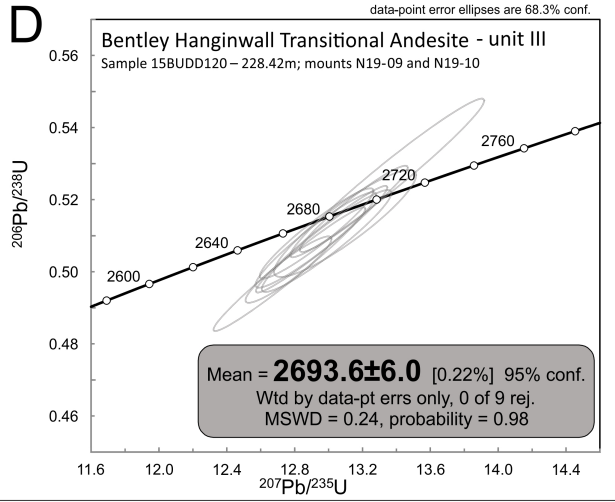
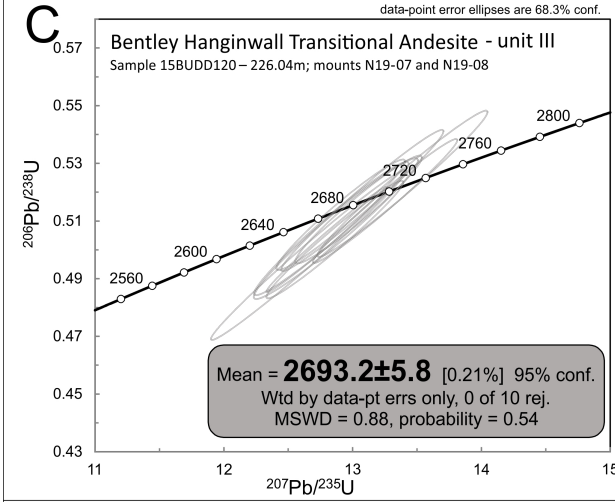
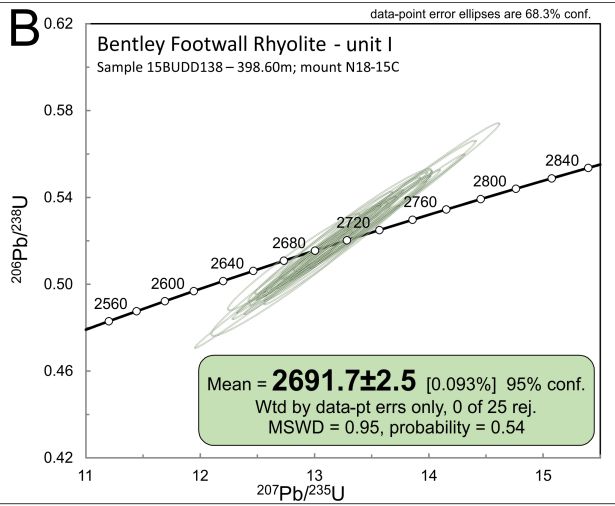
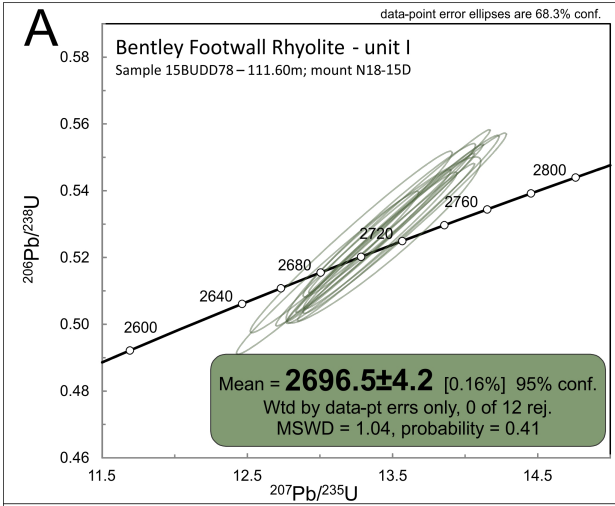
B



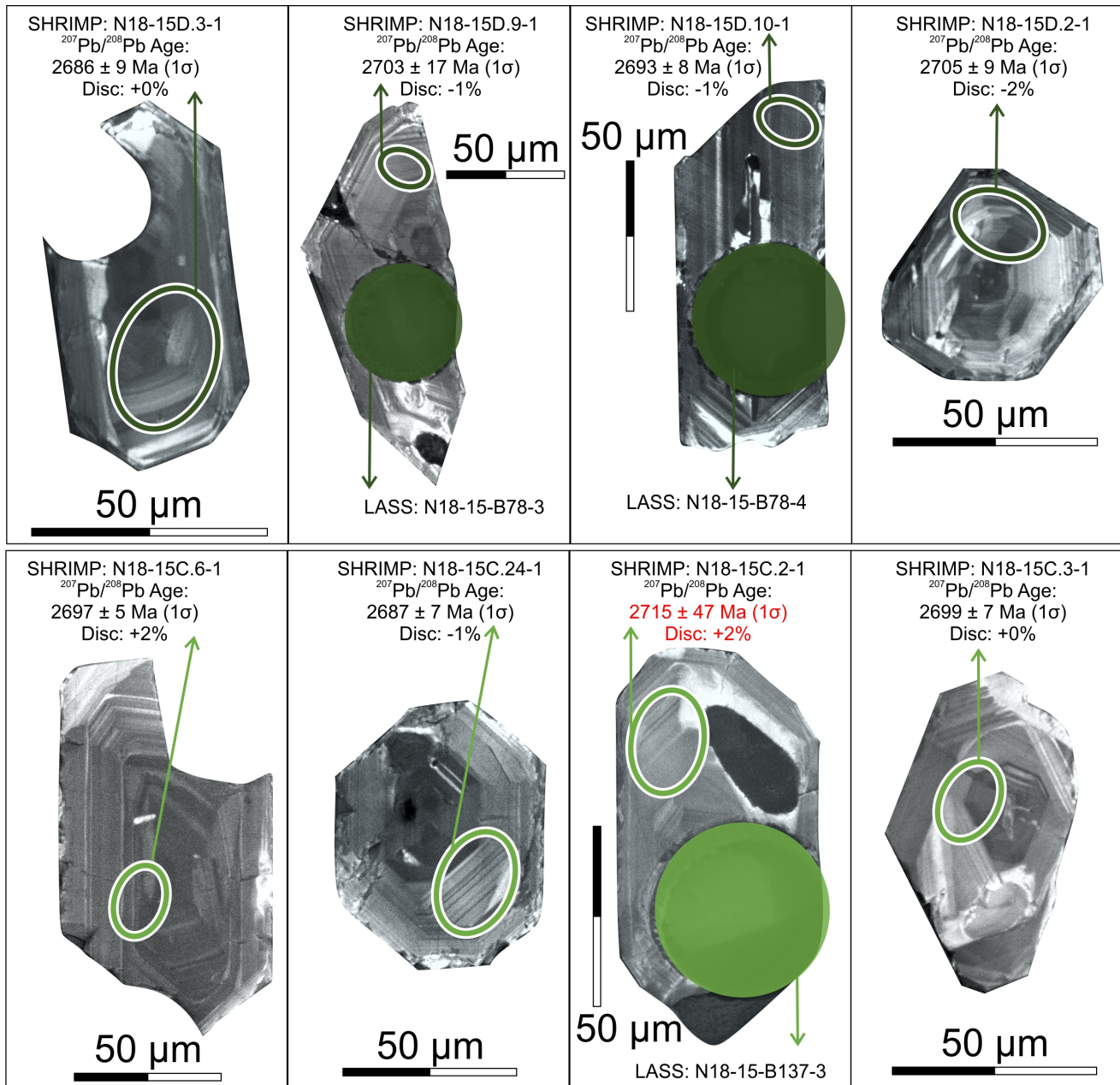
**Legend**

- |   |  |  |               |
|---|--|--|---------------|
| Leucogranite                                      | Andesite, minor basalt and dacite                              | Basalt                                       | Stringer zone |
| Sediments   | Massive sulphide   | Rhyolite                                     |               |
| Geochronology sample location in the stratigraphy | Geochronology sample with unclear location in the stratigraphy | Unclear stratigraphy due to later intrusions |               |
| I to VI Stratigraphical subdivisions              | Uncertain contact  |  |               |

1  
2  
3  
4  
5  
6  
7  
8  
9  
10  
11  
12  
13  
14  
15  
16  
17  
18  
19  
20  
21  
22  
23  
24  
25  
26  
27  
28  
29  
30  
31  
32  
33  
34  
35  
36  
37  
38  
39  
40  
41  
42  
43  
44  
45  
46  
47  
48  
49  
50  
51  
52  
53  
54  
55

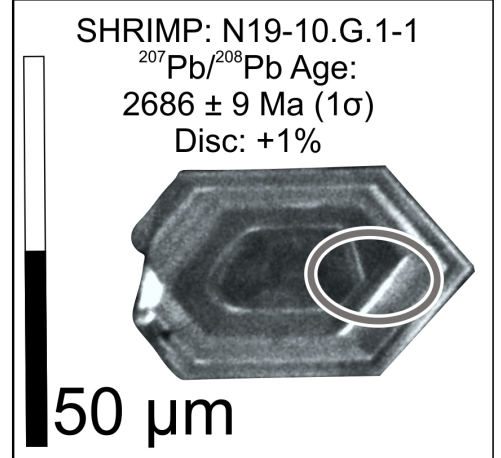
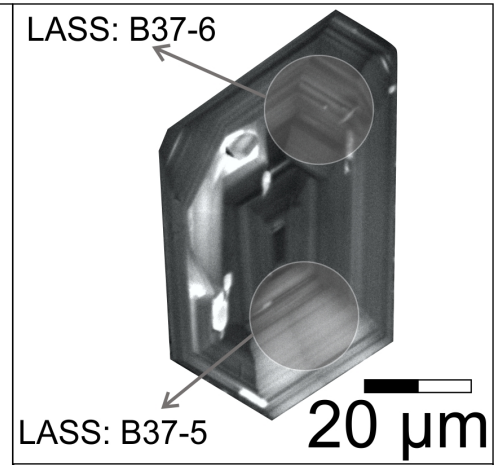
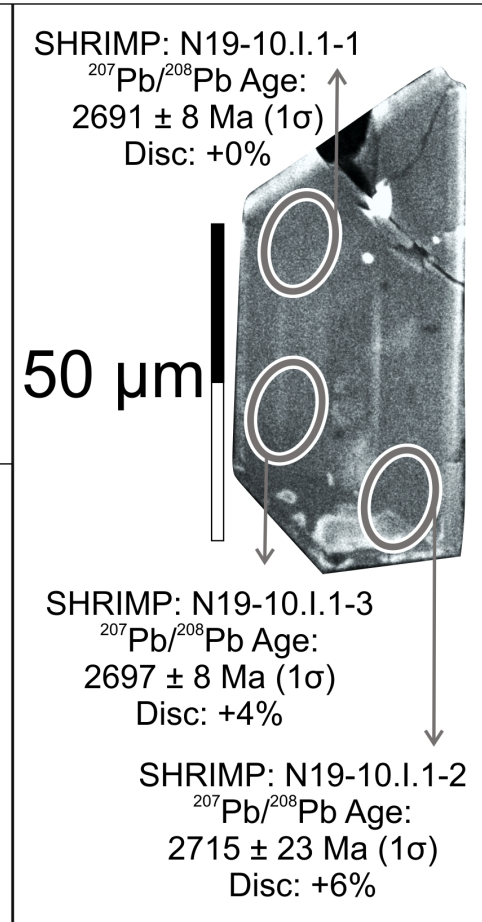
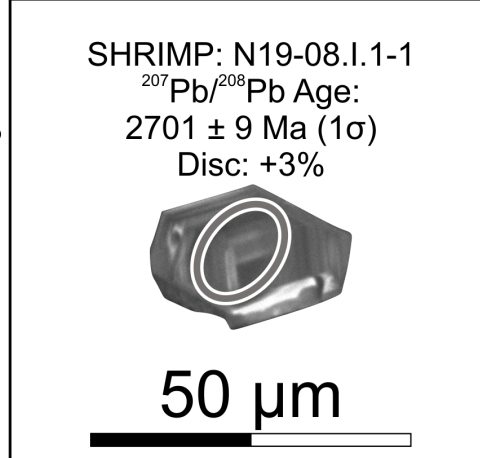
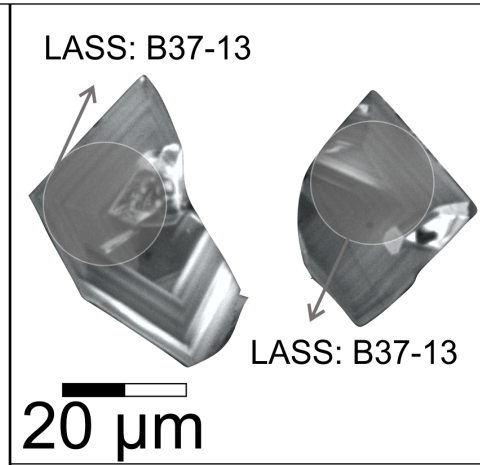
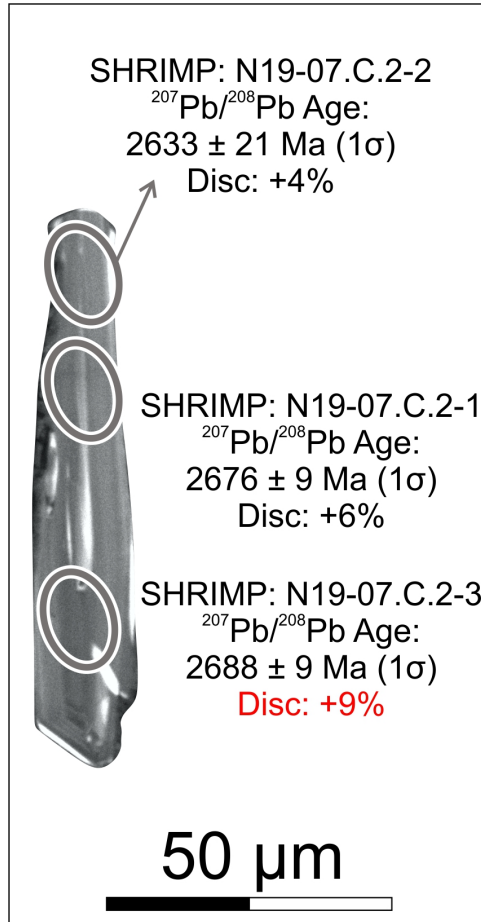


1  
2  
3  
4  
5  
6  
7  
8  
9  
10  
11  
12  
13  
14  
15  
16  
17  
18  
19  
20  
21  
22  
23  
24  
25  
26  
27  
28  
29  
30  
31  
32  
33  
34  
35  
36

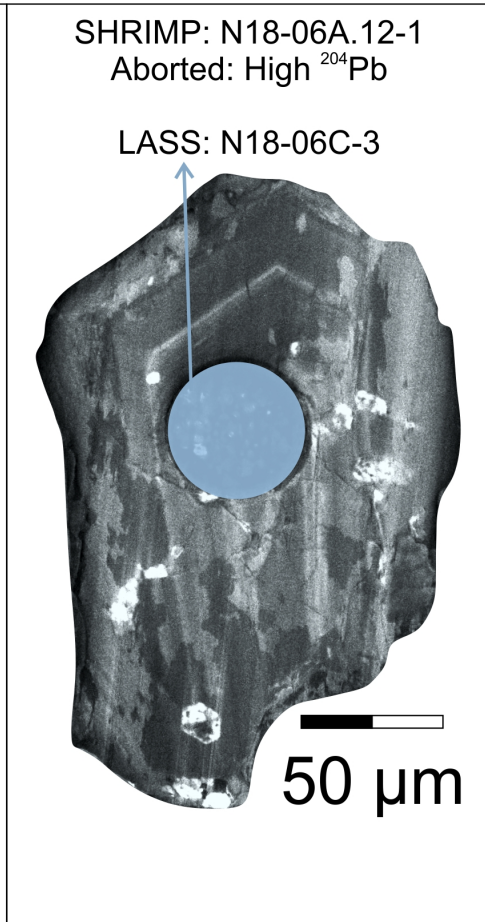
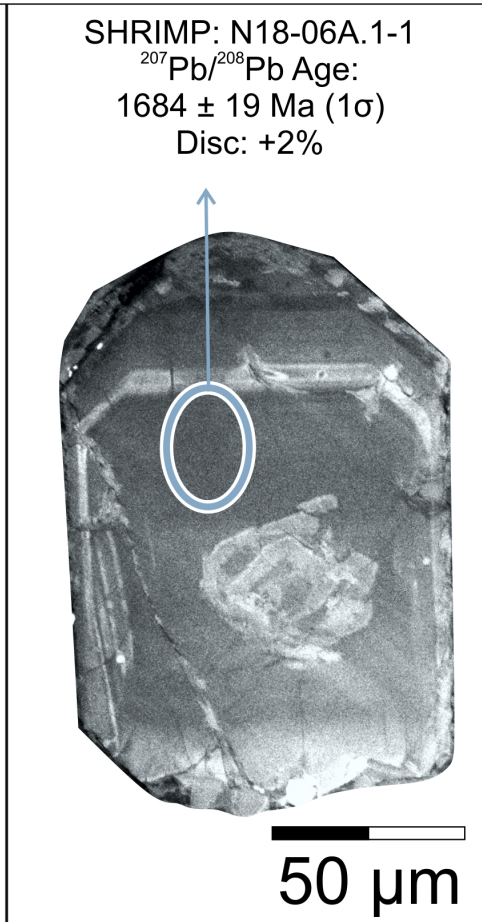
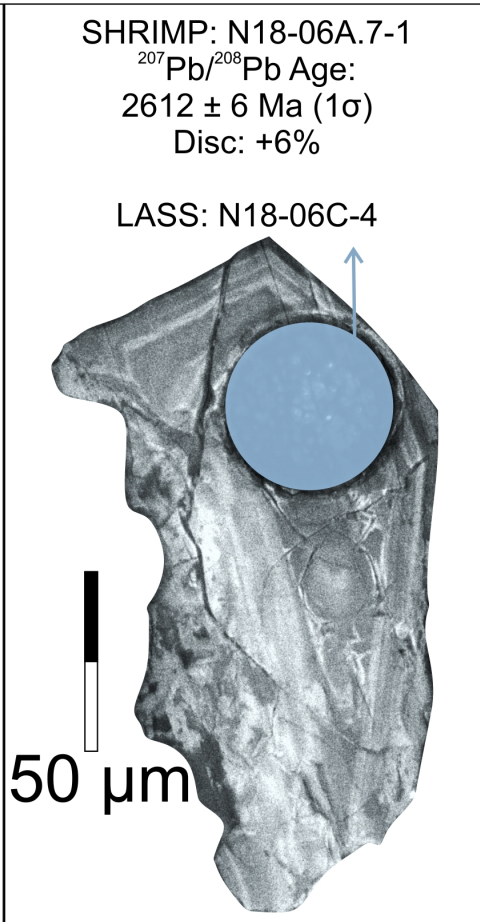
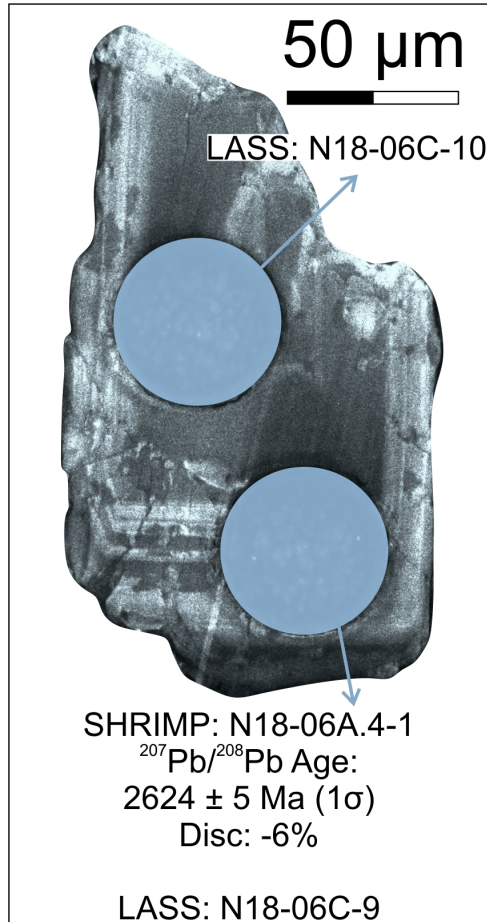




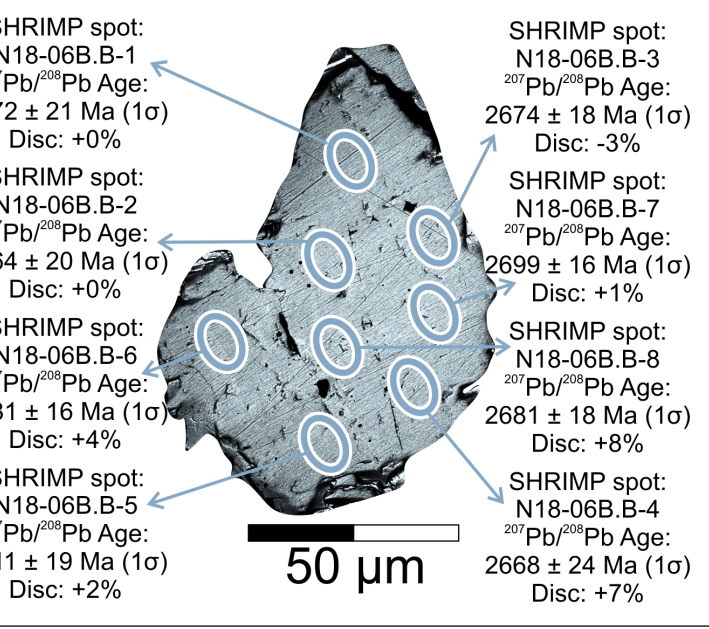
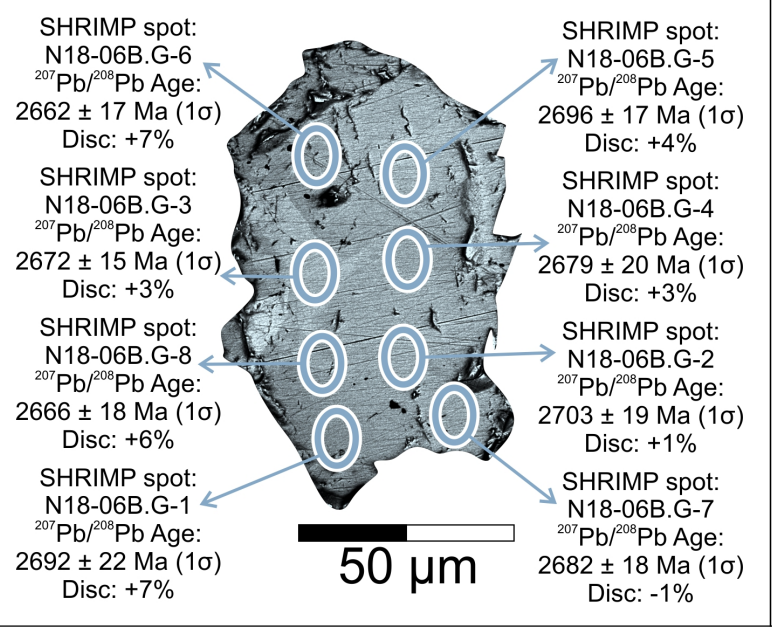
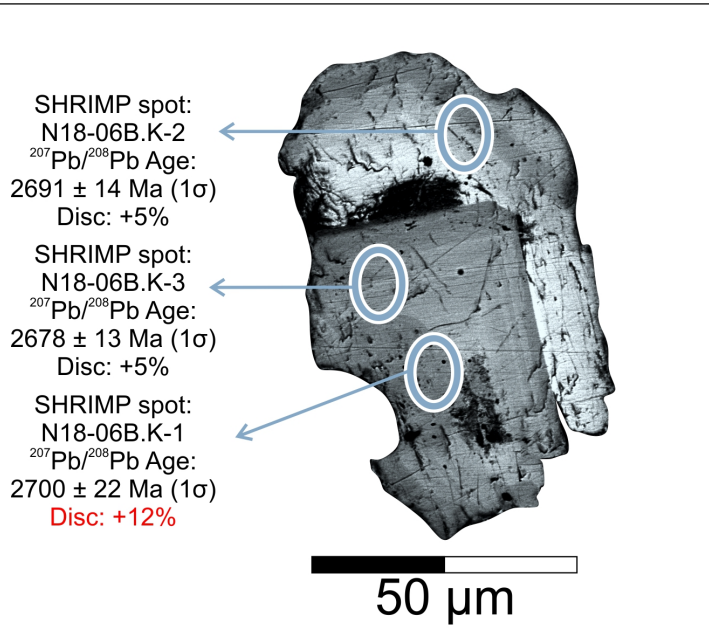
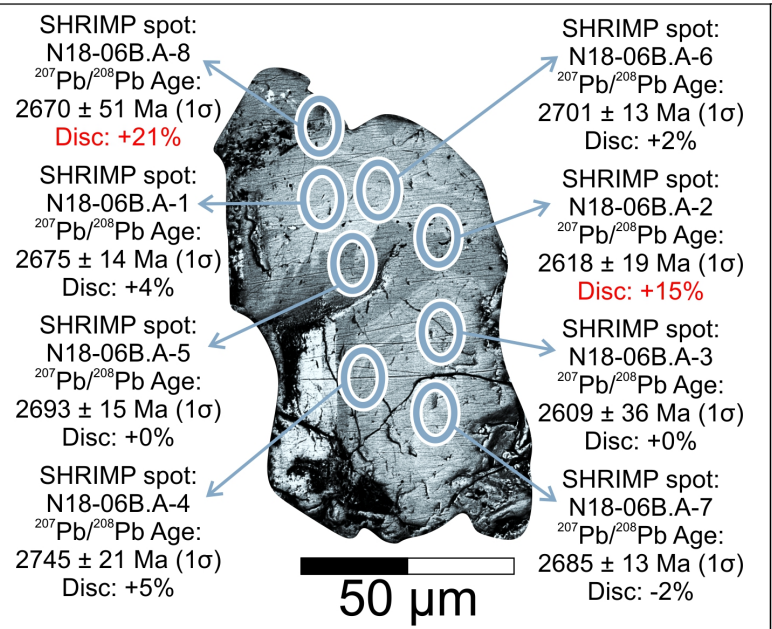
1  
2  
3  
4  
5  
6  
7  
8  
9  
10  
11  
12  
13  
14  
15  
16  
17  
18  
19  
20  
21  
22  
23  
24  
25  
26  
27  
28  
29  
30  
31  
32  
33  
34  
35  
36

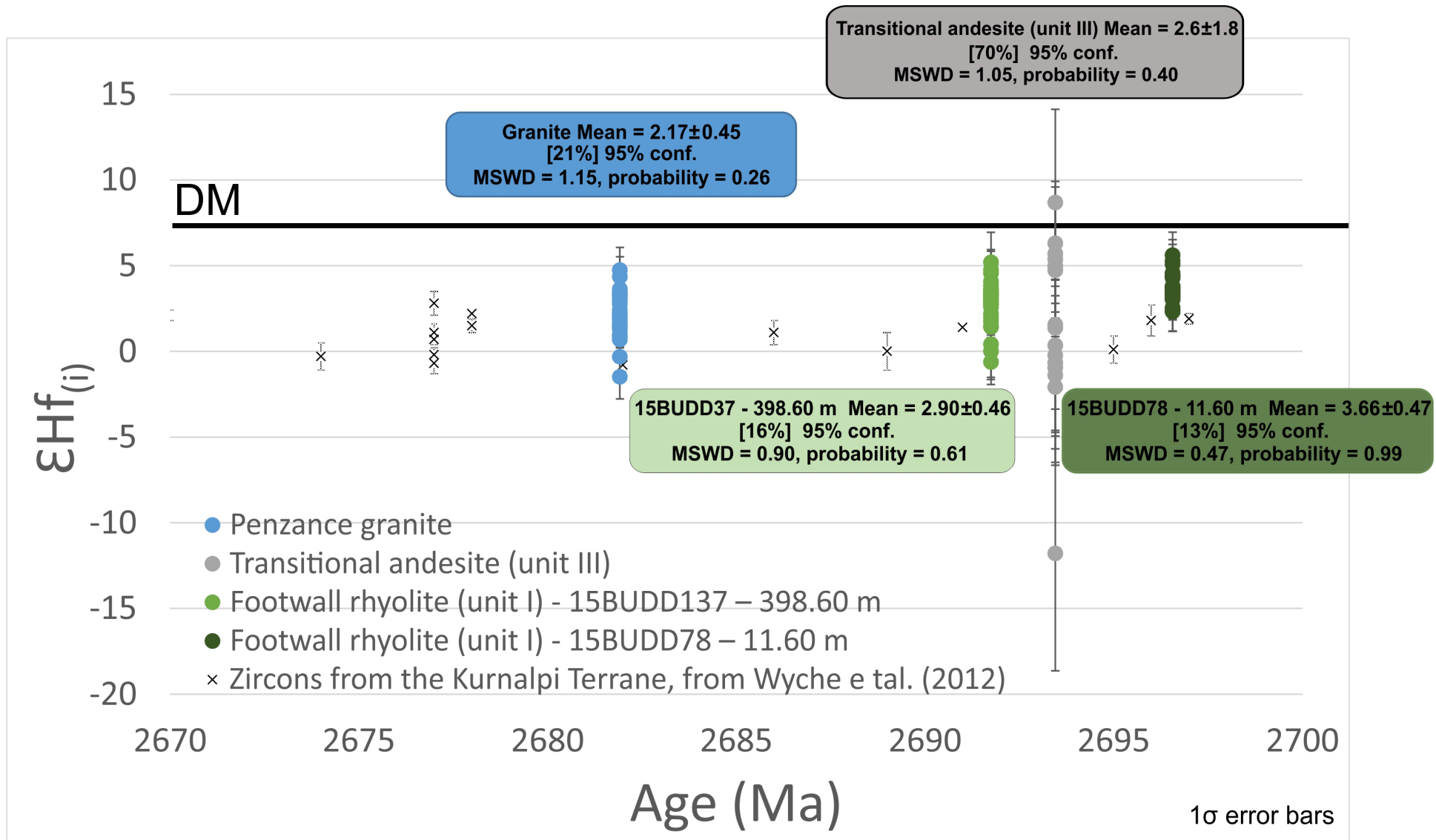


1  
2  
3  
4  
5  
6  
7  
8  
9  
10  
11  
12  
13  
14  
15  
16  
17  
18  
19  
20  
21  
22  
23  
24  
25  
26  
27  
28  
29  
30  
31  
32  
33  
34  
35  
36

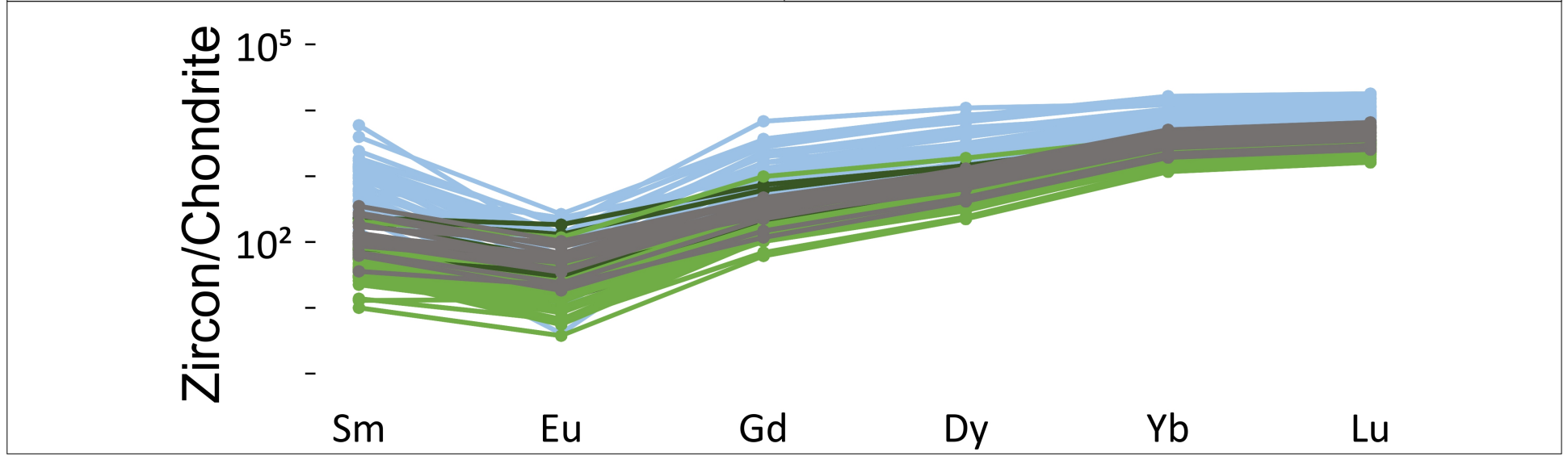
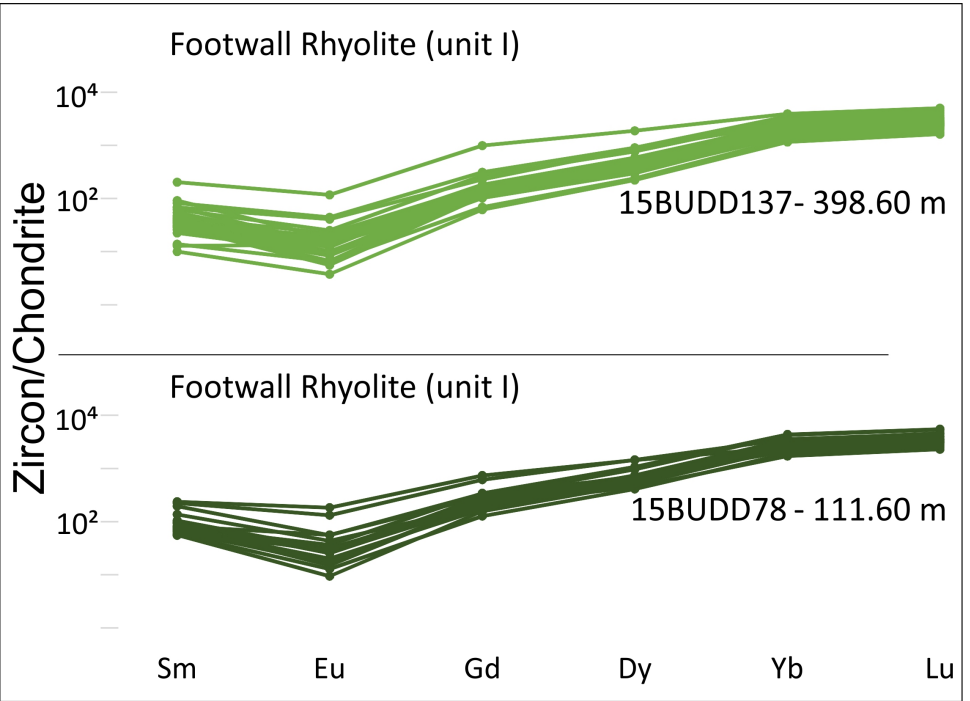
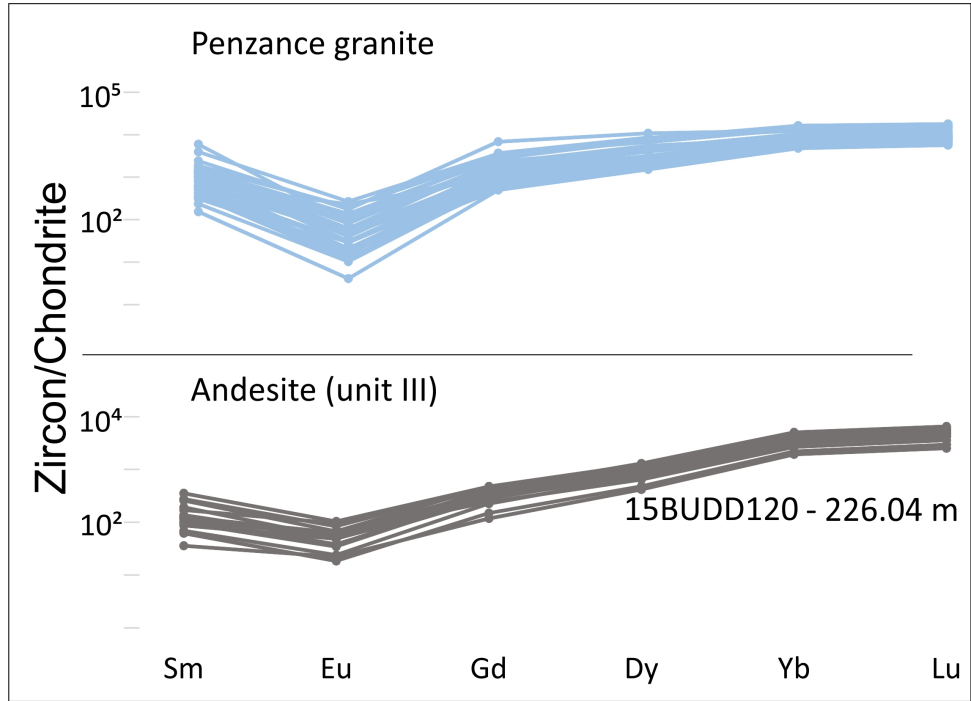


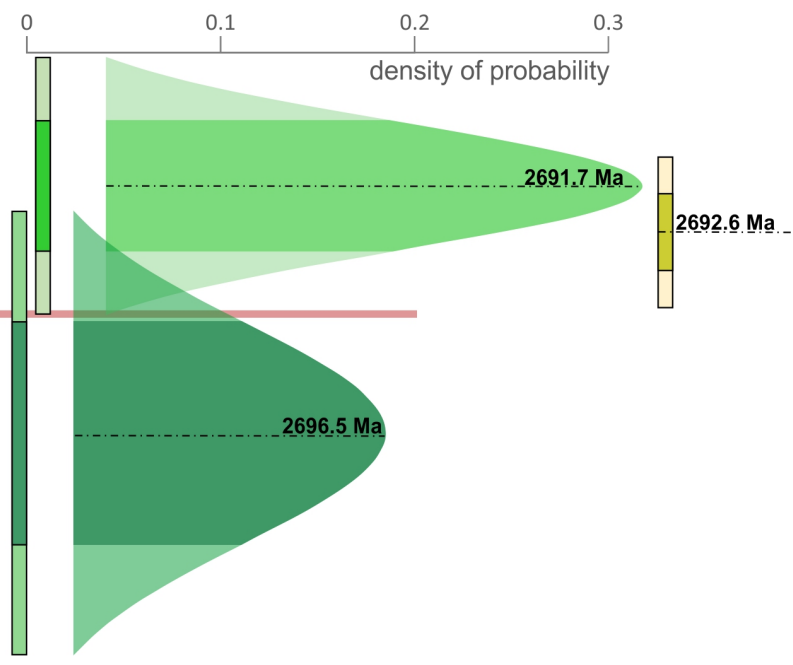
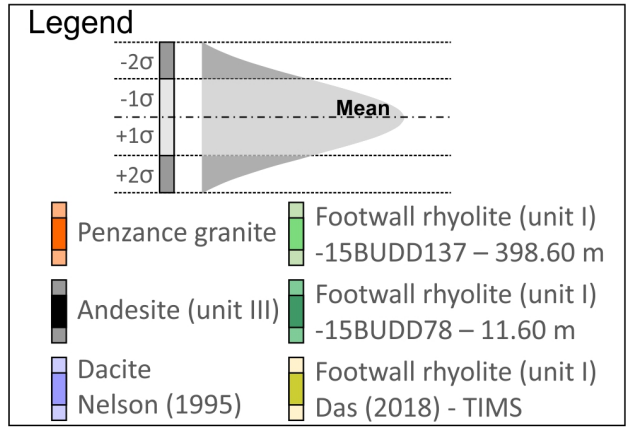
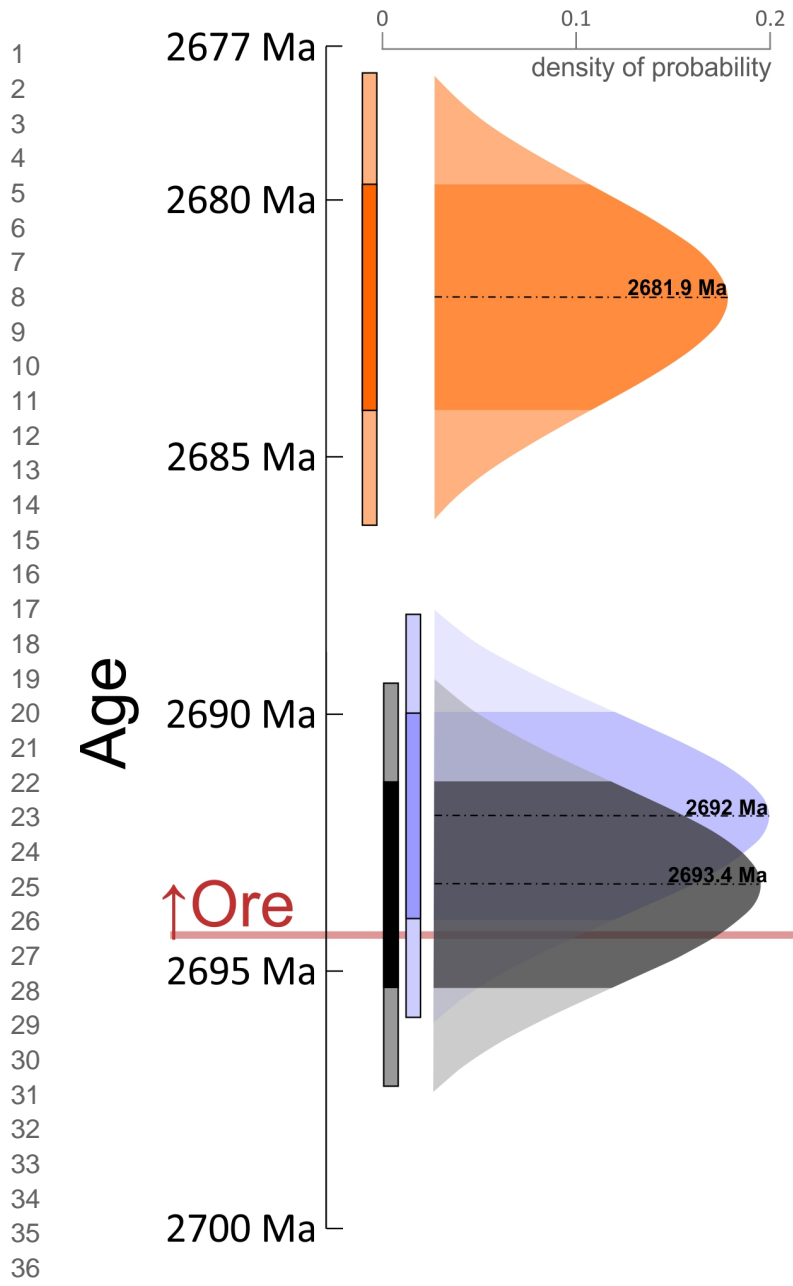
1  
2  
3  
4  
5  
6  
7  
8  
9  
10  
11  
12  
13  
14  
15  
16  
17  
18  
19  
20  
21  
22  
23  
24  
25  
26  
27  
28  
29  
30  
31  
32  
33  
34  
35  
36

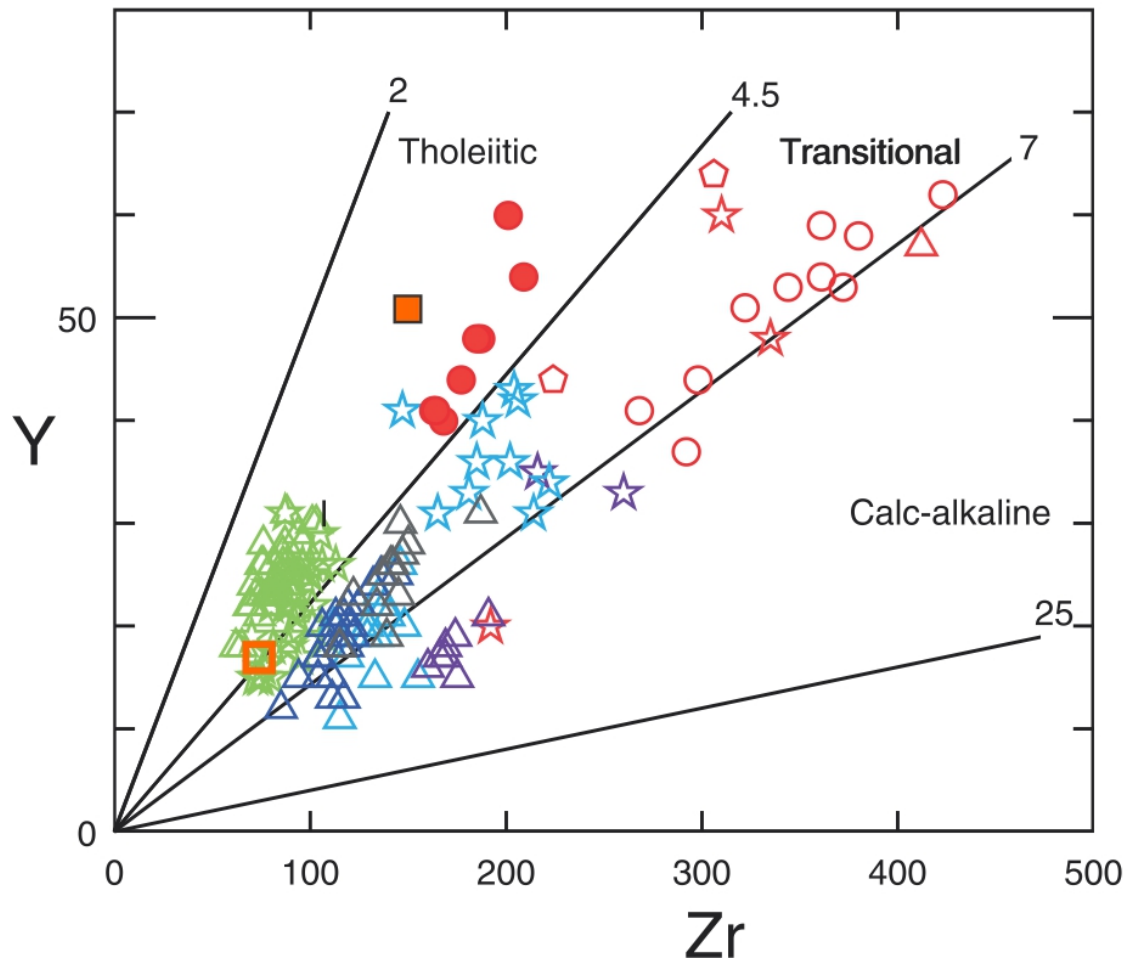




1  
2  
3  
4  
5  
6  
7  
8  
9  
10  
11  
12  
13  
14  
15  
16  
17  
18  
19  
20  
21  
22  
23  
24  
25  
26  
27  
28  
29  
30  
31  
32  
33  
34  
35  
36







**OZCHEM**

- Penzance (Kent) granite (96969076)\* Zr/Y = 2.9
- Penzance granite (92969084)\* Zr/Y = 4.6

**Belford et al. (2015)**

- △ hangingwall upper rhyolite
  - △ hangingwall upper andesite
  - △ hangingwall basalt
  - △ hangingwall andesite 3
  - △ hangingwall andesite 2
  - △ hangingwall andesite 1
  - mineralized package felsics (thol)
  - ◻ mineralized package felsics (trans)
  - mineralized package felsics (calc-alk)
  - ☆ footwall basalts
  - ☆ footwall andesites
  - ☆ footwall felsics
  - ☆ deep footwall andesite
- unit VI
- unit V
- unit IV
- unit III
- unit I

### Declaration of conflict of interests

The authors declare that they have no known competing financial interests or personal relationships that could have appeared to influence the work reported in this paper.

The authors declare the following financial interests/personal relationships which may be considered as potential competing interests:



Vitor Rodrigues Barrote



# SUPPLEMENTARY MATERIAL 1

## 1.1 SHRIMP U-Pb dating of Zircon and Monazite

### 1.1.1 Mount preparation

Zircon and monazite grains were separated from crushed rock samples using a Frantz magnetic separator and heavy liquids (methylene iodide). Grains were handpicked, mounted in epoxy resin discs and polished to expose their interiors. The zircon crystals were characterized by cathodoluminescence (CL) imaging, and monazite crystals by back-scattered electron (BSE) microscopy using the Mira3, at the Microscopy and Microanalysis Facility, John de Laeter Centre, Curtin University. The epoxy mounts were carbon coated for SEM imaging and Au-coated before each SHRIMP analytical session.

Polished thin sections prepared from samples of transitional andesite (unit III) were examined to identify suitable zircon grains for SHRIMP geochronology using the Tescan Integrated Mineral Analyzer (TIMA GM) and back-scattered electron (BSE) microscopy using the Mira3, at the Microscopy and Microanalysis Facility, John de Laeter Centre, Curtin University. Portions of the thin sections containing grains large enough ( $>15\ \mu\text{m}$ ) for ion microprobe analysis were drilled out, in  $\sim 3\ \text{mm}$  plugs, and cast in 25 mm epoxy mounts. The reference materials were in a separate mount that was cleaned and Au-coated with the sample mounts before each SHRIMP analytical session.

### 1.1.2 Zircon

Selected areas of the imaged zircon were analysed on the SHRIMP II at the John de Laeter Centre, Curtin University (JdLC). The analytical procedures for the Curtin consortium SHRIMP II have been described by de Laeter and Kennedy (1998) and Kennedy and de Laeter (1994) and are similar to those described by Compston et al. (1984) and Williams (1998). For the larger zircons in grain mounts, a 20-25  $\mu\text{m}$  elliptical spot was used, with a mass-filtered  $\text{O}_2^-$

60  
61  
62 primary beam of ~2.8-3.0 nA, whereas a 10-12  $\mu\text{m}$  spot of ~0.5 nA was used on the smaller  
63  
64 zircons in polished thin sections. Data for each spot was collected in sets of six scans on the  
65  
66 zircons through the mass range of  $^{196}\text{Zr}2\text{O}^+$ ,  $^{204}\text{Pb}^+$ , Background,  $^{206}\text{Pb}^+$ ,  $^{207}\text{Pb}^+$ ,  $^{208}\text{Pb}^+$ ,  $^{238}\text{U}^+$ ,  
67  
68  $^{248}\text{ThO}^+$  and  $^{254}\text{UO}^+$ . The  $^{206}\text{Pb}/^{238}\text{U}$  age standard and U-content standard used was M257  
69  
70 (561.3 Ma and 840 ppm U; Nasdala et al., 2008) while OGC zircon was utilized as the  
71  
72  $^{207}\text{Pb}/^{206}\text{Pb}$  standard, to monitor instrument induced mass fractionation ( $3465.4 \pm 0.6$  Ma; Stern  
73  
74 et al., 2009). The  $^{207}\text{Pb}/^{206}\text{Pb}$  dates obtained on OGC zircons during the SHRIMP sessions  
75  
76 matched the  $^{207}\text{Pb}/^{206}\text{Pb}$  standard age within uncertainty and no fractionation correction was  
77  
78 warranted. The common Pb correction was based on the measured  $^{204}\text{Pb}$ -content (Compston et  
79  
80 al., 1984). The correction formula for Pb/U fractionation is  $^{206}\text{Pb}^+ / ^{238}\text{U}^+ = a (^{254}\text{UO}^+ / ^{238}\text{U}^+)^b$   
81  
82 (Claoué-Long et al., 1995) using the parameter values of Black et al. (2003). The constant “a”  
83  
84 is determined empirically from analyses of the standard during each analytical session. The  
85  
86 programs SQUID II and Isoplot (Ludwig, 2011, 2009) were used for data processing.  
87  
88  
89

### 90 91 *1.1.3 Monazite*

92  
93 The U–Th–Pb analyses were performed using the high spatial-resolution capability of the  
94  
95 SHRIMP II at the JdLC. Monazite was analysed in two analytical sessions. Grains were  
96  
97 analysed using a 30  $\mu\text{m}$  Köhler aperture, ~0.3 nA primary ion beam ( $\text{O}_2^-$ ) and a ~10  $\mu\text{m}$   
98  
99 analysis spot. Energy filtering was not applied, and the post-collector retardation lens was  
100  
101 activated to reduce stray ion arrivals. The mass resolution ( $M/\Delta M$  at 1% peak height) was  
102  
103 >5000. French ( $^{206}\text{Pb}/^{238}\text{U}$  age 514 Ma) was used as the primary Pb/U reference material, and  
104  
105 Z2908 and Z2234 were the secondary reference materials used to monitor matrix effects  
106  
107 (Fletcher et al., 2010). Z2908 ( $^{207}\text{Pb}/^{206}\text{Pb}$  age 1796 Ma) was also analysed to monitor and  
108  
109 correct for instrumental mass fractionation of  $^{207}\text{Pb}$  from  $^{206}\text{Pb}$ . SQUID II software (Ludwig,  
110  
111 2009) was used for initial data reduction including  $^{204}\text{Pb}$  correction. Matrix effects in  $^{206}\text{Pb}/^{238}\text{U}$   
112  
113 were corrected following established protocols detailed by Fletcher et al. (2010). 9 analyses of  
114  
115  
116  
117  
118

119  
120  
121 Z2908 yielded a mean  $^{207}\text{Pb}/^{206}\text{Pb}$  age of  $1796.7 \pm 5.4$  Ma (mean square weighted deviation,  
122  
123 MSWD = 1.7). An insignificant fractionation correction (0.02%) was applied to sample data,  
124  
125 with no augmentation of sample precision required based on the reproducibility of  $^{207}\text{Pb}/^{206}\text{Pb}$   
126  
127 in the reference materials.  $^{207}\text{Pb}/^{206}\text{Pb}$  dates from individual analyses are presented with  $1\sigma$   
128  
129 internal precision, whereas weighted mean  $^{207}\text{Pb}/^{206}\text{Pb}$  dates are reported at 95% confidence  
130  
131 limits.  
132

## 133 **1.2 LA-SS-ICPMS of Zircon – Trace elements and Hf isotopes**

134  
135  
136 Zircon Lu–Hf isotopes and rare earth element (REE) abundances were measured over two  
137  
138 analytical sessions using laser ablation split stream inductively coupled plasma mass  
139  
140 spectrometry (LA-SS-ICPMS). The analyses were conducted in zircons from the same samples  
141  
142 that were analysed by SHRIMP, but not necessarily on the same grain or over the same spot as  
143  
144 the SHRIMP analysis. Isotopic and elemental data were collected simultaneously using a  
145  
146 Resonetics S-155-LR 193 nm excimer laser coupled to a Nu Plasma II multicollector and  
147  
148 Agilent 7700s quadrupole mass spectrometer in the GeoHistory Facility, JdLC at Curtin  
149  
150 University.  
151  
152

153  
154 Samples 15BUDD120 – 228.42 and 15BUDD120 – 226.04 m, from the Transitional  
155  
156 andesite (unit III) were analysed with a laser spot diameter of 24  $\mu\text{m}$ , with 2.7  $\text{J}/\text{cm}^2$  on-sample  
157  
158 laser energy, repetition rate of 10 Hz, ablation time of 25 seconds and ~30 seconds of  
159  
160 background capture before and after each analysis. Two cleaning pulse preceded analysis. The  
161  
162 spot size and ablation time in this case were limited by the smaller size of the zircons.  
163

164  
165 The remaining samples were analysed with a laser spot diameter of 50  $\mu\text{m}$ , with 2.7  $\text{J}/\text{cm}^2$   
166  
167 on-sample laser energy, repetition rate of 10 Hz, ablation time of 40 seconds and ~45 seconds  
168  
169 of total baseline acquisition.  
170

171  
172 Zircon standard P1 (Li et al., 2010; chips of Penglai zircon characterised in-house for trace  
173  
174 element composition) was used as the primary standard to calculate element concentrations  
175  
176  
177

178 using  $^{91}\text{Zr}$  as the internal reference isotope and assuming 43.14% Zr in zircon, and to correct  
 179 for instrument drift.

180 Lu–Hf isotopic data were measured simultaneously for  $^{172}\text{Yb}$ ,  $^{173}\text{Yb}$ ,  $^{175}\text{Lu}$ ,  $^{176}\text{Hf}+\text{Yb}+\text{Lu}$ ,  
 181  $^{177}\text{Hf}$ ,  $^{178}\text{Hf}$ ,  $^{179}\text{Hf}$  and  $^{180}\text{Hf}$  on the Faraday array. Time resolved data was baseline subtracted  
 182 and reduced using Iolite3.5 (DRS after Woodhead et al., 2004), where  $^{176}\text{Yb}$  and  $^{176}\text{Lu}$  were  
 183 removed from the 176 mass signal using  $^{176}\text{Yb}/^{173}\text{Yb} = 0.7962$  (Chu et al., 2002) and  
 184  $^{176}\text{Lu}/^{175}\text{Lu} = 0.02655$  (Chu et al., 2002) with an exponential law mass bias correction assuming  
 185  $^{172}\text{Yb}/^{173}\text{Yb} = 1.35274$  (Chu et al., 2002). The interference corrected  $^{176}\text{Hf}/^{177}\text{Hf}$  was  
 186 normalized to  $^{179}\text{Hf}/^{177}\text{Hf} = 0.7325$  (Patchett and Tatsumoto, 1980) for mass bias correction.  
 187 Zircons from the Mud Tank carbonatite locality were analysed together with the samples in  
 188 each session to determine corrected, standard referenced  $^{176}\text{Hf}/^{177}\text{Hf}$  (Table 1). Zircon  
 189 standards with a range of REE contents (FC1 91500, Plešovice and GJ-1; references and data  
 190 in Table 1) were run to verify the method. All analysed standards fell within  $2\sigma$  error of reported  
 191  $^{176}\text{Hf}/^{177}\text{Hf}$  values, although uncertainties on the 24 micron beam run were, understandably,  
 192 significantly higher. In addition, the corrected  $^{178}\text{Hf}/^{177}\text{Hf}$  and  $^{180}\text{Hf}/^{177}\text{Hf}$  ratios (for the 50  
 193 micron beam run) were calculated to monitor the accuracy of the mass bias correction and  
 194 yielded an average value of  $1.467193 \pm 12$  and  $1.886808 \pm 11$  (n=184), which is within the  
 195 range of values reported by Thirlwall and Anczkiewicz (2004). Calculation of  $\epsilon\text{Hf}$  values  
 196 employed the decay constant of Scherer et al. (2001) and the Chondritic Uniform Reservoir  
 197 (CHUR) values of Blichert-Toft and Albarède (1997).

223 Table 1: Summary of the Hf isotope measurements of standard materials used interspersed  
 224 with analyses of unknown zircons. Mean values were calculated using the built-in statistics  
 225 from the Iolite software (Paton et al., 2011)

Standard Material	50 $\mu\text{m}$	24 $\mu\text{m}$	Reference Value
	Corrected $^{176}\text{Hf}/^{177}\text{Hf}$	Corrected $^{176}\text{Hf}/^{177}\text{Hf}$	
Mud Tank	<b><math>0.282505 \pm 14</math></b> (MSWD = 0.70, n = 14)	<b><math>0.282507 \pm 64</math></b> (MSWD = 2.9, n = 6)	$0.282505 \pm 44$ (Woodhead and Hergt, 2005)
FC1	<b><math>0.282182 \pm 9</math></b> (MSWD = 0.31, n = 9)	<b><math>0.282229 \pm 150</math></b> (MSWD = 3.9, n = 6)	$0.282172 \pm 42$ (Woodhead and Hergt, 2005)

91500	<b>0.282306 ± 11</b> (MSWD = 0.71, n = 14)	<b>0.282235 ± 130</b> (MSWD = 2.4, n = 6)	0.282306 ± 40 (Woodhead et al., 2004)
Plešovice	<b>0.282477 ± 8</b> (MSWD = 0.3, n = 10)	<b>0.282470 ± 51</b> (MSWD = 0.49, n = 6)	0.282482 ± 13 (Sláma et al., 2008)
GJ-1	<b>0.282016 ± 12</b> (MSWD = 0.69, n = 14)	<b>0.281201 ± 110</b> (MSWD = 1.1, n = 6)	0.282000 ± 5 (Morel et al., 2008)

### 1.3 References

- Black, L.P., Kamo, S.L., Allen, C.M., Aleinikoff, J.N., Davis, D.W., Korsch, R.J., Foudoulis, C., 2003. TEMORA 1: a new zircon standard for Phanerozoic U–Pb geochronology. *Chem. Geol.* 200, 155–170. [https://doi.org/10.1016/S0009-2541\(03\)00165-7](https://doi.org/10.1016/S0009-2541(03)00165-7)
- Blichert-Toft, J., Albarède, F., 1997. The Lu–Hf isotope geochemistry of chondrites and the evolution of the mantle–crust system. *Earth Planet. Sci. Lett.* 148, 243–258. [https://doi.org/10.1016/S0012-821X\(97\)00040-X](https://doi.org/10.1016/S0012-821X(97)00040-X)
- Claoué-Long, J.C., Compston, W., Roberts, J., Fanning, C.M., 1995. Two Carboniferous Ages: A Comparison of Shrimp Zircon Dating with Conventional Zircon Ages and <sup>40</sup>Ar/<sup>39</sup>Ar Analysis, in: Berggren, W.A., Kent, D.V., Aubry, M.-P., Hardenbol, J. (Eds.), *Geochronology, Time Scales, and Global Stratigraphic Correlation*, Society for Sedimentary Geology Special Publications. SEPM (Society for Sedimentary Geology), pp. 3–21. <https://doi.org/10.2110/pec.95.54>
- Compston, W., Williams, I.S., Meyer, C., 1984. U–Pb geochronology of zircons from lunar breccia 73217 using a sensitive high mass-resolution ion microprobe. *Proc. 14th Lunar Planet. Sci. Conf. J. Geophys. Res. Suppl.* 89, B525–B534. <https://doi.org/10.1029/JB089iS02p0B525>
- Chu, N.-C., Taylor, R.N., Chavagnac, V., Nesbitt, R.W., Boella, R.M., Milton, J.A., German, C.R., Bayon, G., Burton, K., 2002. Hf isotope ratio analysis using multi-collector inductively coupled plasma mass spectrometry: an evaluation of isobaric interference corrections. *J. Anal. At. Spectrom.* 17, 1567–1574. <https://doi.org/10.1039/b206707b>
- de Laeter, J.R., Kennedy, A.K., 1998. A double focusing mass spectrometer for geochronology. *Int. J. Mass Spectrom.* 178, 43–50. [https://doi.org/10.1016/S1387-3806\(98\)14092-7](https://doi.org/10.1016/S1387-3806(98)14092-7)
- Fletcher, I.R., McNaughton, N.J., Davis, W.J., Rasmussen, B., 2010. Matrix effects and calibration limitations in ion probe U–Pb and Th–Pb dating of monazite. *Chem. Geol.* 270, 31–44. <https://doi.org/10.1016/j.chemgeo.2009.11.003>
- Kennedy, A.K., De Laeter, J.R., 1994. The performance characteristics of the WA SHRIMP II ion microprobe., in: *Abstracts Vol., U.S. Geological Survey Circular. Presented at the Eighth International Conference on Geochronology, Cosmochronology and Isotope Geology, Berkeley, USA*, p. 166.
- Li, X.-H., Long, W.-G., Li, Q.-L., Liu, Y., Zheng, Y.-F., Yang, Y.-H., Chamberlain, K.R., Wan, D.-F., Guo, C.-H., Wang, X.-C., Tao, H., 2010. Penglai Zircon Megacrysts: A Potential New Working Reference Material for Microbeam Determination of Hf–O Isotopes and U–Pb Age. *Geostand. Geoanalytical Res.* 34, 117–134. <https://doi.org/10.1111/j.1751-908X.2010.00036.x>
- Ludwig, K.R., 2011. User’s manual for Isoplot 4.15: a geochronological toolkit for Microsoft Excel, Berkeley Geochronology Center Special Publication.
- Ludwig, K.R., 2009. *Squid 2.50, A User’s Manual*, Berkeley Geochronology Centre Special Publication.
- Morel, M.L.A., Nebel, O., Nebel-Jacobsen, Y.J., Miller, J.S., Vroon, P.Z., 2008. Hafnium isotope characterization of the GJ-1 zircon reference material by solution and laser-

- 296  
297  
298 ablation MC-ICPMS. Chem. Geol. 255, 231–235.  
299 <https://doi.org/10.1016/j.chemgeo.2008.06.040>  
300  
301 Nasdala, L., Hofmeister, W., Norberg, N., Martinson, J.M., Corfu, F., Dörr, W., Kamo, S.L.,  
302 Kennedy, A.K., Kronz, A., Reiners, P.W., Frei, D., Kosler, J., Wan, Y., Götze, J.,  
303 Häger, T., Kröner, A., Valley, J.W., 2008. Zircon M257 - a Homogeneous Natural  
304 Reference Material for the Ion Microprobe U-Pb Analysis of Zircon. *Geostand.*  
305 *Geoanalytical Res.* 32, 247–265. <https://doi.org/10.1111/j.1751-908X.2008.00914.x>  
306 Patchett, P.J., Tatsumoto, M., 1980. Hafnium isotope variations in oceanic basalts. *Geophys.*  
307 *Res. Lett.* 7, 1077–1080. <https://doi.org/10.1029/GL007i012p01077>  
308 Paton, C., Hellstrom, J., Paul, B., Woodhead, J., Hergt, J., 2011. Iolite: Freeware for the  
309 visualisation and processing of mass spectrometric data. *J. Anal. At. Spectrom.* 26,  
310 2508. <https://doi.org/10.1039/c1ja10172b>  
311 Scherer, E., 2001. Calibration of the Lutetium-Hafnium Clock. *Science* 293, 683–687.  
312 <https://doi.org/10.1126/science.1061372>  
313 Sláma, J., Košler, J., Condon, D.J., Crowley, J.L., Gerdes, A., Hanchar, J.M., Horstwood,  
314 M.S.A., Morris, G.A., Nasdala, L., Norberg, N., Schaltegger, U., Schoene, B., Tubrett,  
315 M.N., Whitehouse, M.J., 2008. Plešovice zircon — A new natural reference material  
316 for U–Pb and Hf isotopic microanalysis. *Chem. Geol.* 249, 1–35.  
317 <https://doi.org/10.1016/j.chemgeo.2007.11.005>  
318 Stern, R.A., Bodorkos, S., Kamo, S.L., Hickman, A.H., Corfu, F., 2009. Measurement of SIMS  
319 Instrumental Mass Fractionation of Pb Isotopes During Zircon Dating. *Geostand.*  
320 *Geoanalytical Res.* 33, 145–168. <https://doi.org/10.1111/j.1751-908X.2009.00023.x>  
321 Thirlwall, M.F., Anczkiewicz, R., 2004. Multidynamic isotope ratio analysis using MC–ICP–  
322 MS and the causes of secular drift in Hf, Nd and Pb isotope ratios. *Int. J. Mass*  
323 *Spectrom.* 235, 59–81. <https://doi.org/10.1016/j.ijms.2004.04.002>  
324 Williams, I.S., 1998. Geochronology by Ion Microprobe, in: McKibben, M.A., Shanks, W.C.,  
325 Ridley, W.I. (Eds.), *Applications of Microanalytical Techniques to Understanding*  
326 *Mineralizing Processes, Reviews in Economic Geology.* pp. 1–35.  
327 Woodhead, J., Hergt, J., Shelley, M., Eggins, S., Kemp, R., 2004. Zircon Hf-isotope analysis  
328 with an excimer laser, depth profiling, ablation of complex geometries, and  
329 concomitant age estimation. *Chem. Geol.* 209, 121–135.  
330 <https://doi.org/10.1016/j.chemgeo.2004.04.026>  
331 Woodhead, J.D., Hergt, J.M., 2005. A Preliminary Appraisal of Seven Natural Zircon  
332 Reference Materials for In Situ Hf Isotope Determination. *Geostand. Geoanalytical*  
333 *Res.* 29, 183–195. <https://doi.org/10.1111/j.1751-908X.2005.tb00891.x>  
334  
335  
336  
337  
338  
339  
340  
341  
342  
343  
344  
345  
346  
347  
348  
349  
350  
351  
352  
353  
354